The 4D evolution of the Teutonic Bore Camp VHMS deposits, Yilgarn Craton, Western Australia

Manuscript Details

Manuscript number	ORGEO_2019_778_R1
Title	The 4D evolution of the Teutonic Bore Camp VHMS deposits, Yilgarn Craton, Western Australia
Article type	Research paper

Abstract

The Teutonic Bore Camp, comprised of the Teutonic Bore, Jaguar and Bentley deposits, is one of the most significant volcanic-hosted massive sulphide (VHMS) camps in Western Australia. Despite being extensively studied, only recently there have been advances in the understanding of the mechanism that drove the formation of mineralisation. It has been recognized by recent studies that the volcanic-hosted deposits from the Teutonic Bore Camp represent replacement-type VHMS systems, with significant input of fluids and metals from a magmatic source. This paper tests the existing hypothesis that the nearby Penzance granite acted as the metals source and/or thermal engine driving the development of these ore deposits. New age constraints on the formation of the host volcanic sequence at the Bentley deposit and the crystallization of the Penzance granite allows for the construction of a 4D evolutionary model for the ore system. A new U-Pb SHRIMP monazite age of 2681.9 ± 4.5 Ma indicates that the Penzance granite post-dates the host stratigraphy at Bentley (ca. 2693 Ma) and is probably coeval with mineralisation. All zircons (Penzance, Bentley units I and III) have very similar ƐHf(i), with most values between -1 and +6, slightly higher than the ƐHf(i) of zircons from other granites and volcanics within the Kurnalpi Terrain, and indicative of juvenile sources. The mean Th/U ratios are ~0.7 and ~0.6 for the Penzance and Bentley zircons, respectively. All zircons have similar Ce/Nd(CN) ratios. The chemical similarities between the zircons from the granite and the volcanic rocks at Bentley support a shared magmatic source between the Penzance and the Teutonic Bore Camp sequence. The Penzance granite is the likely source of heat, and potentially metals, which drove the VHMS mineralisation at the Teutonic Bore Camp.

Keywords	Penzance; Teutonic Bore; Volcanic-hosted massive sulphide; Archean; Geochronology; 4D modelling

Corresponding Author	Vitor Rodrigues Barrote
Corresponding Author's Institution	Curtin University
Order of Authors	Vitor Rodrigues Barrote, Neal McNaughton, Svetlana Tessalina, Noreen Evans, Cristina Talavera, Jian-Wei Zi, Bradley McDonald
Suggested reviewers	Susan Belford, John Percival, Haoyang Zhou, Christopher Yeats

Submission Files Included in this PDF

File Name [File Type]

Cover letter.docx [Cover Letter]

Reply to reviwers.docx [Response to Reviewers]

MS with changes marked.docx [Revised Manuscript with Changes Marked]

Highlights.docx [Highlights]

GraphicAbstract.tif [Graphical Abstract]

MS with no changes marked.docx [Manuscript File]

Figure Captions.docx [Figure]

Fig1.jpg [Figure]

Fig2.jpg [Figure]

Fig3.jpg [Figure]

Fig4.jpg [Figure]

Fig5.jpg [Figure]

Fig6.jpg [Figure]

Fig7.jpg [Figure]

Fig8.jpg [Figure]

Fig9.jpg [Figure]

Fig10.jpg [Figure]

Fig11.jpg [Figure]

declaration-of-conflict of-interests.docx [Conflict of Interest]

Sup1_Methods.docx [e-Component]

Submission Files Not Included in this PDF

File Name [File Type]

Table 1.xlsx [Table]

Sup2_SHRIMP_Zircon.xlsx [e-Component]

Sup3_Hf_Zircon.xlsx [e-Component]

Sup4_TE_Zircon.xlsx [e-Component]

To view all the submission files, including those not included in the PDF, click on the manuscript title on your EVISE Homepage, then click 'Download zip file'.

Research Data Related to this Submission

Data set https://data.mendeley.com/datasets/jpwjnwcnv2/draft?a=97413372-af5a-4ce3-96d8-180bf090118b

Data for: The magmatic 4D evolution of the Teutonic Bore Camp VHMS deposits, Yilgarn Craton, Western Australia

Eletronic Supplementary Material for "The 4D evolution of the Teutonic Bore Camp VHMS deposits, Yilgarn Craton, Western Australia" The Teutonic Bore Camp, comprised of the Teutonic Bore, Jaguar and Bentley deposits, is one of the most significant volcanic-hosted massive sulphide (VHMS) camps in Western Australia. Despite being extensively studied, only recently there have been advances in the understanding of the mechanism that drove the formation of mineralisation. It has been recognized by recent studies that the volcanic-hosted deposits from the Teutonic Bore Camp represent replacement-type VHMS systems, with significant input of fluids and metals from a magmatic source. This paper tests the existing hypothesis that the nearby Penzance granite acted as the metals source and/or thermal engine driving the development of these ore deposits. New age constraints on the formation of the host volcanic sequence at the Bentley deposit and the crystallization of the Penzance granite allows for the construction of a 4D evolutionary model for the ore system. A new U-Pb SHRIMP monazite age of 2681.9 ± 4.5 Ma indicates that the Penzance granite post-dates the host stratigraphy at Bentley (ca. 2693 Ma) and is probably coeval with mineralisation. All zircons (Penzance, Bentley units I and III) have very similar ƐHf(i), with most values between -1 and +6, slightly higher than the ƐHf(i) of zircons from other granites and volcanics within the Kurnalpi Terrain, and indicative of juvenile sources. The mean Th/U ratios are ~0.7 and ~0.6 for the Penzance and Bentley zircons, respectively. All zircons have similar Ce/Nd(CN) ratios. The chemical similarities between the zircons from the granite and the volcanic rocks at Bentley support a shared magmatic source between the Penzance and the Teutonic Bore Camp sequence. The Penzance granite is the likely source of heat, and potentially metals, which drove the VHMS mineralisation at the Teutonic Bore Camp.

Vitor Barrote
School of Earth and Planetary Sciences
Curtin University
Kent St, Bentley WA 6102
Phone: +6145 1929556
Email: vitorbarrote@hotmail.com

28.01.2020

Dear Editor,

I am pleased to re-submit the manuscript “The magmatic 4D evolution of the Teutonic Bore Camp VHMS deposits, Yilgarn Craton, Western Australia”, on behalf of myself, Vitor Barrote and my co-authors.

We have greatly appreciated the helpful and constructive revisions to this important work and continue to appreciate your consideration. We have addressed the concerns raised by the reviewers and editors and believe that the manuscript should be now suitable for publication.

We attach a rebuttal letter that indicates how we have addressed the comments as well as a version of the manuscript with tracked changes.

Sincerely,

Vitor Barrote

Authors' response to reviewers' comments

Manuscript title: ¬The 4D evolution of the Teutonic Bore Camp VHMS deposits, Yilgarn Craton, Western Australia

Authors: Vitor Barrote, Neal McNaughton, Svetlana Tessalina, Noreen Evans, Cristina Talavera, Jian-Wei Zi, Bradley McDonald

Manuscript number: ORGEO_2019_778

Date: 28th January 2020

Dear editor,

The authors would like to thank you for your positive reviews, advice, and critiques in how to further correct and improve this manuscript. We have addressed comments below; editor and reviewer's comments are indicated in red font, whereas our response is indicated in black font, for easy reading. In addition to the main comments presented below we have also accepted and appropriately modified the manuscript based on all the comments made by reviewer 1 in the tracked version of the revised manuscript. Our response to these comments can be seen in the tracked version that we have re-submitted.

Comments from the editors and reviewers:

-Editor

In addition to the reviewers comment, I think that you should try to frame your study within a broader context. As it stands your paper is very much a local study which should be better integrated within the broader context of VHMS in Precambrian time. Also you should limit the use of acronyms to the minimum.

We have attempted to better clarify the broader impact of our observations to VHMS systems in the Precambrian, as suggested. We have re-phrased the last paragraph of the introduction to present to the reader our intention to reflect upon this broader subject aided by the upcoming study presented. We have also re-shaped our final paragraph of section 5.5 where we expose how the observations presented in this study could potentially impact the exploration of Precambrian VHMS.

Apart from well established acronyms such as VHMS, HFSE and MSWD we have altered the text and limited our use of acronyms (e.g. Teutonic Bore and Eastern Goldfields Superterrane).

-Reviewer 1

This work reports original geochronological data on the volcanic stratigraphy of the Teutonic Bore Camp, it adds important constraints on the evolution of the associated VHMS deposits, and is therefore worthy of publication on Ore Geology Review.

I have attached a track change version of the manuscript with some recommendations, but, in particular, I'd like to emphasise some aspects that should be considered by the authors with care.

1- The first section of the geological background (paragraph 1.1) needs to be revised to improve its clarity. This is a pivotal part of the manuscript that should be crystal clear to the readers, otherwise the following parts will miss of a solid base of understanding.

We have addressed the Geological Background section and based on the additional comments from this reviewer we have modified it to improve its clarity. We believe that this modified version will be much easier for the readers to understand.

2- All the tables, apart from table 3, should be moved to the ESMs in a spreadsheet form, in order to be more accessible and to avoid large text gaps within the final manuscript.

We intend to do this, if agreed upon by the Editors and we submit the revised version of the manuscript with tables 1, 2, 4 and 5 as supplementary material. Also as suggested by the reviewer within the text we have re-shaped the Methods section and added much of the information to the ESM.

3- There is bold claim in the discussion that needs to be further discussed or modified. I am referring to the end of paragraph 4.4 where it is suggested that "the Penzance granite is a strong candidate to have acted as the probable magmatic source of sulphur to the mineralisation, and consequently, metals." Whereas the suggestion that the Penzance granite could have acted as a sulfur source is coherent with the isotopic data discussed in Chen et al. (2015), the assumption that metals were sourced from the granite magma is unsupported.

We have modified this part of the text as not to extrapolate on the proposed discussions and present to the reader unsupported arguments. We have limited ourselves to affirm that Chen et al. (2015) presents evidence for sulphur supply from magmatic sources only. The supply of metals remains a possibility, although there is no evidence at this point that this is the case.

-Reviewer 2

The manuscript provides geochronological constraints on the granite and host sequences for the Teutonic Bore (TB) camp. The authors suggest the involvement of granite in the VHMS mineralization. The topic of the study is suitable for Ore Geology Reviews. However, two important points require attention in preparing your revision so that the resulting manuscript can be evaluated for publication.

1. I am confused with the term “magmatic 4D evolution”. I read the manuscript several times and haven’t found it out. In my view, magmatic evolution should involve the geochemical evolution and dynamical processes, rather than solely providing age data. I think the authors should clarify what the 4D evolution really means.

We have refrained from using the term “magmatic 4D evolution” and instead consistently use “4D evolution”, including modification of the title. The concept of 4D evolution or 4D evolutionary model in this article refers to the addition of time constrains to previously known processes involving magmatism and volcanism, which include geochemical evolution, development of the stratigraphical sequence and development of mineralisation as a consequence of these processes. We have added our definition of the concept to the introduction in order to clarify to the reader the meaning of 4D evolutionary model in this context.

2. The authors also declare that they constructed a 4D evolutionary model for the ore system (lines 24-26 and section 5.4). I definitely do not see this point in the text. Actually, in this manuscript, the authors just conduct geochronological study on the host rock and a granite in the deposits. They even do not obtain the direct ages for mineralization. How do this reveal the 4D evolution of ore systems?

As addressed in the first comment, the 4D evolutionary model refers to the constrain of processes in time, which was achieved by combining extensive new original geochronological observations with previous studies that focused on geochemistry, stratigraphy and other techniques. We have added our definition of the concept to the introduction in order to clarify to the reader the meaning of 4D evolutionary model in this context. We have also added an explanation of the concept in section 5.4 in order not to confuse the reader and to clarify the outcome of the study.

Additionally, do not overstate the temporal association between granite intrusion and mineralization.

We understand the reviewers concern and share his view. We have replaced likely coeval to possibly coeval. We have evidence that the mineralisation is younger than the host rocks that are dated in this study based on stratigraphic observation presented in Belford et al. (2015). However the lack of a reliable age for the Teutonic Bore mineralisation prevents us from demonstrating the association between granite and ore formation.

Some minor comments are:

Q1 Lines 483-484: Why do similar Th/U ratios of zircon suggest a magma consanguinity? Any reference?

According to Kirkland et al. (2015), parental magma composition is one of four factors that may contribute to variations in the Th/U of a zircon crystal.

We have added that information to the main text and included the reference in our Bibliography.

Q2 Lines 499-506: The authors argue the possible involvement of granite in VHMS mineralization. What do you mean for "interaction" (line 499)? I do not see the speciality of granitoid veins within the volcanics as well as volcanic xenoliths within the granite. In my view, it just indicates that granite postdate the volcanics.

We have re-phrased this passage to clarify the ideas presented. The argument presented here absolutely indicates only that the granite postdates the volcanics. The reason why we demonstrate that these rocks interact is to refute the idea that granite and volcanics are part of separate systems that were tectonically placed in contact.

Q3 Conclusion section: "The age of the TB camp mineralisation is likely coeval to the intrusion of the Penzance granite at ca. 2682 Ma." How do you draw the synchronicity for the mineralization and granite intrusion? Do not overstate their association before you can offer a reliable age for the TB mineralization.

We understand the reviewers concern and share his view. We have replaced likely coeval to possibly coeval. We have evidence that the mineralisation is younger than the host rocks that are dated in this study based on stratigraphic observation presented in Belford et al. (2015). However the lack of a reliable age for the Teutonic Bore mineralisation prevents us from demonstrating the association between granite and ore formation.

The ~~magmatic~~ 4D evolution of the Teutonic Bore Camp VHMS deposits, Yilgarn Craton, Western Australia

Vitor R. Barrote[1,2,3], Neal J. McNaughton[1], Svetlana G. Tessalina[1], Noreen J. Evans[1,2], Cristina Talavera[1,4,3], Jian-Wei Zi[1,5,4], Bradley J. McDonald[1,2]

1- John de Laeter Centre and The Institute for Geoscience Research (TIGeR), Curtin University, Kent St, Bentley, WA 6102, Australia

2- School of Earth and Planetary Sciences, Curtin University, Kent St, Bentley, WA 6102, Australia

~~2-~~3- School of Earth, Atmosphere and Environment, Monash University, Clayton, Victoria 3800, Australia

~~3-~~4- School of Geosciences, University of Edinburgh, The King's Building, James Hutton Road, EH9 3FE, Edinburgh, UK

~~4-~~5- State Key Lab of Geological Processes and Mineral Resources, China University of Geosciences

Declarations of interest: none

ABSTRACT

The Teutonic Bore ~~(TB)~~ ~~e~~Camp, comprised of the Teutonic Bore, Jaguar and Bentley deposits, is one of the most significant volcanic-hosted massive sulphide (VHMS) camps in Western Australia. Despite being extensively studied ~~in the past~~, only recently there have been advances in the understanding of the mechanism that drove the formation of mineralisation. It has been recognized by recent studies that the volcanic-hosted deposits from the ~~TB~~Teutonic Bore Camp represent replacement-type VHMS systems, with significant input of fluids and metals from a magmatic source. This paper tests the existing hypothesis that the nearby

Commented [1]: Be consistent with the capital letter. Personally I do not have any preference, but keep it uniform throughout the text.

Commented [2R2]: We made sure to keep it consistently capital throughout the text.

Penzance granite acted as the metals source and/or thermal engine driving the development of these ore deposits.

New age constraints on the formation of the host volcanic sequence at the Bentley deposit and the crystallization of the Penzance granite allows for the construction of a 4D evolutionary model for the ore system. A new U-Pb SHRIMP monazite age of 2681.9 ± 4.5 Ma indicates that the Penzance granite post-dates the host stratigraphy at Bentley (ca. 2693 Ma) and is probably coeval with mineralisation. All zircons (Penzance, Bentley units I and III) have very similar $\varepsilon Hf_{(i)}$, with most values between -1 and +6, slightly higher than the $\varepsilon Hf_{(i)}$ of zircons from other granites and volcanics within the Kurnalpi Terrain, and indicative of juvenile sources. The mean Th/U ratios are ~0.7 and ~0.6 for the Penzance and Bentley zircons, respectively. All zircons have similar $Ce/Nd_{(CN)}$ ratios. The chemical similarities between the zircons from the granite and the volcanic rocks at Bentley support a shared magmatic source between the Penzance and the ~~TB~~Teutonic Bore Camp sequence. The Penzance granite is the likely source of heat, and potentially metals, which drove the VHMS mineralisation at the ~~TB~~Teutonic Bore Camp.

Keywords: Penzance; Teutonic Bore; Volcanic-hosted massive sulphide; Archean; Geochronology; 4D modelling

1 INTRODUCTION

Using an extensive database of compiled whole-rock geochemistry and U-Pb geochronology, Hollis et al (2015) proposed a link between VHMS mineralisation and the emplacement of HFSE-enriched syn-volcanic intrusions, throughout the Archean Yilgarn Craton, including the Eastern Goldfield Superterrane ~~(EGS)~~. Despite the apparent geographical and broadly coeval association between VHMS ores and HFSE-enriched intrusions, the identification of a genetic link ~~link requires~~would benefit from further geochronological and isotopic evidence~~demonstration by detailed geochronology and isotopic geochemistry~~.

The number of significant VHMS occurrences in the Yilgarn Craton is small compared to other Archean terrains with similar characteristics such as the Superior Province of Canada (Hollis et al., 2015). Previous studies suggested that this ~~is~~ could be due to under-exploration and the use of techniques inappropriate for mineral prospecting in the Yilgarn Craton (Butt et al., 2017; Ellis, 2004; Hollis et al., 2017, 2015; McConachy et al., 2004). Unlike classic VHMS systems, replacement-type VHMS systems, such as those in the ~~EGS~~Eastern Goldfield Superterrane, do not precipitate onto the seafloor and ~~, but rather replace slightly older host stratigraphy. As a consequence,~~ although some stratigraphic control can be observed within replacement-type mineralisation, it is not an inevitable feature (Doyle and Allen, 2003).

Historically, ~~the search~~exploration for VHMS occurrences within the Teutonic Bore ~~(TB)~~ area was focused on key stratigraphic horizons. However, the known deposits formed at different stratigraphic positions and show significant differences in the geometry of mineralisation, compared to ~~TB~~Teutonic Bore (Chen et al., 2015; Parker et al., 2017). This led to a significant time gap between the discoveries of the ~~TB~~Teutonic Bore deposit in 1976, and the Jaguar and Bentley deposits ~~(~~in 2004 and 2008, respectively~~)~~ (Ellis, 2004; ~~Independence Group NL (IGO), 2015~~ ~~;~~ Parker et al., 2017).

To better understand thise ~~inconsistent~~ lack of stratigraphic control on the position of orebodies ~~within the stratigraphy~~ at the ~~TB~~Teutonic Bore ~~e~~Camp, and a possible link between high-field-strength-elements (HFSE)-enriched granite emplacement and ore precipitation, this work re-examines and expands the database of geochronology and isotopic/geochemical fingerprints for the igneous rock units. This includes re-assessment of the geochronological data from the nearby HFSE-enriched granite, the Penzance granite (Champion and Cassidy, 2002; Geoscience Australia ~~(GA),~~ 2019), and the volcanic sequence from the ~~TB~~Teutonic Bore ~~e~~Camp (Nelson, 1995), with additional U-Pb Sensitive High-Resolution Ion Microprobe (SHRIMP) dating of zircon and monazite~~s~~.

Commented [3]: Such as… please mention an example.

Commented [4R4]: We have provided an example.

Commented [5]: I recommend to rephrase this sentence. The main clause depends on the subordinate, it should be the opposite. It might be difficult to understand to those readers which are not familiar with the topic.

Commented [6R6]: We have merged the information from the subordinate to the main clause.

Commented [7]: Brackets are not necessary

Commented [8R8]: Change accepted

Commented [9]: I recommend to minimise the use of unpublished references when it is not indispensable, as they are a not transparent means by nature.

Commented [10R10]: Reference removed

Commented [11]: I recommend to clarify to the reader the nature of the inconsistency. It is mentioned above that the VHMS being of a replacive nature are expected to form in the same stratigrafic position, but it is not clear enough, I believe this is an important point that should be emphasised more.

Commented [12R12]: We have modified the sentence to clarify the inconsistency (i.e. lack of stratigraphic control).

Commented [13]: This acronym is never utilised I the text, so it can be deleted.

Commented [14R14]: Ok

Commented [15]: The acronym needs to be resolved once at the beginning, but being a known technique it can be omitted in the abstract.

Commented [16R16]: Ok

Commented [17]: Mineral names are uncountable.

Commented [18R18]: We have modified the text to adhere to this rule.

These geochronological studies are complemented by zircon Hf-isotop~~iee~~ and trace element analys~~e~~is ~~on zircons~~ ~~o~~from the Bentley volcanic sequence and Penzance granite, and compilation of detailed stratigraphy, whole-rock geochemistry and sulphur isotope data from previous studies (Belford et al., 2015; Chen et al., 2015; Das, 2018; Isaac, 2015; Sedgmen et al., 2007). The present work combines the improved geochronological constrains presented here to the current 3D understanding of the geological processes at place, to develop a 4D evolutionary model of the deposits at the Teutonic Bore Camp.

Reliable and precise ages for magmatism and ore-hosting volcanism, combined with traditional and isotopic geochemistry, allows testing of the hypothesis of a genetic relationship between the HFSE-rich Penzance granite and the ~~TB~~Teutonic Bore Camp deposits. The results could have implications for future exploration for Precambrian VHMS deposits, not only in the well-established ~~TB~~Teutonic Bore ~~e~~Camp, but also in *greenfields* throughout the ~~EGS~~Eastern Goldfield Superterrane and, potentially, ~~other terranes~~elsewhere in the Yilgarn Craton.

~~1~~2 GEOLOGICAL BACKGROUND

~~1.1~~2.1 Geology of the Teutonic Bore Camp

The Teutonic Bore, Jaguar and Bentley VHMS deposits, along with several other smaller occurrences, form the ~~TB~~Teutonic Bore Camp (Independence Group NL (~~x~~IGO), 2015). The ~~TB~~Teutonic Bore Camp is located near the town of Leonora, within the Kurnalpi Terrane of the ~~EGS~~Eastern Goldfield Superterrane, Yilgarn Craton (Figure 1). The deposits ~~from~~in the ~~TB~~Teutonic Bore ~~e~~Camp are hosted by the ~~TB~~Teutonic Bore volcanic complex, which comprises pillow basalt, overlain and interlayered with volcanoclastic units, coherent rhyolite, andesite and thin sedimentary units (Belford et al., 2015; Parker et al., 2017 and references therein). The prefix "meta" is assumed but omitted when addressing the Archean

Commented [19]: Elsewhere in the Yilgarn or specifically in certain terrenes? Please specify.

Commented [20R20]: The other Terranes within the Yilgarn are understudied, so studies similar to this if conducted in such regions could impact the understanding and consequently exploration strategies for these locations. Due to the unavailability of such constrains we refrain from specifying which Terranes.

"More data is required in the South West, Burtville and Yamarna terranes, and a number of greenstone belts of the Youanmi Terrane (e.g. Twin Peaks, Tallering) in order to clearly delineate regions of prospectivity and establish temporal, geochemical and stratigraphic associations to mineralization. Localized studies are required in order to establish volcanological settings for a number of deposits and their controlling factors."Hollis et al 2015

Commented [21]: If you want to provide a geographical reference, the location of town of Leonara should be included in the geological map.

Commented [22R22]: We have included the town of Leonora in the geological map and have described the symbology in the caption.

stratigraphic sequence of the Yilgarn Craton, because all rocks are metamorphosed to some extent (Czarnota et al., 2010).

The volcanic stratigraphy and the distribution of the three deposits, as well as other known uneconomic ore bodies, have a NW-SE trend (Figure 1). Tthis trend coincides with the general alignment of regional structures, such as the fault that bounds the ~~TB~~Teutonic Bore volcanic complex to the west (Hallberg and Thompson, 1985; Parker et al., 2017). ~~The TB volcanic sequence is bounded by a syenogranite to the east. Although the nature of the contact with the volcanics is unclear, its attitude follows the general trend of stratigraphy and orebody distribution. Additionally, this trend coincides with the general alignment of regional structures, such as the fault that bounds the TB volcanic complex to the west (Hallberg and Thompson, 1985; Parker et al., 2017).~~

The stratigraphy at the ~~TB~~Teutonic Bore ~~c~~Camp comprises a predominantly laterally continuous lithofacies association between the three deposits (Figure 2A). ~~Disruption of the stratigraphic sequence by later dolerite intrusions causes inconsistencies in the stratigraphic continuity between deposits (Belford et al., 2015; Das, 2018). although individual deposits can occur in locally restricted facies (Das, 2018). The prefix "meta" is assumed but omitted when addressing the Archean stratigraphic sequence of the Yilgarn Craton, because all rocks are metamorphosed to some extent (Czarnota et al., 2010).~~

~~Disruption of the stratigraphic sequence by later dolerite intrusions causes inconsistencies in the stratigraphic continuity between deposits (Belford et al., 2015; Das, 2018).~~ ~~Nonetheless~~Therefore, the volcanic sequence that hosts the mineralisation can be broadly subdivided in six units as follow from bottom to top (Figure 2B; Belford et al., 2015; Parker et al., 2017)~~, as depicted in Figure 2B, and comprises six units, from bottom to top~~:

I. Footwall Rhyolite: from 200 m to over 1 km thick. Mainly coherent, either massive or flow-banded, with minor breccia (Parker et al., 2017), and with calc-alkaline to

Commented [23]: I recommend to anticipate this at L91 when you first mention the rocks within the TB complex. Here this sentence creates a logic gap between the sentence that precedes and the one that follows.

Commented [24R24]: We repositioned the passage.

Commented [25]: This sentence continues the regional analysis started in L92-93. I recommend to avoid logic gaps and to keep this sentence close and connected with the one in L92-93.

Commented [26R26]: We have re-shaped the paragraph to satisfy that.

Commented [27]: This sentence is unclear. Please rephrase trying to be more specific and avoiding the use of generic terminology such as "the attitude of the contact".

Commented [28R28]: We have erased this sentence and focused on describing the interaction between granite and volcanics further down. It was repetitive as well.

Commented [29]: This sentence continues the regional analysis started in L92-93. I recommend to avoid logic gaps and to keep this sentence close and connected with the one in L92-93.

Commented [30R30]: We have re-shaped the paragraph to satisfy that.

Commented [31]: This sentence is redundant, I recommend to simplify it.

Commented [32R32]: We removed this information from this section, we agree with the reviewer that it was unclear. Furthermore it was not necessary to the understanding of the stratigraphy.

Commented [33]: This part of the sentence is unclear. Please rephrase in a way in which the spatial relationships can be clearer, in particular in respect to the VHMS deposits.

Commented [34R34]: We removed this information from this section, we agree with the reviewer that it was unclear. Furthermore it was not necessary to the understanding of the stratigraphy and relationship between deposits.

Commented [35]: I recommend to anticipate this at L91 when you first mention the rocks within the TB complex. Here this sentence creates a logic gap between the sentence that precedes and the one that follows.

Commented [36R36]: We have moved this part to the first paragraph of this section.

Commented [37]: This sentence is redundant, I recommend to simplify it.

Commented [38R38]: We removed this information from this section, we agree with the reviewer that it was unclear. Furthermore it was not necessary to the understanding of the stratigraphy and relationship between deposits.

Commented [39]: Citation should always be located at the end of the sentence before punctuation.

Commented [40R40]: Ok

Commented [41]: Of the six units listed, for only the first is reported the thickness. I recommend to be consistent

Commented [42R42]: We have added the requested information to the text.

transitional . ~~The~~ magmatic affinity ~~is calc-alkaline to transitional~~ (Belford et al., 2015). This package is footwall to all three deposits.

II. Sedimentary rocks partly derived from the rhyolite, locally coarse but grading to arenite, siltstone and shale. This is the host unit to the Bentley deposit. The thickness range from 0 to 70 m according to Parker et al. (2017)

III. Transitional to tholeiitic basalt/ transitional andesite with thickness between 30 and 170 m, with~~: display~~ massive or pillowed habit, commonly intercalated with shale rich sediments (Parker et al., 2017). This package is host to the ~~TB~~Teutonic Bore deposit and upper lens at Bentley (e.g.: Flying Spur, Brooklands, Comet: Independence Group NL (IGO), 2015) and overlays the lower orebody at the Bentley deposit (Arnage: Independence Group NL (IGO), 2015). Belford et al. (2015) names this unit Footwall Andesite (FA) and Footwall Basalt (FB), relative to their position to the mineralised zone at Jaguar.

IV. Upper sedimentary horizon (mineralised package from Belford et al., 2015)~~.~~ consist~~ings~~ of a ~~C~~complex assemblage of intercalated dacite (called MPD by Belford et al., 2015), conglomerate, pumice-rich breccia, laminated sediment, laminated chert and massive sulphide (Belford et al., 2015). Unit IV marks a geochemical break in magmatic affinity, from tholeiitic/transitional of the underlying basalts/andesites to calc-alkaline in the overlying lavas. The thickness is typically within 20 to 40 m (Parker et al., 2017).

V. Upper basalt and andesite of calc-alkaline affinity~~:~~ consist~~ings~~ of massive and pillowed basalt and andesite lavas with minor volcanic breccias, and~~.~~ ~~I~~intercalated with mostly carbonaceous shales (Belford et al., 2015). The total thickness of this unit ranges between about 200 to 700 m (Parker et al., 2017).

VI. Hangingwall rhyolite: uppermost stratigraphic unit, described by Belford et al. (2015) from a single drillhole. The thickness of this unit is estimated to be between 100 to 500m according to Parker et al. (2017).

~~VI.~~

The Teutonic Bore volcanic sequence is bounded to the east ~~The area east of TB is occupied~~ by a large composite batholith (Figure 1) named the Kent Complex by Champion and Cassidy (2002) and part of the Penzance Supersuite (Hollis et al., 2015). The Penzance Supersuite consists of HFSE-enriched granites with biotite and/or amphibole in quartz and feldspar rich rocks. These granites are characterised by variably elevated total Fe, MgO, Y, LREE, Zr, coupled with low to moderate Al_2O_3, K_2O, Rb, Sr and moderate Na_2O (Champion and Cassidy, 2002).

The relationship between the Penzance granite and the volcanic sequence in the ~~TB~~Teutonic Bore Camp area remains unclear. Earlier studies (e.g.: Hallberg and Thompson, 1985) suggest an irregular contact between the granite and the volcanic rocks, with anastomosing veins of granitoid extending into adjacent extrusive rocks and a number of xenoliths of volcanic rocks within the intrusive granite. The Penzance granite is one of several HFSE-enriched intrusions in the Yilgarn Craton that occurs in close proximity to VHMS deposits or occurrences hosted by equally HFSE-enriched volcanics (Hollis et al., 2015).

The Jaguar deposit was classified as a replacement-type VHMS deposit by Belford (2010). This classification relied on evidence including replacement front texture, absence of chimney structures, and rapid emplacement of the host volcanic sequence, according to the criteria proposed by Doyle and Allen (2003). Later studies (Chen et al., 2015; Das, 2018; Parker et al., 2017) have identified similar textures in Bentley and other smaller occurrences and, consequently, the replacement-type VHMS model is accepted within the ~~TB~~Teutonic Bore Camp.

Despite the predominance of sub-seafloor replacement processes, Belford (2010) observed features that indicate possible above seafloor activity. The development of thin beds of translucent chert with colloform intergrowths of chert and sulphide is interpreted as products of a waning hydrothermal system that had vented fluid to the sediment–water interface and deposited precipitates onto the seafloor (Belford et al., 2015). Massive sulphides conformably overlain by, and gradational upwards into, ~~these~~ narrow beds of laminated chert intercalated with finely-bedded sulphide-rich mudstone, support the idea of a progressive disruption of the mineral activity and indicate that some sulphide precipitation might have taken place very near or at seafloor (Belford et al., 2015).

The occurrence of massive sulphide clasts in the surrounding breccias and conglomerates, which were the result of rapid erosion and mass flow, indicates that the sulphide body was formed contemporaneously with the deposition of the upper sedimentary horizon (IV) (Belford et al., 2015). Similar features have not been observed in either the Bentley or the ~~TB~~Teutonic Bore deposits.

~~1.~~2.2 Geochronology of the ~~TB~~Teutonic Bore sequence and the Penzance granite

The SHRIMP zircon age of 2692 ± 4 Ma (Nelson, 1995) is the only published age for the volcanic sequence at the ~~TB~~Teutonic Bore ~~e~~Camp and comes from a porphyric dacite with unclear stratigraphic position (Belford et al., 2015). ~~Detailed geochronology was attempted by~~Additionally, Das (2018)~~,~~ reported an ID-TIMS U-Pb age of 2692 ± 1.5 Ma for a sample of coherent Footwall Rhyolite (unit IV) from Jaguar. These analysis remain unpublished and no data table or sample characterization is provided by Das (2018) ~~in felsic rocks well constrained within the stratigraphic sequence, however only one ID-TIMS U-Pb zircon age was reported. The age of 2692 ± 1.5 Ma for a sample of coherent Footwall Rhyolite (unit IV) from Jaguar remains unpublished.~~

Commented [43]: Here you are referring to the content of a Master's thesis not accessible to the readers. Please provide more details as its content is very relevant to this study. Also, I recommend to reword the sentences as it appears that Das has "attempted" (try??) to acquire detailed geochronology, but has managed to obtain a single analysis. Is this true? How is such information relevant to this study?

Commented [44R44]: We have reworded the sentence as suggested.

I wish I could provide more details. The only reference in the thesis to this data is "The rarity of dateable minerals in the mafic succession is a major difficulty in the process of lithostratigraphic correlation. Therefore, the best way to obtain the age of a mafic succession is by dating the crosscutting felsic rocks that have dateable minerals in abundance. Until now, the age of the Teutonic Bore Volcanic Complex was constrained from
a porphyritic dacite from north of Teutonic Bore deposit at SHRIMP zircon age of 2962±4 Ma (Nelson, 1995). The footwall rhyolite samples for dating were selected from the drill core at Teutonic Bore, Jaguar and Bentley after removing the weathered surface and inclusions.
A sample of the coherent footwall rhyolite from Jaguar (Sample # 13JUDD002) was dated using the ID-TIMS U-Pb analysis of Zircon and gave the age of 2692.6±1.5 Ma."

The reported ages for the Penzance granite are 2679 ± 8Ma (Champion and Cassidy, 2002) and 2686 ± 9 Ma (Geoscience Australia ~~(GA),~~ 2019, sample ID 96969076). The two ages are derived from the same analyses and ~~,~~calculated from ~~the same~~ a single dataset ~~from~~ for sample ID 96969076. No explanation is provided by either references as to the reason behind the difference in age calculation from a single set of analysis.

~~2~~3 SAMPLES AND METHODS

~~2.1~~3.1 Penzance samples

Samples from the Penzance granite were collected from three different positions within the same quarry (Lat. -28.264050, Long. 121.077888, Penzance Quarry in Figure 1). They were collected from the same quarry as sample ID 96969076 from the Geochron Delivery database of Geoscience Australia (2019)~~, according to those records~~. Each one of the three samples was processed separately and treated as different samples, the analysi~~c~~s were combined only in the data processing phase of each technique.

~~2.2~~3.2 Bentley samples

Two samples were collected from different positions within the footwall rhyolite (unit I) in the Bentley deposit. Sample 15BUDD78 – 111.60 m was collected from drillhole 15BUDD78 at 111.60 meters depth, from a distal position to the ore. Sample 15BUDD137 – 398.60 m was collected from a ~~younger~~higher stratigraphic position within the sequence, a stringer zone to the lower massive sulphide lens ~~(Arnage)~~, from a different drillhole (15BUDD137).

Two samples (15BUDD120 - 228.42 and 15BUDD120 - 226.04) of the transitional andesite (unit III), were collected from a single drillhole (15BUDD120), within two meters of each other. The transitional andesite at the sampled point is hangingwall to the lower lens (Arnage), but it is in the stringer zone for the upper lens, marked by the occurrence of disseminated sulphides.

Commented [45]: It is unclear whether these two ages are derived from the same analyses, or from distinct analyses from zircon extracted from the same sample. Please explain better. Also, include the sample ID in the citation as it as not been contextualised in the text.

Commented [46R46]: We have modified the text to clarify that the two ages were calculated from the same single dataset. How these two authors have obtained different ages is not clear and there is no detailed information available. That is one of the reasons why we have decided to attempt dating this rock from newly collected samples from the same location. We accepted the insertion of the sample number to the citation.

Commented [47]: Information regarding the sample is redundant as drillcore names and depths are repeated. The coordinate of the samples is available only for sample 96969076. I recommend to simplify this part by summarising the sample info in a table, it would be clearer and shorter.

Commented [48R48]: The description of the sampling procedure for the Penzance is necessary to understanding the significance of the new age determination and how it compared to the previous data available. We have moved the rest of the methods to the ESM

Commented [49]: The methods can be summarised within the manuscript and the full version moved into the ESM.

Commented [50R50]: We moved the methods to the ESM

Commented [51]: This is implied in the citation, it is not necessary to restate it.

Commented [52R52]: Ok

Commented [53]: It is not clear what this is about. If it is the specific name of the lens provide the reader with a scheme that represents the locations of the different lenses. As it is, this name does not provide the reader with any useful information. Please contextualise

Commented [54R54]: We have removed that reference as it is not fundamental to the understanding of the ideas.

3.3 Analytical techniques

Zircon and Monazites were analysed on the SHRIMP II at the John de Laeter Centre, Curtin University (JdLC). Additionally, Zircon Lu–Hf isotopes and rare earth element (REE) abundances were measured over two analytical sessions using laser ablation split stream inductively coupled plasma mass spectrometry (LA-SS-ICPMS). The analyses were conducted in zircons from the same samples that were analysed by SHRIMP, but not necessarily on the same grain or over the same spot as the SHRIMP analysis. Detailed description of the conditions and procedures are provided in Supplementary Material 1.

~~**2.3 SHRIMP U-Pb dating of Zircon and Monazites**~~

~~*2.3.1 Mount preparation*~~

~~Zircon and monazite grains were separated from crushed rock samples using a Frantz magnetic separator and heavy liquids (methylene iodide). Grains were handpicked, mounted in epoxy resin discs and polished to expose their interiors. The zircon crystals were characterized by cathodoluminescence (CL) imaging, and monazite crystals by back-scattered electron (BSE) microscopy using the Mira3, at the Microscopy and Microanalysis Facility, John de Laeter Centre, Curtin University. The epoxy mounts were carbon coated for SEM imaging and Au-coated before each SHRIMP analytical session.~~

~~Polished thin sections prepared from samples of transitional andesite (unit III) were examined to identify suitable zircon grains for SHRIMP geochronology using the Tescan Integrated Mineral Analyzer (TIMA GM) and back-scattered electron (BSE) microscopy using the Mira3, at the Microscopy and Microanalysis Facility, John de Laeter Centre, Curtin University. Portions of the thin sections containing grains large enough (>15 μm) for ion microprobe analysis were drilled out, in ~3 mm plugs, and cast in 25 mm epoxy mounts. The reference materials were in a separate mount that was cleaned and Au-coated with the sample mounts before each SHRIMP analytical session.~~

2.3.2 Zircon

Selected areas of the imaged zircon were analysed on the SHRIMP II at the John de Laeter Centre, Curtin University (JdLC). The analytical procedures for the Curtin consortium SHRIMP II have been described by de Laeter and Kennedy (1998) and Kennedy and de Laeter (1994) and are similar to those described by Compston et al. (1984) and Williams (1998). For the larger zircons in grain mounts, a 20-25 µm elliptical spot was used, with a mass-filtered O_2^--primary beam of ~2.8-3.0 nA, whereas a 10-12 µm spot of ~0.5 nA was used on the smaller zircons in polished thin sections. Data for each spot was collected in sets of six scans on the zircons through the mass range of $^{196}Zr2O^+$, $^{204}Pb^+$, Background, $^{206}Pb^+$, $^{207}Pb^+$, $^{208}Pb^+$, $^{238}U^+$, $^{248}ThO^+$ and $^{254}UO^+$. The $^{206}Pb/^{238}U$ age standard and U-content standard used was M257 (561.3 Ma and 840 ppm U; Nasdala et al., 2008) while OGC zircon was utilized as the $^{207}Pb/^{206}Pb$ standard, to monitor instrument induced mass fractionation (3465.4 ± 0.6 Ma; Stern et al., 2009). The $^{207}Pb/^{206}Pb$ dates obtained on OGC zircons during the SHRIMP sessions matched the $^{207}Pb/^{206}Pb$ standard age within uncertainty and no fractionation correction was warranted. The common Pb correction was based on the measured ^{204}Pb-content (Compston et al., 1984). The correction formula for Pb/U fractionation is $^{206}Pb^+/^{238}U^+ = a\,(^{254}UO^+/^{238}U^+)^b$ (Claoué-Long et al., 1995) using the parameter values of Black et al. (2003). The constant "a" is determined empirically from analyses of the standard during each analytical session. The programs SQUID II and Isoplot (Ludwig, 2011, 2009) were used for data processing.

2.3.3 Monazite

The U–Th–Pb analyses were performed using the high spatial-resolution capability of the SHRIMP II at the JdLC. Monazite was analysed in two analytical sessions. Grains were analysed using a 30 µm Köhler aperture, ~0.3 nA primary ion beam (O_2^-) and a ~10 µm analysis spot. Energy filtering was not applied, and the post-collector retardation lens was activated to reduce stray ion arrivals. The mass resolution (M/ΔM at 1% peak height) was

>5000. French ($^{206}Pb/^{238}U$ age 514 Ma) was used as the primary Pb/U reference material, and Z2908 and Z2234 were the secondary reference materials used to monitor matrix effects (Fletcher et al., 2010). Z2908 ($^{207}Pb/^{206}Pb$ age 1796 Ma) was also analysed to monitor and correct for instrumental mass fractionation of ^{207}Pb from ^{206}Pb. SQUID II software (Ludwig, 2009) was used for initial data reduction including ^{204}Pb correction. Matrix effects in $^{206}Pb/^{238}U$ were corrected following established protocols detailed by Fletcher et al. (2010). 9 analyses of Z2908 yielded a mean $^{207}Pb/^{206}Pb$ age of 1796.7 ± 5.4 Ma (MSWD = 1.7). An insignificant fractionation correction (0.02%) was applied to sample data, with no augmentation of sample precision required based on the reproducibility of $^{207}Pb/^{206}Pb$ in the reference materials. $^{207}Pb/^{206}Pb$ dates from individual analyses are presented with 1σ internal precision, whereas weighted mean $^{207}Pb/^{206}Pb$ dates are reported at 95% confidence limits.

2.4 LA-SS-ICPMS of Zircon – Trace elements and Hf isotopes

Zircon Lu–Hf isotopes and rare earth element (REE) abundances were measured over two analytical sessions using laser ablation split stream inductively coupled plasma mass spectrometry (LA-SS-ICPMS). The analyses were conducted in zircons from the same samples that were analysed by SHRIMP, but not necessarily on the same grain or over the same spot as the SHRIMP analysis. Isotopic and elemental data were collected simultaneously using a Resonetics S-155-LR 193 nm excimer laser coupled to a Nu Plasma II multicollector and Agilent 7700s quadrupole mass spectrometer in the GeoHistory Facility, JdLC at Curtin University.

Samples 15BUDD120 – 228.42 and 15BUDD120 – 226.04 m, from the Transitional andesite (unit III) were analysed with a laser spot diameter of 24 µm, with 2.7 J/cm^2 on-sample laser energy, repetition rate of 10 Hz, ablation time of 25 seconds and ~30 seconds of background capture before and after each analysis. Two cleaning pulse preceded analysis. The spot size and ablation time in this case were limited by the smaller size of the zircons.

Commented [55]: This acronym should be open up once the first time it is mentioned.

Commented [56R56]: Ok

The remaining samples were analysed with a laser spot diameter of 50 µm, with 2.7 J/cm^2 on-sample laser energy, repetition rate of 10 Hz, ablation time of 40 seconds and ~45 seconds of total baseline acquisition.

Zircon standard P1 (Li et al., 2010; chips of Penglai zircon characterised in-house for trace element composition) was used as the primary standard to calculate element concentrations using ^{91}Zr as the internal reference isotope and assuming 43.14% Zr in zircon, and to correct for instrument drift.

Lu–Hf isotopic data were measured simultaneously for ^{172}Yb, ^{173}Yb, ^{175}Lu, ^{176}Hf+Yb+Lu, ^{177}Hf, ^{178}Hf, ^{179}Hf and ^{180}Hf on the Faraday array. Time resolved data was baseline subtracted and reduced using Iolite3.5 (DRS after Woodhead et al., 2004), where ^{176}Yb and ^{176}Lu were removed from the 176 mass signal using ^{176}Yb/^{173}Yb = 0.7962 (Chu et al., 2002) and ^{176}Lu/^{175}Lu = 0.02655 (Chu et al., 2002) with an exponential law mass bias correction assuming ^{172}Yb/^{173}Yb = 1.35274 (Chu et al., 2002). The interference corrected ^{176}Hf/^{177}Hf was normalized to ^{179}Hf/^{177}Hf = 0.7325 (Patchett and Tatsumoto, 1980) for mass bias correction. Zircons from the Mud Tank carbonatite locality were analysed together with the samples in each session to determine corrected, standard referenced ^{176}Hf/^{177}Hf (Table 1). Zircon standards with a range of REE contents (FC1 91500, Plešovice and GJ-1; references and data in Table 1) were run to verify the method. All analysed standards fell within 2σ error of reported ^{176}Hf/^{177}Hf values, although uncertainties on the 24 micron beam run were, understandably, significantly higher. In addition, the corrected ^{178}Hf/^{177}Hf and ^{180}Hf/^{177}Hf ratios (for the 50 micron beam run) were calculated to monitor the accuracy of the mass bias correction and yielded an average value of 1.467193 ± 12 and 1.886808 ± 11 (n=184), which is within the range of values reported by Thirlwall and Anczkiewicz (2004). Calculation of εHf values employed the decay constant of Scherer et al. (2001) and the Chondritic Uniform Reservoir (CHUR) values of Blichert-Toft and Albarède (1997).

Table 1: Summary of the Hf isotope measurements of standard materials used interspersed with analyses of unknown zircons. Mean values were calculated using the built-in statistics from the Iolite software (Paton et al., 2011)

Standard Material	50 µm	24 µm	Reference Value
	Corrected $^{176}Hf/^{177}Hf$	Corrected $^{176}Hf/^{177}Hf$	
Mud Tank	0.282505 ± 14 (MSWD = 0.70, n = 14)	0.282507 ± 64 (MSWD = 2.9, n = 6)	0.282505 ± 44 (Woodhead and Hergt, 2005)
FC1	0.282182 ± 9 (MSWD = 0.31, n = 9)	0.282229 ± 150 (MSWD = 3.9, n = 6)	0.282172 ± 42 (Woodhead and Hergt, 2005)
91500	0.282306 ± 11 (MSWD = 0.71, n = 14)	0.282235 ± 130 (MSWD = 2.4, n = 6)	0.282306 ± 40 (Woodhead et al., 2004)
Plešovice	0.282477 ± 8 (MSWD = 0.3, n = 10)	0.282470 ± 51 (MSWD = 0.49, n = 6)	0.282482 ± 13 (Sláma et al., 2008)
GJ-1	0.282016 ± 12 (MSWD = 0.69, n = 14)	0.281201 ± 110 (MSWD = 1.1, n = 6)	0.282000 ± 5 (Morel et al., 2008)

34 RESULTS

3.14.1 U-Pb SHRIMP Zircon dating

3.1.14.1.1 Footwall rhyolite (unit I) – Bentley Footwall

Fourteen analyses on 14 zircons from sample 15BUDD78 – 111.60 m were performed (Table 2Supplementary Material 2). Using only analyses within 3% of concordant yields a mean $^{207}Pb/^{206}Pb$ age of 2696.5 ± 4.2 Ma (95% c.l., n=12; mean square weighted deviation, MSWD=1.04, Figure 3). The average and range of Th/U ratio from the most concordant SHRIMP analyses for this sample are 0.60 and 0.45-0.72, respectively.

A second sample from unit I was dated, t. Twenty-seven analyses from 27 zircons from sample 15BUDD137 – 398.60 m were collected (Table 2Supplementary Material 2). The mean $^{207}Pb/^{206}Pb$ age obtained for analyses within 4% of concordant and with <0.3% common Pb was 2691.7 ± 2.5 Ma (95% c.l.; n=25; MSWD=0.95, Figure 3). The average and range of Th/U ratio from the most concordant SHRIMP analyses are 0.63 and 0.41-0.84, respectively.

The CL images of zircons from the two unit I, footwall rhyolite samples show grains with continuous oscillatory zoning and no discernible core and/or rims, as shown in Figure 4, and havewith sizes that rangeinge from about 50 to 100 µm (Figure 4). Their morphologies, Th/U and ages are indistinguishable, and combining the most concordant data, the resulting age of

Commented [57]: I recommend to move Table 2 into the ESMs in a spreadsheet format, so that the data can be more easily accessible. We should save colleagues from wasting their time doing copy/pasting from tables within pdf.

Commented [58R58]: Ok

Commented [59]: This sentences should be better linked or combined.

Commented [60R60]: Ok

2692.9 ± 2.1 Ma (95% cl; n=37; MSWD=1.05) is our best estimate of the age of the footwall rhyolite at Bentley.

~~3.1.2~~4.1.2 *Transitional andesite (unit III) – Bentley Hangingwall*

The samples from the transitional andesite were treated as two separate samples for the geochronology portion of this study. However, these samples were taken 2 meters apart, from the same drillcore (15BUDD120), and were within the same stratigraphic facies. The CL images show zircons with continuous oscillatory zoning, and ~~are~~ ranging from 15 to 30 µm in diameter (Figure 5).

Sample 15BUDD120 – 226.04 m yielded 24 dates from 20 zircons. Considering only the 13 results with <5% discordance (~~Table 2~~Supplementary Material 2), the MSWD is 2.7 and indicates an age spread not consistent with a single age population. Omitting the three youngest ages as statistical outliers probably influenced by diffusional Pb-loss, ~~yields a mean age for~~ the remaining population yields a mean age of 2693.2 ± 5.8 Ma (95% cl; n= 10; MSWD=0.88, Figure 3). The average and range of Th/U from the SHRIMP analyses of the more concordant zircons from this sample is 0.90 and 0.39-1.55, respectively.

Sample 15BUDD120 – 228.42 has 18 dates from 16 grains. The ages <5% discordant and <0.1% common Pb yield a mean $^{207}Pb/^{206}Pb$ age of 2693.6 ± 6.0 Ma (95% cl, n=9; MSWD=0.24, Figure 3; ~~Table 2~~Supplementary Material 2). The average and range of Th/U of the more concordant zircons is 0.95 and 0.73-1.31, respectively.

The ages obtained for the two adjacent samples from the same stratigraphical facies agree within error. Hence, the data can be combined to obtain a mean $^{207}Pb/^{206}Pb$ age for the Transitional Andesite (unit III) of 2693.4 ± 4.1 Ma (95% c.l., n=19; MSWD=0.55). The average Th/U from the zircons used in this mean age calculation was 0.92.

361

Table 13: SHRIMP isotopic data for monazite from the Penzance granite (mounts N18-06, 16)

Penzance granite (mount N18-06, 16)

Mount grain-spot	ppm U	ppm Th	$^{232}Th/^{238}U$	4f206 (%)	4f208 (%)	$^{207}Pb^*/^{206}Pb^*$	± 1σ err	$^{206}Pb^*/^{238}U$	± 1σ err	$^{207}Pb^*/^{235}U$	± 1σ err	$^{208}Pb^*/^{232}Th$	± 1σ err	$^{207}Pb/^{206}Pb$ Age (Ma)	1σ err	% Disc.
≤5% discordance and <0.5% 4f206																
N18-06B.B-5	207	12986	63.00	-0.02	0.00	0.1865	0.0022	0.5074	0.0114	13.044	0.3320	0.137	0.0026	2711	19	+2
N18-16C.8-3	629	12531	20.00	-0.01	-0.01	0.1863	0.0010	0.5232	0.0101	13.435	0.2720	0.148	0.0032	2709	9	0
N18-16A.1-6	508	15332	30.00	-0.06	-0.02	0.1862	0.0014	0.5092	0.0069	13.075	0.2050	0.142	0.0030	2709	12	+2
N18-06B.G-2	215	14282	66.00	0.02	0.00	0.1855	0.0022	0.5170	0.0097	13.224	0.2950	0.141	0.0026	2703	19	+1
N18-06B.A-6	789	32172	41.00	0.00	0.00	0.1853	0.0015	0.5092	0.0090	13.010	0.2560	0.140	0.0029	2701	13	+2
N18-16A.1-1	448	11587	26.00	0.00	0.00	0.1852	0.0026	0.5288	0.0091	13.499	0.3020	0.152	0.0032	2700	23	-1
N18-06B.B-7	310	11884	38.00	-0.04	-0.01	0.1851	0.0018	0.5140	0.0088	13.119	0.2620	0.138	0.0028	2699	16	+1
N18-06B.G-5	345	16469	48.00	-0.06	-0.01	0.1847	0.0019	0.4933	0.0085	12.563	0.2540	0.136	0.0024	2696	17	+4
N18-06B.A-5	573	19934	35.00	0.43	0.11	0.1844	0.0017	0.5213	0.0094	13.257	0.2710	0.144	0.0028	2693	15	0
N18-06B.K-2	1134	74444	66.00	0.34	0.04	0.1842	0.0016	0.4894	0.0085	12.430	0.2430	0.136	0.0027	2691	14	+5
N18-16B.6-2	926	62647	68.00	0.05	0.01	0.1842	0.0010	0.4854	0.0078	12.327	0.2130	0.142	0.0030	2691	9	+5
N18-16D.15-1	602	14098	23.00	0.02	0.01	0.1841	0.0009	0.5092	0.0083	12.929	0.2250	0.147	0.0030	2690	8	+1
N18-16C.8-5	664	14242	21.00	-0.05	-0.02	0.1841	0.0012	0.5198	0.0080	13.193	0.2240	0.141	0.0030	2690	11	0
N18-16C.8-6	466	11320	24.00	0.01	0.00	0.1840	0.0013	0.4927	0.0118	12.502	0.3140	0.144	0.0029	2689	12	+4

N18-16D.16-1	1039	19243	19.00	0.03	0.01	0.1839	0.0007	0.5021	0.0120	12.729	0.3110	0.147	0.0033	2688	6	+2
N18-16G.18-1	1002	69393	69.00	0.32	0.04	0.1838	0.0009	0.4905	0.0102	12.430	0.2690	0.149	0.0035	2687	8	+4
N18-06B.A-7	1097	38290	35.00	0.01	0.00	0.1835	0.0014	0.5314	0.0097	13.442	0.2700	0.146	0.0029	2685	13	-2
N18-06B.G-7	216	12340	57.00	0.07	0.01	0.1832	0.0020	0.5244	0.0095	13.249	0.2840	0.143	0.0028	2682	18	-1
N18-16D.14-1	129	6945	54.00	-0.03	-0.01	0.1832	0.0019	0.5022	0.0137	12.685	0.3700	0.152	0.0032	2682	17	+2
N18-16A.1-4	279	15220	54.00	-0.01	0.00	0.1831	0.0016	0.5303	0.0114	13.390	0.3120	0.152	0.0032	2681	14	-2
N18-06B.B-6	308	10496	34.00	0.03	0.01	0.1830	0.0018	0.4883	0.0107	12.323	0.2980	0.137	0.0028	2681	16	+4
N18-06B.G-4	178	11404	64.00	0.04	0.01	0.1828	0.0023	0.4965	0.0095	12.515	0.2870	0.139	0.0026	2679	20	+3
N18-06B.K-3	895	38759	43.00	0.02	0.00	0.1827	0.0015	0.4817	0.0083	12.135	0.2340	0.136	0.0026	2678	13	+5
N18-16A.1-3	515	14308	28.00	-0.01	0.00	0.1827	0.0010	0.5205	0.0105	13.111	0.2760	0.147	0.0032	2677	9	-1
N18-16C.8-1	638	13479	21.00	0.00	0.00	0.1824	0.0014	0.5182	0.0072	13.035	0.2110	0.147	0.0032	2675	13	-1
N18-06B.A-1	863	31292	36.00	-0.02	0.00	0.1824	0.0015	0.5070	0.0088	12.750	0.2490	0.149	0.0030	2675	14	+1
N18-06B.B-3	296	11665	39.00	-0.09	-0.02	0.1823	0.0020	0.5334	0.0095	13.405	0.2850	0.144	0.0029	2674	18	-3
N18-06B.B-1	188	10313	55.00	0.05	0.01	0.1821	0.0023	0.5124	0.0099	12.868	0.2980	0.144	0.0026	2672	21	0
N18-06B.G-3	475	24369	51.00	-0.03	-0.01	0.1821	0.0017	0.4923	0.0083	12.363	0.2420	0.136	0.0026	2672	15	+3
N18-16A.6-1	1052	69743	66.00	-0.01	0.00	0.1821	0.0007	0.5010	0.0077	12.581	0.2020	0.150	0.0033	2672	6	+2
N18-16C.8-2	605	11778	19.00	0.00	0.00	0.1821	0.0010	0.5212	0.0089	13.084	0.2390	0.149	0.0030	2672	9	-1
N18-16C.10-4	587	20801	35.00	0.02	0.00	0.1820	0.0011	0.5089	0.0096	12.772	0.2570	0.146	0.0033	2671	10	+1
N18-16C.10-1	466	14728	32.00	0.10	0.03	0.1819	0.0011	0.5268	0.0110	13.210	0.2900	0.153	0.0039	2670	10	-2

N18-06B.B-2	202	9808	49.00	0.22	0.04	0.1812	0.0022	0.5116	0.0094	12.779	0.2860	0.141	0.0027	2664	20	0
N18-16C.8-4	636	13910	22.00	0.02	0.01	0.1810	0.0010	0.5352	0.0069	13.353	0.1920	0.144	0.0030	2662	9	-4
N18-16D.13-1	389	6592	17.00	0.09	0.04	0.1808	0.0011	0.5403	0.0104	13.471	0.2760	0.155	0.0034	2661	10	-5
N18-06B.D-1	362	26423	73.00	0.04	0.00	0.1808	0.0018	0.4927	0.0099	12.282	0.2780	0.139	0.0026	2660	16	+3
N18-16C.10-3	557	15536	28.00	0.07	0.02	0.1805	0.0012	0.5212	0.0087	12.968	0.2360	0.142	0.0030	2657	11	-2
>5% discordance and/or >0.5% 4f206																
N18-06A.N-3	115	12090	105.00	1.31	0.09	0.1942	0.0046	0.3399	0.0074	9.100	0.2920	0.120	0.0024	2778	38	+32
N18-06B.A-4	484	26279	54.00	0.98	0.17	0.1903	0.0024	0.4979	0.0106	13.063	0.3280	0.134	0.0025	2745	21	+5
N18-06B.E-1	142	5608	40.00	2.70	0.69	0.1879	0.0044	0.5326	0.0107	13.801	0.4280	0.132	0.0024	2724	39	-1
N18-06B.K-1	440	31841	72.00	0.93	0.12	0.1852	0.0025	0.4438	0.0078	11.331	0.2530	0.120	0.0023	2700	22	+12
N18-06B.G-1	173	10873	63.00	0.06	0.01	0.1843	0.0025	0.4764	0.0124	12.104	0.3560	0.133	0.0027	2692	22	+7
N18-06B.B-8	245	13623	56.00	-0.03	-0.01	0.1831	0.0020	0.4666	0.0083	11.780	0.2490	0.123	0.0022	2681	18	+8
N18-16A.1-2	288	14906	52.00	0.08	0.01	0.1819	0.0015	0.5669	0.0127	14.220	0.3420	0.160	0.0036	2670	14	-8
N18-06B.A-8	349	26244	75.00	2.02	0.21	0.1818	0.0056	0.3843	0.0130	9.635	0.4430	0.122	0.0029	2670	51	+21
N18-06B.B-4	143	9993	70.00	0.14	0.02	0.1816	0.0027	0.4682	0.0095	11.725	0.2960	0.128	0.0025	2668	24	+7
N18-06B.G-8	220	14795	67.00	0.26	0.04	0.1814	0.0020	0.4741	0.0101	11.857	0.2890	0.128	0.0025	2666	18	+6
N18-16B.6-3	843	59533	71.00	0.07	0.01	0.1812	0.0010	0.4463	0.0081	11.152	0.2140	0.140	0.0030	2664	9	+11
N18-06A.N-1	76	9566	125.00	1.76	0.15	0.1811	0.0049	0.4884	0.0112	12.191	0.4330	0.110	0.0023	2663	45	+4
N18-06B.G-6	281	13360	48.00	0.06	0.01	0.1810	0.0018	0.4676	0.0182	11.670	0.4720	0.137	0.0027	2662	17	+7

N18-16C.10-2	629	16612	26.00	0.12	0.03	0.1802	0.0019	0.4040	0.0213	10.040	0.5400	0.133	0.0031	2655	17	+18
N18-06B.A-2	814	29448	36.00	1.02	0.23	0.1763	0.0020	0.4132	0.0093	10.042	0.2560	0.124	0.0024	2618	19	+15
N18-06B.A-3	638	36168	57.00	1.50	0.23	0.1753	0.0038	0.4980	0.0173	12.034	0.4960	0.136	0.0027	2609	36	0
N18-16G.23-1	147	17544	120.00	0.89	0.04	0.1270	0.0034	0.2374	0.0127	4.155	0.2490	0.094	0.0021	2056	47	+33
N18-16G.23-2	456	36602	80.00	1.94	0.08	0.0971	0.0042	0.1036	0.0017	1.387	0.0640	0.067	0.0019	1569	81	+59

~~3.1.3~~4.1.3 *Penzance granite*

The CL imaging of abundant zircons from all three samples collected from different locations in a single quarry of the Penzance granite displays textures typical of metamict zircons (Figure 6). These include cavities, fractures, disruption of the original zoning and development of dark CL areas (Corfu, 2003; Kılıç, 2016).

Even when targeting zircon grains seemingly less affected by metamictisation, twenty-seven analysis were aborted throughout ~~the~~a single analytical session due to the unacceptably high ^{204}Pb content. Of the twenty-four analysis which were not aborted, only nine were <5% discordant and had less than 1% common Pb (Figure 6, ~~Table 2~~Supplementary Material 2). The U and Th contents of completed analyses (average of ~580 and ~400 ppm, respectively) were commensurate with the observed metamictisation. The nine near concordant analysis have scattered ages typical of metamict zircons, and only one of the ages is within error of the previously reported age (Geoscience Australia ~~(GA),~~ 2019). We conclude that no reliable age could be calculated from these zircon data. The average and range of Th/U from the completed SHRIMP analyses was 0.72 and 0.52-1.46, respectively.

~~3.2~~4.2 U-Pb SHRIMP monazite dating of the Penzance granite

A significant number of the monazite grains were separated from the three Penzance granite samples. They have euhedral zoning textures on BSE images (Figure 7), which indicates magmatic crystallization. Recent studies (e.g.: Piechocka et al., 2017) have demonstrated the increased reliability of magmatic monazite as a geochronometer for igneous rocks with unreliable zircon age data, when subsequent metamorphic conditions remained under the Pb closure temperature of monazite. Monazite contains high U and Th and incorporates minor common Pb and, unlike zircon, is largely immune to metamictisation and radiogenic Pb loss at low temperatures (Piechocka et al., 2017).

A total of 38 of 56 analysis from 18 grains with low common Pb (f206 <0.5%) and low discordance (≤5%) (Table 13) yield a mean $^{207}Pb/^{206}Pb$ age of 2681.9 ± 4.5 Ma (95% c1; MSWD = 1.4; Figure 3). The slightly high MSWD indicates the possibility of scatter from a single-age population. However, in the absence of any skewness in the age probability plot (not shown), anomalous Th-U chemistry or other evidence for either inheritance or Pb-loss, and given the amount of data collected (n=56) and used (n=38), this is considered to be the age of these igneous monazites.

3.34.3 HF-isotopes in zircon

3.3.14.3.1 Teutonic Bore volcanics

Twenty-five zircon grains from sample 15BUDD78 – 111.60 m of the footwall rhyolite (unit I) were analysed for Lu–Hf by LA-SS-ICP-MS (Table 4Supplementary Material 3, mount N18-15D, sample B78,). The calculated $\varepsilon Hf_{(i)}$, based on the interpreted SHRIMP $^{207}Pb/^{206}Pb$ age (2692.9Ma), plot in a homogeneous population with values ranging between +2.3 and +5.6 (Figure 8), and a mean of 3.7 ± 0.5 (MSWD = 0.47, n = 25). The low MSWD value partly reflects the relatively large $\varepsilon Hf_{(i)}$ errors on individual analyses.

Twenty-nine Lu–Hf analysis (Table 4Supplementary Material 3, mount N18-15C, sample B137) were conducted on zircons from sample 15BUDD137 – 398.60 m of the same footwall rhyolite (unit I), and, once again, the $\varepsilon Hf_{(i)}$ is calculated based on the interpreted SHRIMP $^{207}Pb/^{206}Pb$ age for emplacement. $\varepsilon Hf_{(i)}$ values range between -0.6 and +5.2 with a mean of 2.9 ± 0.5 (MSWD = 0.90, n = 29, Figure 8). Combining the $\varepsilon Hf_{(i)}$ data for the both footwall rhyolite samples (unit I) yields a value of 3.27 ± 0.33 (MSWD = 0.79, n = 54).

Sixteen Lu–Hf analysis (Table 4Supplementary Material 3, B37) were conducted on zircon from both samples of transitional andesite (unit III) and the mean age of the combined SHRIMP analyses of 2693.4 Ma was used to calculate $\varepsilon Hf_{(i)}$ which showed considerable scatter and ranged between -11.7 and +8.6 with significant errors on individual analyses (Table

4Supplementary Material 3). The lower precision is a result of the smaller spot-size necessary for the small zircons from these samples. The mean $\varepsilon Hf_{(i)}$ for the transitional andesite (unit III) is 2.6 ± 1.8 (MSWD = 1.05, n = 16, Figure 8).

~~3.3.2~~4.3.2 *Penzance granite*

Recent studies show that the Lu–Hf system remains relatively undisturbed within metamic zircon that do not undergo significant later alteration (Lenting et al., 2010). Thirty-four Lu–Hf analyses on zircon from the Penzance granite (~~Table 4~~Supplementary Material 3, N18-06) show a range of $\varepsilon Hf_{(i)}$ between -1.5 to +4.7 with mean value of 2.17 ± 0.45 (MSWD = 1.15, n = 34). The $\varepsilon Hf_{(i)}$ values were calculated based on the SHRIMP monazite ages presented herein.

~~3.4~~4.4 Trace elements in zircon

Selected trace elements were measured via LA-SS-ICP-MS (~~Table 5~~Supplementary Material 4). Figure 9 illustrates patterns for selected REEs normalized to chondrite (Anders and Grevesse, 1989) for the two samples from the footwall rhyolite (unit I), the combined samples of andesite (unit III) and the Penzance granite. ~~Despite being represented separately on Figure 9, both samples of footwall rhyolite (unit I) display consistent REE chemistry.~~

The zircons from the footwall rhyolite (unit I) and the andesite (unit III) have similar MREE and HREE content~~, as showed on~~ (Figure 9). The mean Yb/Dy ratio is 4.15 ± 0.85 and 4.45 ± 0.68 (1σ) for the rhyolite and andesite, respectively. The Ce anomaly is estimated by the $Ce/Nd_{(CN)}$ ratio (Loucks et al., 2018) to be positive in both rock types (~~Tables 4~~Supplementary Material 4), with mean $Ce/Nd_{(CN)}$ of 1.04 ± 0.58 and 1.30 ± 0.75 (1σ) for the rhyolite and andesite, respectively. The zircons from the Penzance granite show a mean $Ce/Nd_{(CN)}$ of 0.92 ± 0.23 (1δ), indicating a positive Ce anomaly, and Yb/Dy ratio of 2.5 ± 0.67 (1σ).

Commented [61]: If you believe that this graphical representation might be misleading provide an alternative version. To me it seems clear as it is, and I find this sentence not necessary.

Commented [62R62]: The unnecessary sentence was erased.

~~Table 5: Selected trace element contents (ppm) of zircons from the Penzance granite and the volcanic sequence at the Bentley deposit.~~

Commented [63]: As for Table 2 and 4, also Table 5 should be included in the ESMs. Raw data should have no place in the manuscript. If you think to be necessary provide a small summary-table of the analyses, but your figures already represent well your data.

Commented [64R64]: Ok

~~4~~5 DISCUSSION

~~4.1~~5.1 Age constrains on the Penzance granite

Hollis et al. (2015) proposed a link between VHMS mineralisation at the ~~TB~~Teutonic Bore Camp and the emplacement of the HFSE-enriched Penzance granite, based on geochemical similarities, the proximity and broad synchronicity between the intrusive magmatic activity and the volcanism of the host sequence. These observations were underpinned by a U-Pb zircon age for the volcanism (2692 ± 4 Ma; Nelson, 1995) and the age reported by Champion and Cassidy (2002) of 2679 ± 8 Ma, for the Kent Complex of the Penzance Supersuite. This latter age was obtained by SHRIMP U-Pb zircon dating of sample ID 96969076 of Geoscience Australia's database, after L.Black, AGSO (unpublished) in Champion and Cassidy (2002).

Champion and Cassidy (2002) reported the age but not the data table. However, the geochronological data, as well as location and description for sample ID 96969076, are available from Geoscience Australia's Geochron Delivery database (Geoscience Australia ~~(GA),~~ 2019). The reported age for this sample is 2686 ± 9 Ma with MSWD = 1.6 and probability = 0.044 (Geoscience Australia ~~(GA),~~ 2019), which is within error of the age reported by Champion and Cassidy (2002), but not identical.

We have reprocessed the data available from Geochron Delivery for sample 96969076 and obtained an identical age of 2686 ± 9 Ma, MSWD = 1.6 from 21 analysis. However, given the scatter inferred by the high MSWD, we have filtered the data by only considering analysis with common Pb <0.3%, deriving a more statistically robust age of 2682 ± 9 Ma (n=12; MSWD = 1.3). More importantly, only four zircons were recovered from sample 96969076 and the 21 analyses and calculated age is based on analyses from only three grains, of which one ~~was~~is

a xenocryst. Each of ~~the~~our three samples ~~we~~ collected from the same quarry had hundreds of zircon grains, and after hand-picking the clearest (least metamict) zircons and analysing the best areas based on CL-SE imaging, we only detected one analysis in the relevant time interval, and it was 7% discordant. In view of this discrepancy, we searched for other datable minerals in the Penzance granite and identified igneous monazite. The monazite age of 2681.9 ± 4.5 Ma discussed above is considered to be a statistically valid age of magma crystallization for the Penzance granite, and supersedes the previous zircon age(s).

~~4.2~~5.2 Geochronological associations

The relative timing of ore formation in the ~~TB~~Teutonic Bore C~~e~~amp is well constrained within the stratigraphic sequence at Jaguar, where substantial evidence of seafloor precipitation indicate coeval mineralisation to the development of the upper sedimentary package (unit IV). Such evidence is absent from Bentley and the ~~TB~~Teutonic Bore deposit, which indicates that they were formed at greater depths, probably by replacement of a slightly older stratigraphy (see Figure 2A).

The syn-ore nature of the upper sedimentary package (unit IV) at Jaguar, the deposit hosted within the youngest stratigraphic level in the ~~TB~~Teutonic Bore C~~e~~amp, indicates that the hangingwall sequence at Jaguar post-dates ore formation and could provide a potential minimum mineralisation age. Attempts to date this sequence have proven unsuccessful to date (Das, 2018). The footwall in all three deposits, as well as the hangingwall immediately above the orebodies of the Bentley and the ~~TB~~Teutonic Bore deposits, pre-date the mineralisation and represent a maximum age of ore formation.

The ages obtained in this study for the footwall rhyolite (unit I - 2691.7 ± 2.5 Ma and 2696.5 ± 4.3 Ma) and the transitional andesite (unit III - 2693.4 ± 4.1 Ma) suggest that mineralisation at the ~~TB~~Teutonic Bore C~~e~~amp is younger than c.a~~-~~. 2694 Ma~~, as indicated in~~ (Figure 10). The unpublished TIMS age for the footwall rhyolite sequence (unit I) of 2692.6 ± 1.5 Ma (Das,

2018) is indistinguishable from the SHRIMP age presented here for the pre-ore volcanic sequence at the ~~TB~~Teutonic Bore Ceamp. Similarly, the previous SHRIMP age for the ~~TB~~Teutonic Bore Ceamp sequence (2692 ± 4 Ma; (Nelson, 1995) is similar to the age determined in this study (Figure 10). Therefore, although poorly constrained in the stratigraphy, it is likely that the porphyritic dacite dated by Nelson (1995) is part of the pre-ore stratigraphy (units I, II, or III).

The ages for the footwall rhyolite (unit I) of 2696.5 ± 4.3 Ma and 2691.7 ± 2.5 Ma are within error of each other, when considering a 95% confidence interval. However, considering the normal distribution tendency ~~(Figure 10)~~ of single-population ages obtained from multiple grains (Figure 10; Schoene et al., 2013), it is probable that these could also represent a long duration of volcanic activity during the development of this stratigraphic facies.

The ages for the footwall rhyolite (unit I) and the Penzance granite (2681.9 ± 4.5 Ma) do not overlap (Figure 10) at the 95% confidence interval and are not, therefore, coeval. Furthermore, the porphyritic dacite from Nelson (1995) and the transitional andesite (unit III) do not overlap the age of the Penzance (Figure 10) at a 95% confidence interval. We infer that these rocks pre-date the mineralisation and the syn-ore stratigraphy.

~~4.3~~5.3 Geochemical correlations

~~4.3.1~~5.3.1 Whole-rock geochemistry

Hollis et al. (2015) described similarities in whole-rock REE distribution between the Penzance granite (Kent Complex) and the felsic volcanics that host the mineralisation at Jaguar (footwall rhyolite – unit I). Based on these observations and the HFSE enrichment of both rock types they suggested a possible genetic link between these rocks, proposing that the footwall volcanic sequence at Jaguar would be the extrusive equivalent to the Penzance granite.

The geochronological results presented here indicate that the crystallization of the Penzance granite is not coeval to the formation of the footwall rhyolite (unit I) or the transitional andesite

(unit III) at Bentley. However, these processes occur within a ~12 M.y. interval. Given the chemical similarities between these rock types and their proximity in age it is conceivable that they are both the product of a single magmatic system or had a common source.

Additionally, based on whole-rock geochemistry observations, other stratigraphic facies within the younger, syn-ore, portion of the volcanic sequence at the ~~TB~~Teutonic Bore C~~e~~amp are alternative candidates to be the extrusive correspondent to the Penzance granite.

The dacite that can be observed at the sedimentary-volcanic package of the upper sedimentary horizon (unit IV) in the Jaguar deposit (MPD from Belford et al., 2015) has Y/Zr ratios that indicates a tholeiitic affinity (Belford et al., 2015), which is also the case for the Penzance granite (ID 96969076, sampled from the same locality of the geochronological study; Sedgmen et al., 2007) (Figure 11). Furthermore, the MPD dacite yields a La/Yb_{CN} ratio of 3.4 – 5.5 (Belford, 2010), which indicates a significant LREE/HREE enrichment, equal to what is indicated by whole-rock REE content for the Penzance granite (Hollis et al., 2015).

~~4.3.2~~5.3.2 *Zircon geochemistry*

The Hf-isotopes corroborate Hollis et al. (2015)'s hypothesis of a genetic link between the ~~TB~~Teutonic Bore Camp volcanic sequence and the Penzance granite. All zircons (Penzance, units I and III) have very similar $\varepsilon Hf_{(i)}$, with most values between -1 and +6 (Figure 8). The $\varepsilon Hf_{(i)}$ values show little contribution from evolved sources ~~as shown in~~ (Figure 8). Indeed, Nd and Pb isotopes indicate that the ~~TB~~Teutonic Bore ~~e~~Camp is located within a more juvenile zone of the Yilgarn craton, the Teutonic zone (Huston et al., 2014). The $\varepsilon Hf_{(i)}$ for the zircons from the Penzance granite and the volcanic rocks from the ~~TB~~Teutonic Bore C~~e~~amp plot above the CHUR line (Figure 8), indicating a juvenile depleted mantle source component. These $\varepsilon Hf_{(i)}$ are slightly higher than the $\varepsilon Hf_{(i)}$ of zircons from other granites and volcanics within the Kurnalpi Terrain (Isaac, 2015; Wyche et al., 2012).

According to Kirkland et al. (2015), parental magma composition is one of four factors that may contribute to variations in the Th/U of a zircon crystal.Therefore, the similar Th/U ratios (~~Table 2~~Supplementary Material 2) of the Penzance (~0.7) and Bentley zircons (Unit I: ~0.6) also suggest they could have a shared magma source. Furthermore, all zircons have similar $Ce/Nd_{(CN)}$ ratios (~~Table 5~~Supplementary Material 4), which indicates comparable redox conditions, as this ratio is a proxy for the Ce anomaly (Loucks et al., 2018).

The zircons from the Penzance granite have higher overall REE content and MREE/HREE enrichment (indicated by the Yb/Dy ratio), when compared to the Bentley units I and III zircons (~~Table 5~~Supplementary Material 4). These chemical differences indicate that the Penzance granite is more fractionated but do not resolve whether this is the result of igneous differentiation from a common magma or magma production from a common source. The ~12 M.y. interval between the units I and III volcanics, and the Penzance granite suggests the latter.

~~4.4~~5.4 ~~The~~ Contribution to the 4D evolutionary model of the ~~TB~~Teutonic Bore Camp ore

The 4D evolutionary model of the Teutonic Bore Camp is achieved by the addition of the time dimension to the current understanding of the geological evolution of the deposits, including stratigraphy and geochemistry (Figure 2; Belford, 2010; Belford et al., 2015; Chen et al., 2015; Das, 2018; Hallberg and Thompson, 1985; Macklin, 2010; Parker et al., 2017). The geochronology data presented in this study constrain in time several processes within the Teutonic Bore Camp, including the intrusion of the Penzance granite, which could be linked to the development of the mineral system.

Similarities in zircon chemistry (i.e.: $\varepsilon Hf_{(i)}$ and Th/U ratio; see section 5.3: Geochemical correlations) complemented by the geochemical correspondences between the Penzance granite and the ~~TB~~Teutonic Bore volcanics (i.e.: HFSE-enrichment and REE pattern, see

section 5.3: Geochemical correlations), suggest a genetic association between the intrusive granite and the extrusive rocks that constitute the ~~TB~~Teutonic Bore Camp host sequence.

~~Additionally, there is evidence of interaction between the Penzance and the volcanic rocks that are intruded by it, such as the i~~Irregular contact between the Penzance granite and the volcanic sequence, as well as, the recognition of intrusive veins of granitoid within the volcanics, and xenoliths of volcanic rocks within the ~~intrusive~~ granite (Hallberg and Thompson, 1985) indicate that the Penzance intrudes the volcanic Teutonic Bore sequence and that their proximity is not the result of subsequent tectonic processes. Considering the close geographic position of the granite and the ore-bearing volcanic sequence (Figure 1), their shared geochemical features and broad synchronicity, it is ~~probable~~ possible that the Penzance granite was involved in the process that generated the VHMS mineralisation at the ~~TB~~Teutonic Bore Ceamp.

~~The role of granites in the development of VHMS systems has been the focus of numerous studies (...).~~ Magmatic-hydrothermal contribution of metals is not necessary in the development of VHMS deposits (Huston et al., 2011) and syn-ore intrusions do not always directly supply metal to the system, but rather act as a heating source, driving hydrothermal circulation that leaches metals from the country host rock (Lode et al., 2017). However, in a number of cases there is evidence of a significant contribution of metals and/or volatiles from the magmatic source, in addition to the supply of heat (e.g.: Chen et al., 2015; Lode et al., 2017; ~~e.g.:~~ Yang and Scott, 1996).

Chen et al. (2015) used S-isotopes as a proxy for the hydrothermal fluid composition in the ~~TB~~Teutonic Bore Camp and interpreted that the supply of sulphur to the hydrothermal ore fluid was the result of a mixture between seawater and a hydrothermal fluid of magmatic origin. These authors did not find compelling evidence for leaching of sulphur from the host sequence into the ore fluid in the ~~TB~~Teutonic Bore Camp. Therefore, the Penzance granite is a strong

Commented [65]: References are required.

Commented [66R66]: I simply erased the sentence. It was not necessary to the understanding of the paragraph and the studies that would be referenced are presented through the rest of the text.

candidate to have acted as the probable magmatic source of sulphur to the mineralisation, and consequentlypossibly, metals.

4.55.5 Exploration strategies

Our observations show that the HFSE-enriched Penzance granite probably played a fundamental role in the supply of metals and heat that culminated in the development of the replacement-type VHMS deposits of the TBTeutonic Bore Ceamp. Therefore, future exploration efforts within the camp should focus on fluid pathways from the similar granites. The emphasis should be on mapping syn- or pre-intrusive structures that could facilitate fluid flow from the granite to the host sequence. Fertile zones are likely to be discovered where these fluid paths find the appropriate conditions for metal precipitation, which has been suggested by previous studies to be sediment-rich horizons (Parker et al., 2017) and/or depositional breaks (Belford et al., 2015).

This paper supports conclusions proposed by Hollis et al. (2015), of a connection between HFSE-enriched granites and VHMS (± base metals) deposits within the Yilgarn Craton. Following the identification of fertile terrains, populated with HFSE-enriched granites, *greenfield* exploration campaigns should employ a multi-disciplinary approach to test the processes involved in the formation of an ore deposit. The development of 4D models (i.e. constrain in time of 3D geological processes) allows for a better understanding of the timing and nature of the magmatic and stratigraphical processes necessary for the development of such ore deposits. This is particular true in Archean replacement-type VHMS deposits, where the syn-volcanic timing of the mineralisation is not always clear (e.g. Barrote et al., 2019)

56 CONCLUSIONS

- Three mined VHMS orebodies in the Teutonic Bore eCamp (Teutonic Bore deposit, Jaguar and Bentley) formed at different stratigraphic levels.

Commented [67]: Whereas the suggestion that the Penzance granite could have acted as a sulfur source is coherent with the isotopic data discussed in Chen et al. (2015), the assumption that metals were sourced from the the granite magma needs to be supported from further evidence.

Commented [68R68]: We understand the reviewers concern and have re-phrased the text as to not point the reader towards unsupported affirmations.

- Jaguar formed coeval with its host sequence, whereas the ore in Teutonic Bore and Bentley replaces slightly older stratigraphy.
- The age of the host sequence at the stratigraphic level of the Bentley deposit is ca. 2693 Ma.
- The age of the ~~TB~~Teutonic Bore ~~e~~Camp mineralisation is ~~likely~~ possibly coeval to the intrusion of the Penzance granite at ca. 2682 Ma.
- Monazite has been shown to be a more reliable chronometer than high-U-Th zircons in the HFSE-enriched Penzance granite.
- The Penzance granite possibly acted as the source of heat and potentially fluid/metals to the ore formation at the ~~TB~~Teutonic Bore C~~e~~amp.
- VHMS exploration in the Yilgarn Craton should focus in finding fluid pathways between HFSE-enriched intrusives and potential host sequences to orebodies.

~~6~~7 ACKNOWLEGMENTS

The authors acknowledge: Dr Steve Bereford and Mr. Kyle Hodges from IGO for their wisdom, access to samples, drill core and internal data; Thermo Fisher, GSWA and MRIWA for financial support; and the John de Laeter Centre (JdLC) for the facilities, scientific and technical assistance. We thank Dr. Haoyang Zhou, Dr. Nicolas Thebaud and an anonymous reviewer whose comments helped improve and clarify this manuscript. JdLC facilities are supported by a university-government consortium, ARC and AuScope via NCRIS. GeoHistory Facility instruments in the John de Laeter Centre, Curtin University were funded via an Australian Geophysical Observing System grant provided to AuScope Pty Ltd. by the AQ44 Australian Education Investment Fund program. The NPII multi-collector was obtained via funding from the Australian Research Council LIEF program (LE150100013).

~~7~~8 BIBLIOGRAPHY

Anders, E., Grevesse, N., 1989. Abundances of the elements: Meteoritic and solar. Geochim. Cosmochim. Acta 53, 197–214. https://doi.org/10.1016/0016-7037(89)90286-X

Barrett, T.J., MacLean, W.H., 1994. Chemostratigraphy and hydrothermal alterationin exploration for VHMS deposits in greenstones and younger volcanic rocks., in: Lentz, D.R. (Ed.), Alteration and Alteration Processes Associated with Ore-Forming Systems, Short Course Notes / Geological Association of Canada. Geological Assoc. of Canada, St.John's, Newfoundland, pp. 433–467.

Barrote, V., Tessalina, S., McNaughton, N., Jourdan, F., Hollis, S.P., Ware, B., Zi, J.-W., 2020. 4D history of the Nimbus VHMS ore deposit in the Yilgarn Craton, Western Australia. Precambrian Research 337, 105536. https://doi.org/10.1016/j.precamres.2019.105536

Belford, S.M., 2010. Genetic and chemical characterisation of the host succession to the archean Jaguar VHMS deposit. (Doctoral dissertation). University of Tasmania, UTAS, Hobart, Tasmania, Australia.

Belford, S.M., Davidson, G.J., McPhie, J., Large, R.R., 2015. Architecture of the Neoarchaean Jaguar VHMS deposit, Western Australia: Implications for prospectivity and the presence of depositional breaks. Precambrian Res. 260, 136–160. https://doi.org/10.1016/j.precamres.2014.12.019

~~Black, L.P., Kamo, S.L., Allen, C.M., Aleinikoff, J.N., Davis, D.W., Korsch, R.J., Foudoulis, C., 2003. TEMORA 1: a new zircon standard for Phanerozoic U–Pb geochronology. Chem. Geol. 200, 155–170. https://doi.org/10.1016/S0009-2541(03)00165-7~~

~~Blichert-Toft, J., Albarède, F., 1997. The Lu-Hf isotope geochemistry of chondrites and the evolution of the mantle-crust system. Earth Planet. Sci. Lett. 148, 243–258. https://doi.org/10.1016/S0012-821X(97)00040-X~~

Butt, C.R.M., Anand, R.R., Smith, R.E., 2017. Geology of the Australian regolith, in: Phillips, G.N. (Ed.), Australian Ore Deposits. The Australian Institute of Mining and Metallurgy, Melbourne, pp. 27–34.

Champion, D.C., Cassidy, K.F., 2002. Granites of the Northern Eastern Goldfields: their Distribution, Age, Geochemistry, Petrogenesis, Relationship with Mineralisation, and Implications for Tectonic Environment, AMIRA P482/MERIWAM281-Yilgarn Granitoids. AMIRA P482/MERIWAM281-Yilgarn Granitoids.

Chen, M., Campbell, I.H., Xue, Y., Tian, W., Ireland, T.R., Holden, P., Cas, R.A.F., Hayman, P.C., Das, R., 2015. Multiple Sulfur Isotope Analyses Support a Magmatic Model for the Volcanogenic Massive Sulfide Deposits of the Teutonic Bore Volcanic Complex, Yilgarn Craton, Western Australia. Econ. Geol. 110, 1411–1423. https://doi.org/10.2113/econgeo.110.6.1411

~~Chu, N.-C., Taylor, R.N., Chavagnac, V., Nesbitt, R.W., Boella, R.M., Milton, J.A., German, C.R., Bayon, G., Burton, K., 2002. Hf isotope ratio analysis using multi-collector inductively coupled plasma mass spectrometry: an evaluation of isobaric interference corrections. J. Anal. At. Spectrom. 17, 1567–1574. https://doi.org/10.1039/b206707b~~

~~Claoué-Long, J.C., Compston, W., Roberts, J., Fanning, C.M., 1995. Two Carboniferous Ages: A Comparison of Shrimp Zircon Dating with Conventional Zircon Ages and 40Ar/39Ar Analysis, in: Berggren, W.A., Kent, D.V., Aubry, M.-P., Hardenbol, J. (Eds.), Geochronology, Time Scales, and Global Stratigraphic Correlation, Society for Sedimentary Geology Special Publications. SEPM (Society for Sedimentary Geology), pp. 3–21. https://doi.org/10.2110/pec.95.54~~

~~Compston, W., Williams, I.S., Meyer, C., 1984. U-Pb geochronology of zircons from lunar breccia 73217 using a sensitive high mass-resolution ion microprobe. Proc. 14th Lunar~~

~~Planet. Sci. Conf. J. Geophys. Res. Suppl 89, B525–B534. https://doi.org/10.1029/JB089iS02p0B525~~

Corfu, F., 2003. Atlas of Zircon Textures. Rev. Mineral. Geochem. 53, 469–500. https://doi.org/10.2113/0530469

Czarnota, K., Champion, D.C., Goscombe, B., Blewett, R.S., Cassidy, K.F., Henson, P.A., Groenewald, P.B., 2010. Geodynamics of the eastern Yilgarn Craton. Precambrian Res. 183, 175–202. https://doi.org/10.1016/j.precamres.2010.08.004

Das, R., 2018. Understanding the Palaeovolcanological and Palaeoenvironmental setting of Archaean VMS Deposit: Stratigraphic Architecture and Volcanology of the Archaean VMS host rock succession of the Teutonic Bore, Jaguar and Bentley Mine corridor, Eastern Goldfields Province, Western Australia (Master thesis). Melbourne University, Melbourne.

~~De Laeter, J.R., Kennedy, A.K., 1998. A double focusing mass spectrometer for geochronology. Int. J. Mass Spectrom. 178, 43–50. https://doi.org/10.1016/S1387-3806(98)14092-7~~

Doyle, M.G., Allen, R.L., 2003. Subsea-floor replacement in volcanic-hosted massive sulfide deposits. Ore Geol. Rev. 23, 183–222. https://doi.org/10.1016/S0169-1368(03)00035-0

Ellis, P., 2004. Geology and mineralisation of the Jaguar copper-zinc deposit, Western Australia, in: McConachy, T.F., McInnes, B.I.A. (Eds.), Copper-Zinc Massive Sulphide Deposits in Western Australia. CSIRO Exploration and Mining, Melbourne, pp. 39–46.

~~Fletcher, I.R., McNaughton, N.J., Davis, W.J., Rasmussen, B., 2010. Matrix effects and calibration limitations in ion probe U–Pb and Th–Pb dating of monazite. Chem. Geol. 270, 31–44. https://doi.org/10.1016/j.chemgeo.2009.11.003~~

Geoscience Australia~~ (GA),~~ 2019. Geochron Delivery Database. Accessed June 2019. http://www.ga.gov.au/geochron-sapub-web/geochronology/shrimp/search.htm.

GeoVIEW.WA, 2016. 1:500 000 State interpreted bedrock geology polygons, 2016.

Hallberg, J.A., Thompson, J.F.H., 1985. Geologic setting of the Teutonic Bore massive sulfide deposit, Archean Yilgarn Block, Western Australia. Econ. Geol. 80, 1953–1964. https://doi.org/10.2113/gsecongeo.80.7.1953

Hollis, S.P., Mole, D.R., Gillespie, P., Barnes, S.J., Tessalina, S., Cas, R.A.F., Hildrew, C., Pumphrey, A., Goodz, M.D., Caruso, S., Yeats, C.J., Verbeeten, A., Belford, S.M., Wyche, S., Martin, L.A.J., 2017. 2.7 Ga plume associated VHMS mineralization in the Eastern Goldfields Superterrane, Yilgarn Craton: Insights from the low temperature and shallow water, Ag-Zn-(Au) Nimbus deposit. Precambrian Res. 291, 119–142. https://doi.org/10.1016/j.precamres.2017.01.002

Hollis, S.P., Yeats, C.J., Wyche, S., Barnes, S.J., Ivanic, T.J., Belford, S.M., Davidson, G.J., Roache, A.J., Wingate, M.T.D., 2015. A review of volcanic-hosted massive sulfide (VHMS) mineralization in the Archaean Yilgarn Craton, Western Australia: Tectonic, stratigraphic and geochemical associations. Precambrian Res. 260, 113–135. https://doi.org/10.1016/j.precamres.2014.11.002

Huston, D.L., Champion, D.C., Cassidy, K.F., 2014. Tectonic Controls on the Endowment of Neoarchean Cratons in Volcanic-Hosted Massive Sulfide Deposits: Evidence from Lead and Neodymium Isotopes. Econ. Geol. 109, 11–26. https://doi.org/10.2113/econgeo.109.1.11

Huston, D.L., Relvas, J.M.R.S., Gemmell, J.B., Drieberg, S., 2011. The role of granites in volcanic-hosted massive sulphide ore-forming systems: an assessment of magmatic–hydrothermal contributions. Miner. Deposita 46, 473–507. https://doi.org/10.1007/s00126-010-0322-7

Independence Group NL (IGO), 2015. Annual Report 2015 (Unpublished Annual Report). Independence Group NL (IGO), Perth, W.A.

Isaac, C., 2015. Geochemistry of the north Eastern Goldfields, Western Australia: examining the processes that produce nickel sulphide camps (Masters Thesis). The University of Western Australia, Perth, W.A.

~~Kennedy, A.K., De Laeter, J.R., 1994. The performance characteristics of the WA SHRIMP II ion microprobe., in: Abstracts Vol., U.S. Geological Survey Circular. Presented at the Eighth International Conference on Geochronology, Cosmochronology and Isotope Geology, Berkeley, USA, p. 166.~~Kirkland, C.L., Smithies, R.H., Taylor, R.J.M., Evans, N., McDonald, B., 2015. Zircon Th/U ratios in magmatic environs. Lithos 212–215, 397–414. https://doi.org/10.1016/j.lithos.2014.11.021

Kılıç, A.D., 2016. Investigation of zircon by CL (Cathodoluminescence) and Raman Spectroscopy. IOP Conf. Ser. Earth Environ. Sci. 44, 042006. https://doi.org/10.1088/1755-1315/44/4/042006

Lenting, C., Geisler, T., Gerdes, A., Kooijman, E., Scherer, E.E., Zeh, A., 2010. The behavior of the Hf isotope system in radiation-damaged zircon during experimental hydrothermal alteration. Am. Mineral. 95, 1343–1348. https://doi.org/10.2138/am.2010.3521

~~Li, X.-H., Long, W.-G., Li, Q.-L., Liu, Y., Zheng, Y.-F., Yang, Y.-H., Chamberlain, K.R., Wan, D.-F., Guo, C.-H., Wang, X.-C., Tao, H., 2010. Penglai Zircon Megacrysts: A Potential New Working Reference Material for Microbeam Determination of Hf-O Isotopes and U-Pb Age. Geostand. Geoanalytical Res. 34, 117–134. https://doi.org/10.1111/j.1751-908X.2010.00036.x~~

Lode, S., Piercey, S.J., Layne, G.D., Piercey, G., Cloutier, J., 2017. Multiple sulphur and lead sources recorded in hydrothermal exhalites associated with the Lemarchant volcanogenic massive sulphide deposit, central Newfoundland, Canada. Miner. Deposita 52, 105–128. https://doi.org/10.1007/s00126-016-0652-1

Loucks, R.R., Fiorentini, M.L., Rohrlach, B.D., 2018. Divergent T–*f*O2 paths during crystallisation of H2O-rich and H2O-poor magmas as recorded by Ce and U in zircon, with implications for TitaniQ and TitaniZ geothermometry. Contrib. Mineral. Petrol. 173. https://doi.org/10.1007/s00410-018-1529-3

~~Ludwig, K.R., 2011. User's manual for Isoplot 4.15: a geochronological toolkit for Microsoft Excel, Berkeley Geochronology Center Special Publication.~~

~~Ludwig, K.R., 2009. Squid 2.50, A User's Manual, Berkeley Geochronology Centre Special Publication,.~~

Macklin, D., 2010. Alteration at the Teutonic Bore (VHMS) Deposit, Western Australia (B.Sc with honours thesis). University of Tasmania, UTAS.

McConachy, T.F., McInnes, B.I.A., Carr, G.R., 2004. Is Western Australia intrinsically impoverished in volcanogenic massive sulphide deposits, or under explored?, in: McConachy, T.F., McInnes, B.I.A. (Eds.), Copper-Zinc Massive Sulphide Deposits in Western Australia. CSIRO Exploration and Mining, Melbourne, pp. 15–32.

~~Morel, M.L.A., Nebel, O., Nebel-Jacobsen, Y.J., Miller, J.S., Vroon, P.Z., 2008. Hafnium isotope characterization of the GJ-1 zircon reference material by solution and laser-ablation MC-ICPMS. Chem. Geol. 255, 231–235. https://doi.org/10.1016/j.chemgeo.2008.06.040~~

~~Nasdala, L., Hofmeister, W., Norberg, N., Martinson, J.M., Corfu, F., Dörr, W., Kamo, S.L., Kennedy, A.K., Kronz, A., Reiners, P.W., Frei, D., Kosler, J., Wan, Y., Götze, J., Häger, T., Kröner, A., Valley, J.W., 2008. Zircon M257 - a Homogeneous Natural Reference Material for the Ion Microprobe U-Pb Analysis of Zircon. Geostand. Geoanalytical Res. 32, 247–265. https://doi.org/10.1111/j.1751-908X.2008.00914.x~~

Nelson, D.R., 1995. Compilation of SHIRMP U-Pb zircon geochronology data, 1994, Record / Geological Survey of Western Australia. Geological Survey of Western Australia, Perth.

Parker, P., Belford, S.M., Maier, R., Lynn, S., Stewart, W., 2017. Teutonic Bore - Jaguar - Bentley volcanogenic massive sulfide field, in: Phillips, G.N. (Ed.), Australian Ore Deposits. The Australian Institute of Mining and Metallurgy, Melbourne, pp. 167–172.

Patchett, P.J., Tatsumoto, M., 1980. Hafnium isotope variations in oceanic basalts. Geophys. Res. Lett. 7, 1077–1080. https://doi.org/10.1029/GL007i012p01077

Paton, C., Hellstrom, J., Paul, B., Woodhead, J., Hergt, J., 2011. Iolite: Freeware for the visualisation and processing of mass spectrometric data. J. Anal. At. Spectrom. 26, 2508. https://doi.org/10.1039/c1ja10172b

Piechocka, A.M., Gregory, C.J., Zi, J.-W., Sheppard, S., Wingate, M.T.D., Rasmussen, B., 2017. Monazite trumps zircon: applying SHRIMP U–Pb geochronology to systematically evaluate emplacement ages of leucocratic, low-temperature granites in a complex Precambrian orogen. Contrib. Mineral. Petrol. 172. https://doi.org/10.1007/s00410-017-1386-5

Scherer, E., 2001. Calibration of the Lutetium-Hafnium Clock. Science 293, 683–687. https://doi.org/10.1126/science.1061372

Schoene, B., Condon, D.J., Morgan, L., McLean, N., 2013. Precision and Accuracy in Geochronology. Elements 9, 19–24. https://doi.org/10.2113/gselements.9.1.19

Sedgmen, A., Hazell, M.S., Budd, A.R., Champion, D.C., 2007. OZCHEM National Whole Rock Geochemistry Dataset.

Sláma, J., Košler, J., Condon, D.J., Crowley, J.L., Gerdes, A., Hanchar, J.M., Horstwood, M.S.A., Morris, G.A., Nasdala, L., Norberg, N., Schaltegger, U., Schoene, B., Tubrett, M.N., Whitehouse, M.J., 2008. Plešovice zircon — A new natural reference material for U–Pb and Hf isotopic microanalysis. Chem. Geol. 249, 1–35. https://doi.org/10.1016/j.chemgeo.2007.11.005

Stern, R.A., Bodorkos, S., Kamo, S.L., Hickman, A.H., Corfu, F., 2009. Measurement of SIMS Instrumental Mass Fractionation of Pb Isotopes During Zircon Dating. Geostand. Geoanalytical Res. 33, 145–168. https://doi.org/10.1111/j.1751-908X.2009.00023.x

Thirlwall, M.F., Anczkiewicz, R., 2004. Multidynamic isotope ratio analysis using MC–ICP–MS and the causes of secular drift in Hf, Nd and Pb isotope ratios. Int. J. Mass Spectrom. 235, 59–81. https://doi.org/10.1016/j.ijms.2004.04.002

Williams, I.S., 1998. Geochronology by Ion Microprobe, in: McKibben, M.A., Shanks, W.C., Ridley, W.I. (Eds.), Applications of Microanalytical Techniques to Understanding Mineralizing Processes, Reviews in Economic Geology. pp. 1–35.

Woodhead, J., Hergt, J., Shelley, M., Eggins, S., Kemp, R., 2004. Zircon Hf-isotope analysis with an excimer laser, depth profiling, ablation of complex geometries, and concomitant age estimation. Chem. Geol. 209, 121–135. https://doi.org/10.1016/j.chemgeo.2004.04.026

Woodhead, J.D., Hergt, J.M., 2005. A Preliminary Appraisal of Seven Natural Zircon Reference Materials for In Situ Hf Isotope Determination. Geostand. Geoanalytical Res. 29, 183–195. https://doi.org/10.1111/j.1751-908X.2005.tb00891.x

Wyche, S., Kirkland, C.L., Riganti, A., Pawley, M.J., Belousova, E., Wingate, M.T.D., 2012. Isotopic constraints on stratigraphy in the central and eastern Yilgarn Craton, Western Australia. Aust. J. Earth Sci. 59, 657–670. https://doi.org/10.1080/08120099.2012.697677

Yang, K., Scott, S.D., 1996. Possible contribution of a metal-rich magmatic fluid to a sea-floor hydrothermal system. Nature 383, 420–423. https://doi.org/10.1038/383420a0https://doi.org/10.1038/383420a0

829

Table 2: SHRIMP isotopic data for zircons in samples 15BUDD78 (mount N18-15D), 15BUDD138 (mount N18-15C), 15BUDD120 -226.04 (mount N19-07, 08), 15BUDD120 - 228.42 (mount N19-09, 10) and Penzance granite (mount N18-06).

Mount grain-spot	ppm U	ppm Th	$^{232}Th/^{238}U$	%com 206Pb	$^{207}Pb^*/^{206}Pb^*$	% 1σ err	$^{207}Pb^*/^{235}U$	% 1σ err	$^{206}Pb^*/^{238}U$	% 1σ err	err corr	$^{207}Pb/^{206}Pb$ Age (Ma)	1σ err	% Disc.
15BUDD78 (mount N18-15D)														
≤3% discordance														
N18-15D.11-1	126	72	0.59	0.01	0.1860	0.38	13.46	3.0	0.525	3.0	0.992	2707	6	-1
N18-15D.2-1	65	29	0.46	0.04	0.1858	0.54	13.58	3.4	0.530	3.4	0.987	2705	9	-2
N18-15D.9-1	75	33	0.45	-0.11	0.1856	1.04	13.44	3.3	0.525	3.1	0.948	2703	17	-1
N18-15D.8-1	71	33	0.48	-0.07	0.1854	0.55	13.56	3.3	0.531	3.2	0.986	2701	9	-2
N18-15D.7-1	214	129	0.62	0.05	0.1853	0.49	13.36	2.9	0.523	2.9	0.986	2700	8	-1
N18-15D.1-1	182	123	0.70	0.03	0.1850	0.32	13.42	3.2	0.526	3.2	0.995	2698	5	-1
N18-15D.14-1	185	129	0.72	0.03	0.1849	0.33	13.48	3.2	0.529	3.2	0.995	2697	5	-2
N18-15D.10-1	85	54	0.65	0.02	0.1845	0.46	13.30	3.0	0.523	3.0	0.988	2693	8	-1
N18-15D.13-1	148	101	0.70	0.04	0.1841	0.37	13.55	3.0	0.534	3.0	0.993	2690	6	-3
N18-15D.12-1	75	48	0.66	0.21	0.1840	0.57	13.48	2.9	0.531	2.9	0.981	2690	9	-3
N18-15D.3-1	73	38	0.53	0.11	0.1837	0.54	13.05	3.2	0.515	3.1	0.985	2686	9	+0
N18-15D.6-1	77	48	0.65	0.21	0.1827	0.62	13.22	3.5	0.525	3.4	0.984	2678	10	-2
>3% discordance														
N18-15D.4-1	125	74	0.62	0.00	0.1857	0.42	14.52	3.3	0.567	3.2	0.992	2705	7	-9
N18-15D.5-1	175	124	0.73	0.07	0.1848	0.71	14.32	3.1	0.562	3.0	0.973	2696	12	-8
15BUDD138 (mount N18-15C)														

Mount grain-spot	ppm U	ppm Th	$^{232}Th/^{238}U$	%com 206Pb	$^{207}Pb^*/^{206}Pb^*$	% 1σ err	$^{207}Pb^*/^{235}U$	% 1σ err	$^{206}Pb^*/^{238}U$	% 1σ err	err corr	$^{207}Pb/^{206}Pb$ Age (Ma)	1σ err	% Disc.
<5% discordance and <0.3% common Pb														
N18-15C.22-1	136	83	0.63	0.04	0.1857	0.37	13.15	3.0	0.513	2.9	0.992	2705	6	+2
N18-15C.26-1	174	128	0.76	0.04	0.1853	0.32	13.64	3.3	0.534	3.3	0.995	2701	5	-3
N18-15C.3-1	103	78	0.78	0.07	0.1851	0.44	13.27	3.5	0.520	3.5	0.992	2699	7	0
N18-15C.17-1	175	120	0.71	0.03	0.1849	0.34	13.44	3.2	0.527	3.2	0.994	2698	6	-1
N18-15C.6-1	250	173	0.71	0.02	0.1849	0.28	13.03	3.2	0.511	3.2	0.996	2697	5	+2
N18-15C.21-1	85	39	0.47	-0.03	0.1847	0.48	13.40	3.0	0.526	3.0	0.987	2696	8	-1
N18-15C.4-1	35	15	0.44	0.23	0.1846	0.85	12.77	3.5	0.502	3.4	0.969	2694	14	+3
N18-15C.7-1	189	113	0.61	0.08	0.1845	0.33	13.35	3.4	0.525	3.3	0.995	2694	5	-1
N18-15C.9-1	91	51	0.58	0.10	0.1845	0.49	13.92	3.3	0.547	3.3	0.989	2694	8	-5
N18-15C.10-1	89	48	0.55	0.02	0.1845	0.49	13.67	3.6	0.537	3.5	0.990	2694	8	-4
N18-15C.16-1	178	111	0.64	0.02	0.1843	0.35	12.64	3.6	0.498	3.6	0.995	2692	6	+4
N18-15C.14-1	181	123	0.70	0.03	0.1842	0.32	12.86	3.0	0.506	2.9	0.994	2691	5	+2
N18-15C.15-1	65	29	0.47	0.12	0.1841	0.57	13.08	3.3	0.515	3.2	0.99	2690	9	1
N18-15C.18-1	238	180	0.78	0.01	0.1840	0.28	13.16	3.1	0.519	3.0	0.996	2689	5	0
N18-15C.5-1	264	195	0.77	0.01	0.1840	0.27	13.10	3.1	0.516	3.0	0.996	2689	4	0
N18-15C.20-1	53	21	0.41	0.040	0.184	0.63	13.42	3	0.529	2.9	0.98	2689	10	-2
N18-15C.1-1	84	38	0.47	0.02	0.1839	0.46	13.08	2.9	0.516	2.8	0.987	2688	8	0
N18-15C.11-1	165	98	0.61	0.09	0.1839	0.36	13.30	3.4	0.525	3.4	0.994	2688	6	-1
N18-15C.8-1	169	98	0.60	0.05	0.1838	0.35	13.33	3.0	0.526	2.9	0.993	2688	6	-2
N18-15C.24-1	91	74	0.84	0.00	0.1838	0.42	13.17	3.0	0.520	3.0	0.990	2687	7	-1
N18-15C.12-1	102	59	0.60	0.04	0.1837	0.82	13.36	3.3	0.528	3.2	0.968	2686	14	-2
N18-15C.19-1	304	264	0.90	0.06	0.1836	0.27	12.95	3.2	0.511	3.2	0.997	2686	4	+1
N18-15C.23-1	60	24	0.42	0.09	0.1833	0.59	13.00	2.9	0.514	2.9	0.980	2683	10	0
N18-15C.25-1	94	66	0.73	0.12	0.1828	0.47	13.08	3.0	0.519	3.0	0.988	2678	8	-1
N18-15C.13-1	51	25	0.50	0.24	0.1822	0.68	12.82	3.0	0.510	2.9	0.973	2673	11	+1

>5% discordance or >0.3% common Pb														
N18-15C.2-1	52	21	0.43	1.77	0.1869	2.85	13.19	4.2	0.512	3.1	0.739	2715	47	+2
N18-15C.27-1	192	171	0.92	0.12	0.1826	0.36	12.12	3.6	0.481	3.6	0.995	2676	6	+6

15BUDD120 -226.04 (mount N19-07, 08)

Mount grain-spot	ppm U	ppm Th	$^{232}Th/^{238}U$	%com 206Pb	$^{207}Pb^*/^{206}Pb^*$	% 1σ err	$^{207}Pb^*/^{235}U$	% 1σ err	$^{206}Pb^*/^{238}U$	% 1σ err	err corr	$^{207}Pb/^{206}Pb$ Age (Ma)	1σ err	% Disc.
<5% discordance														
N19-08.K.1-1	156	163	1.08	0.070	0.1859	0.51	13.25	2.8	0.517	2.7	0.98	2707	8	1
N19-07.G.1-1	107	85	0.82	0.09	0.1857	0.61	13.39	3.3	0.523	3.2	0.982	2704	10	0
N19-08.I.1-1	149	158	1.10	0.13	0.1853	0.57	12.86	2.7	0.504	2.7	0.978	2701	9	+3
N19-07.C.1-1	298	445	1.55	0.16	0.1844	0.36	12.80	2.4	0.504	2.4	0.989	2692	6	+3
N19-08.A.1-1	134	110	0.84	0.10	0.1843	0.58	12.66	4.0	0.498	3.9	0.989	2692	10	+4
N19-07.B.1-1	107	75	0.73	0.07	0.1841	0.65	13.05	2.5	0.514	2.4	0.965	2690	11	+1
N19-07.L.1-2	60	23	0.39	0.08	0.1840	0.79	12.87	3.3	0.507	3.2	0.971	2689	13	+2
N19-07.L.1-1	83	46	0.58	-0.04	0.1835	0.70	12.84	3.1	0.507	3.0	0.974	2685	12	+2
N19-07.H.1-1	115	85	0.76	0.09	0.1834	0.60	13.08	3.2	0.517	3.1	0.982	2684	10	0
N19-07.C.2-1	126	93	0.76	0.37	0.1828	0.65	12.91	2.6	0.512	2.5	0.968	2678	11	+1
N19-07.J.1-1#	153	156	1.05	0.19	0.1804	0.64	12.75	2.4	0.512	2.3	0.962	2657	11	0
N19-08.H.1-1#	177	205	1.20	0.11	0.1789	1.04	11.99	3.9	0.486	3.7	0.963	2643	17	+4
N19-07.C.2-2#	120	88	0.76	0.10	0.1779	1.29	11.87	2.7	0.484	2.3	0.875	2633	21	+4
>5% discordance														
N19-03B.1-1	497	1322	2.75	0.39	0.2230	0.72	7.37	4.9	0.240	4.9	0.989	3003	12	+60
N19-07.J.2-2	130	131	1.04	0.11	0.1848	0.62	10.74	5.0	0.422	5.0	0.992	2697	10	+19
N19-07.C.2-3	196	171	0.9	0.200	0.1839	0.57	11.96	2.9	0.472	2.8	0.98	2688	9	9
N19-08.G.1-1	124	113	0.94	0.09	0.1833	0.57	13.76	1.4	0.544	1.3	0.918	2683	9	-5
N19-07.A.1-2	107	98	0.95	0.14	0.1832	0.95	12.03	2.9	0.476	2.7	0.944	2682	16	+8
N19-07.K.1-1	128	115	0.93	0.26	0.1832	0.62	12.14	2.6	0.481	2.6	0.972	2682	10	+7
N19-08.C.1-1	344	359	1.08	0.03	0.1826	0.57	12.21	3.5	0.485	3.4	0.987	2676	9	+6

N19-08.J.1-1	113	77	0.70	0.23	0.1779	1.21	11.47	3.1	0.468	2.8	0.918	2633	20	+7
N19-07.A.1-1	430	422	1.01	0.18	0.1777	0.63	11.23	5.0	0.458	5.0	0.992	2632	10	+9
N19-08.E.1-1	186	148	0.82	0.17	0.1740	0.95	10.91	4.8	0.455	4.7	0.980	2597	16	+8
N19-07.J.2-1	136	134	1.01	0.41	0.1725	1.48	9.66	5.4	0.406	5.2	0.962	2582	25	+18

15BUDD120 - 228.42 (mount N19-09, 10)

Mount grain-spot	ppm U	ppm Th	$^{232}Th/^{238}U$	%com 206Pb	$^{207}Pb^*/^{206}Pb^*$	% 1σ err	$^{207}Pb^*/^{235}U$	% 1σ err	$^{206}Pb^*/^{238}U$	% 1σ err	err corr	$^{207}Pb/^{206}Pb$ Age (Ma)	1σ err	% Disc.
<5% discordant and common Pb <0.1%														
N19-09.C.1-1	107	76	0.73	0.00	0.1852	0.64	12.99	1.9	0.509	1.8	0.940	2700	11	+2
N19-09.G.2-1	178	184	1.06	0.01	0.1850	0.9	13.1	2.1	0.514	1.9	0.9	2698	15	1
N19-10.D.2-1	162	181	1.16	-0.03	0.1849	0.50	12.77	2.3	0.501	2.3	0.980	2697	8	+4
N19-10.I.1-3	252	210	0.86	-0.04	0.1849	0.50	12.76	1.3	0.501	1.2	0.920	2697	8	+4
N19-09.G.1-1	215	273	1.31	0.050	0.1846	0.47	12.96	2	0.509	1.9	0.97	2695	8	2
N19-10.I.1-1	226	181	0.83	0.05	0.1842	0.47	13.15	1.6	0.518	1.5	0.960	2691	8	0
N19-10.F.1-1	139	122	0.90	0.00	0.1842	0.60	12.92	1.8	0.509	1.7	0.940	2691	10	+2
N19-09.F.1-1	128	113	0.91	0.03	0.1840	0.62	13.35	2.8	0.526	2.8	0.980	2689	10	-2
N19-10.G.1-1	177	164	0.96	0.08	0.1836	0.56	12.93	1.7	0.511	1.6	0.940	2686	9	+1
>5% discordant or common Pb >0.1%														
N19-10.H.1-1	132	109	0.85	-0.03	0.1884	0.61	13.05	1.5	0.502	1.3	0.910	2728	10	+5
N19-10.D.1-1	49	33	0.70	-0.14	0.1875	1.06	12.36	2.3	0.478	2.0	0.890	2721	17	+9
N19-10.I.1-2	305	289	0.98	0.33	0.1868	1.39	12.66	2.8	0.491	2.4	0.870	2715	23	+6
N19-10.E.1-1	152	138	0.93	0.02	0.1854	0.59	12.55	2.7	0.491	2.6	0.980	2701	10	+6
N19-10.C.1-1	143	150	1.08	-0.02	0.1842	0.59	12.14	2.2	0.478	2.1	0.960	2691	10	+8
N19-09.H.1-1	146	133	0.94	0.09	0.1823	0.57	12.23	2.3	0.486	2.2	0.970	2674	9	+5
N19-10.A.1-1	108	86	0.82	0.61	0.1815	0.92	12.33	1.6	0.493	1.4	0.830	2666	15	+4
N19-10.B.1-1	115	86	0.77	0.07	0.1799	1.2	11.33	8.5	0.457	8.4	0.99	2652	20	10
N19-10.J.1-1	223	247	1.14	0.17	0.1789	0.46	12.01	2.5	0.487	2.4	0.980	2643	8	+4

Penzance granite (mount N18-06)

Mount grain-spot	ppm U	ppm Th	$^{232}Th/^{238}U$	%com 206Pb	$^{207}Pb^*/^{206}Pb^*$	% 1σ err	$^{207}Pb^*/^{235}U$	% 1σ err	$^{206}Pb^*/^{238}U$	% 1σ err	err corr	$^{207}Pb/^{206}Pb$ Age (Ma)	1σ err	% Disc.
N18-06B.16-1	476	378	0.82	0.43	0.1830	0.34	12.10	1.1	0.480	1.1	0.960	2676	6	+7
N18-06A.4-1	534	246	0.48	0.11	0.1790	0.25	13.20	1.1	0.536	1.1	0.970	2640	4	-6
N18-06C.9-1	462	381	0.85	0.75	0.1750	0.56	10.90	1.2	0.454	1.1	0.890	2602	9	+9
N18-06C.1-1	513	335	0.68	0.24	0.1750	0.29	12.20	1.1	0.509	1.1	0.970	2601	5	-2
N18-06A.7-1	475	250	0.54	0.46	0.1740	0.36	11.10	1.2	0.465	1.1	0.950	2593	6	+6
N18-06A.10-1	502	252	0.52	0.67	0.1730	0.37	11.30	1.1	0.475	1.1	0.950	2589	6	+4
N18-06C.12-1	542	451	0.86	0.28	0.1730	0.31	11.00	1.1	0.463	1.1	0.960	2583	5	+6
N18-06A.3-1	401	295	0.76	0.64	0.1700	0.61	11.00	1.3	0.469	1.1	0.870	2554	10	+3
N18-06B.8-1	641	350	0.56	0.31	0.1680	0.28	11.30	1.1	0.486	1.1	0.970	2541	5	-1
N18-06A.3-2	535	555	1.07	0.97	0.1610	0.43	9.50	1.3	0.429	1.2	0.940	2463	7	+8
N18-06C.5-1	594	344	0.60	0.20	0.1610	0.66	9.90	1.3	0.449	1.1	0.850	2463	11	+4
N18-06C.2-1	540	313	0.60	0.38	0.1550	0.85	8.80	1.6	0.414	1.3	0.840	2401	14	+8
N18-06B.2-1	556	356	0.66	0.38	0.1510	0.35	8.6	1.1	0.413	1.1	0.95	2352	6	6
N18-06A.19-1	601	363	0.62	0.95	0.1460	0.44	8.00	1.2	0.394	1.1	0.930	2304	8	+8
N18-06C.6-1	622	445	0.74	0.50	0.1410	0.41	7.50	1.2	0.383	1.1	0.930	2243	7	+8
N18-06A.8-1	568	354	0.64	1.910	0.141	0.58	8.1	1.2	0.416	1.1	0.88	2237	10	0
N18-06A.14-1	591	360	0.63	0.96	0.1410	0.48	7.70	1.2	0.395	1.1	0.910	2234	8	+5
N18-06B.12-1	605	339	0.58	0.54	0.1380	0.38	7.50	1.1	0.393	1.1	0.940	2198	7	+3
N18-06A.2-1	623	442	0.73	1.87	0.1370	1.43	6.70	1.8	0.357	1.0	0.580	2190	25	+12
N18-06B.11-1	601	850	1.46	0.94	0.1370	0.47	7.30	1.2	0.387	1.1	0.920	2185	8	+4
N18-06C.8-1	652	442	0.70	0.61	0.1330	0.42	6.80	1.1	0.369	1.1	0.930	2138	7	+6
N18-06B.9-1	676	514	0.79	0.86	0.1320	0.44	6.80	1.2	0.374	1.1	0.920	2127	8	+4
N18-06A.1-1	830	539	0.67	2.80	0.1200	1.62	5.70	1.9	0.347	1.0	0.530	1951	29	+2
N18-06B.13-1	801	567	0.73	0.74	0.1180	0.70	5.30	1.4	0.324	1.2	0.860	1934	12	+7

young outlier: omitted from age calculation

Table 3: SHRIMP isotopic data for monazite from the Penzance granite (mounts N18-06, 16)

Penzance granite (mount N18-06, 16)																
Mount grain-spot	ppm U	ppm Th	$^{232}Th/^{238}U$	f206 (%)	f208 (%)	$^{207}Pb^*/^{206}Pb^*$	± 1σ err	$^{206}Pb^*/^{238}U$	± 1σ err	$^{207}Pb^*/^{235}U$	± 1σ err	$^{208}Pb^*/^{232}Th$	± 1σ err	$^{207}Pb/^{206}Pb$ Age (Ma)	1σ err	% Disc.
≤5% discordance and <0.5% f206																
N18-06B.B-5	207	12986	63.00	-0.02	0.00	0.1865	0.0022	0.5074	0.0114	13.044	0.3320	0.137	0.0026	2711	19	+2
N18-16C.8-3	629	12531	20.00	-0.01	-0.01	0.1863	0.0010	0.5232	0.0101	13.435	0.2720	0.148	0.0032	2709	9	0
N18-16A.1-6	508	15332	30.00	-0.06	-0.02	0.1862	0.0014	0.5092	0.0069	13.075	0.2050	0.142	0.0030	2709	12	+2
N18-06B.G-2	215	14282	66.00	0.02	0.00	0.1855	0.0022	0.5170	0.0097	13.224	0.2950	0.141	0.0026	2703	19	+1
N18-06B.A-6	789	32172	41.00	0.00	0.00	0.1853	0.0015	0.5092	0.0090	13.010	0.2560	0.140	0.0029	2701	13	+2
N18-16A.1-1	448	11587	26.00	0.00	0.00	0.1852	0.0026	0.5288	0.0091	13.499	0.3020	0.152	0.0032	2700	23	-1
N18-06B.B-7	310	11884	38.00	-0.04	-0.01	0.1851	0.0018	0.5140	0.0088	13.119	0.2620	0.138	0.0028	2699	16	+1
N18-06B.G-5	345	16469	48.00	-0.06	-0.01	0.1847	0.0019	0.4933	0.0085	12.563	0.2540	0.136	0.0024	2696	17	+4
N18-06B.A-5	573	19934	35.00	0.43	0.11	0.1844	0.0017	0.5213	0.0094	13.257	0.2710	0.144	0.0028	2693	15	0
N18-06B.K-2	1134	74444	66.00	0.34	0.04	0.1842	0.0016	0.4894	0.0085	12.430	0.2430	0.136	0.0027	2691	14	+5
N18-16B.6-2	926	62647	68.00	0.05	0.01	0.1842	0.0010	0.4854	0.0078	12.327	0.2130	0.142	0.0030	2691	9	+5

N18-16D.15-1	602	14098	23.00	0.02	0.01	0.1841	0.0009	0.5092	0.0083	12.929	0.2250	0.147	0.0030	2690	8	+1
N18-16C.8-5	664	14242	21.00	-0.05	-0.02	0.1841	0.0012	0.5198	0.0080	13.193	0.2240	0.141	0.0030	2690	11	0
N18-16C.8-6	466	11320	24.00	0.01	0.00	0.1840	0.0013	0.4927	0.0118	12.502	0.3140	0.144	0.0029	2689	12	+4
N18-16D.16-1	1039	19243	19.00	0.03	0.01	0.1839	0.0007	0.5021	0.0120	12.729	0.3110	0.147	0.0033	2688	6	+2
N18-16G.18-1	1002	69393	69.00	0.32	0.04	0.1838	0.0009	0.4905	0.0102	12.430	0.2690	0.149	0.0035	2687	8	+4
N18-06B.A-7	1097	38290	35.00	0.01	0.00	0.1835	0.0014	0.5314	0.0097	13.442	0.2700	0.146	0.0029	2685	13	-2
N18-06B.G-7	216	12340	57.00	0.07	0.01	0.1832	0.0020	0.5244	0.0095	13.249	0.2840	0.143	0.0028	2682	18	-1
N18-16D.14-1	129	6945	54.00	-0.03	-0.01	0.1832	0.0019	0.5022	0.0137	12.685	0.3700	0.152	0.0032	2682	17	+2
N18-16A.1-4	279	15220	54.00	-0.01	0.00	0.1831	0.0016	0.5303	0.0114	13.390	0.3120	0.152	0.0032	2681	14	-2
N18-06B.B-6	308	10496	34.00	0.03	0.01	0.1830	0.0018	0.4883	0.0107	12.323	0.2980	0.137	0.0028	2681	16	+4
N18-06B.G-4	178	11404	64.00	0.04	0.01	0.1828	0.0023	0.4965	0.0095	12.515	0.2870	0.139	0.0026	2679	20	+3
N18-06B.K-3	895	38759	43.00	0.02	0.00	0.1827	0.0015	0.4817	0.0083	12.135	0.2340	0.136	0.0026	2678	13	+5
N18-16A.1-3	515	14308	28.00	-0.01	0.00	0.1827	0.0010	0.5205	0.0105	13.111	0.2760	0.147	0.0032	2677	9	-1
N18-16C.8-1	638	13479	21.00	0.00	0.00	0.1824	0.0014	0.5182	0.0072	13.035	0.2110	0.147	0.0032	2675	13	-1
N18-06B.A-1	863	31292	36.00	-0.02	0.00	0.1824	0.0015	0.5070	0.0088	12.750	0.2490	0.149	0.0030	2675	14	+1
N18-06B.B-3	296	11665	39.00	-0.09	-0.02	0.1823	0.0020	0.5334	0.0095	13.405	0.2850	0.144	0.0029	2674	18	-3
N18-06B.B-1	188	10313	55.00	0.05	0.01	0.1821	0.0023	0.5124	0.0099	12.868	0.2980	0.144	0.0026	2672	21	0
N18-06B.G-3	475	24369	51.00	-0.03	-0.01	0.1821	0.0017	0.4923	0.0083	12.363	0.2420	0.136	0.0026	2672	15	+3
N18-16A.6-1	1052	69743	66.00	-0.01	0.00	0.1821	0.0007	0.5010	0.0077	12.581	0.2020	0.150	0.0033	2672	6	+2

N18-16C.8-2	605	11778	19.00	0.00	0.00	0.1821	0.0010	0.5212	0.0089	13.084	0.2390	0.149	0.0030	2672	9	-1
N18-16C.10-4	587	20801	35.00	0.02	0.00	0.1820	0.0011	0.5089	0.0096	12.772	0.2570	0.146	0.0033	2671	10	+1
N18-16C.10-1	466	14728	32.00	0.10	0.03	0.1819	0.0011	0.5268	0.0110	13.210	0.2900	0.153	0.0039	2670	10	-2
N18-06B.B-2	202	9808	49.00	0.22	0.04	0.1812	0.0022	0.5116	0.0094	12.779	0.2860	0.141	0.0027	2664	20	0
N18-16C.8-4	636	13910	22.00	0.02	0.01	0.1810	0.0010	0.5352	0.0069	13.353	0.1920	0.144	0.0030	2662	9	-4
N18-16D.13-1	389	6592	17.00	0.09	0.04	0.1808	0.0011	0.5403	0.0104	13.471	0.2760	0.155	0.0034	2661	10	-5
N18-06B.D-1	362	26423	73.00	0.04	0.00	0.1808	0.0018	0.4927	0.0099	12.282	0.2780	0.139	0.0026	2660	16	+3
N18-16C.10-3	557	15536	28.00	0.07	0.02	0.1805	0.0012	0.5212	0.0087	12.968	0.2360	0.142	0.0030	2657	11	-2
≥5% discordance and/or ≥0.5% 4f206																
N18-06A.N-3	115	12090	105.00	1.31	0.09	0.1942	0.0046	0.3399	0.0074	9.100	0.2920	0.120	0.0024	2778	38	+32
N18-06B.A-4	484	26279	54.00	0.98	0.17	0.1903	0.0024	0.4979	0.0106	13.063	0.3280	0.134	0.0025	2745	21	+5
N18-06B.E-1	142	5608	40.00	2.70	0.69	0.1879	0.0044	0.5326	0.0107	13.801	0.4280	0.132	0.0024	2724	39	-1
N18-06B.K-1	440	31841	72.00	0.93	0.12	0.1852	0.0025	0.4438	0.0078	11.331	0.2530	0.120	0.0023	2700	22	+12
N18-06B.G-1	173	10873	63.00	0.06	0.01	0.1843	0.0025	0.4764	0.0124	12.104	0.3560	0.133	0.0027	2692	22	+7
N18-06B.B-8	245	13623	56.00	-0.03	-0.01	0.1831	0.0020	0.4666	0.0083	11.780	0.2490	0.123	0.0022	2681	18	+8
N18-16A.1-2	288	14906	52.00	0.08	0.01	0.1819	0.0015	0.5669	0.0127	14.220	0.3420	0.160	0.0036	2670	14	-8
N18-06B.A-8	349	26244	75.00	2.02	0.21	0.1818	0.0056	0.3843	0.0130	9.635	0.4430	0.122	0.0029	2670	51	+21
N18-06B.B-4	143	9993	70.00	0.14	0.02	0.1816	0.0027	0.4682	0.0095	11.725	0.2960	0.128	0.0025	2668	24	+7
N18-06B.G-8	220	14795	67.00	0.26	0.04	0.1814	0.0020	0.4741	0.0101	11.857	0.2890	0.128	0.0025	2666	18	+6

N18-16B.6-3	843	59533	71.00	0.07	0.01	0.1812	0.0010	0.4463	0.0081	11.152	0.2140	0.140	0.0030	2664	9	+11
N18-06A.N-1	76	9566	125.00	1.76	0.15	0.1811	0.0049	0.4884	0.0112	12.191	0.4330	0.110	0.0023	2663	45	+4
N18-06B.G-6	281	13360	48.00	0.06	0.01	0.1810	0.0018	0.4676	0.0182	11.670	0.4720	0.137	0.0027	2662	17	+7
N18-16C.10-2	629	16612	26.00	0.12	0.03	0.1802	0.0019	0.4040	0.0213	10.040	0.5400	0.133	0.0031	2655	17	+18
N18-06B.A-2	814	29448	36.00	1.02	0.23	0.1763	0.0020	0.4132	0.0093	10.042	0.2560	0.124	0.0024	2618	19	+15
N18-06B.A-3	638	36168	57.00	1.50	0.23	0.1753	0.0038	0.4980	0.0173	12.034	0.4960	0.136	0.0027	2609	36	0
N18-16G.23-1	147	17544	120.00	0.89	0.04	0.1270	0.0034	0.2374	0.0127	4.155	0.2490	0.094	0.0021	2056	47	+33
N18-16G.23-2	456	36602	80.00	1.94	0.08	0.0971	0.0042	0.1036	0.0017	1.387	0.0640	0.067	0.0019	1569	81	+59

Figure 1: Location of the ~~TB~~Teutonic Bore Camp on a map showing the major subdivisions of the Eastern Goldfields Superterrane, Yilgarn Craton, Western Australia. The town of Leonora is indicated by a black diamond. ~~Also~~ The inset map shows the location of the three deposits (Teutonic Bore, Jaguar and Bentley) and the sampled Penzance granite on the 1:500 000 State interpreted bedrock geological map from the GSWA online database GeoVIEW.WA (2016).

Figure 2: A) Schematic geological model for the ~~TB~~Teutonic Bore Ceamp showing the position of each deposit within the stratigraphic sequence and illustrating the sub-seafloor replacement feature of the VHMS mineralisation and possible relationship of the host stratigraphy and the intrusive leucogranite described by Hallberg and Thompson (1985). B) Simplified stratigraphic sequence and stratigraphical subdivisions for each of the three deposits within the ~~TB~~Teutonic Bore Camp (Belford, 2010; Belford et al., 2015; Chen et al., 2015; Das, 2018 and complemented by this study; stratigraphic sequence modified from Hallberg and Thompson, 1985; Macklin, 2010; Parker et al., 2017). The U-Pb zircon age, drillhole and depth for the dacite are from Nelson (1995).

Figure 3: U-Pb Concordia diagram showing the SHRIMP spot analyses and mean $^{207}Pb/^{206}Pb$ ages for: A) Footwall rhyolite (unit I) – Bentley footwall zircons (sample 15BUDD78; mount N18-15D). B) Footwall rhyolite (unit I) – Bentley footwall zircons (sample 15BUDD138; mount N18-15C). C) Transitional andesite (unit III) – Bentley hangingwall zircons (sample 15BUDD120 - 226.04m; mount N19-07, 08). D) Transitional andesite (unit III) – Bentley hangingwall zircons (sample 15BUDD120 - 228.42m; mount N19-09, 10). E) Penzance granite zircons (mount N18-06, 16). F) Penzance granite monazites (mounts N18-06, N18-16). Error ellipses are ±1σ.

Figure 4: Cathodoluminescence electron microscope images of zircon grains separated from the footwall rhyolite (unit I) at the Bentley deposit, and analysed with SHRIMP and/or LA-SS-ICPMS. The location of the spots are indicated within each grain as well as the name (and $^{207}Pb/^{206}Pb$ age for SHRIMP spots).

Figure 5: Cathodoluminescence electron microscope images of zircon grains separated from the transitional andesite (unit III) at the Bentley deposit, and analysed with SHRIMP or LA-SS-ICPMS. The location of the spots are indicated within each grain as well as the name (and $^{207}Pb/^{206}Pb$ age and discordance for SHRIMP spots).

Figure 6: Cathodoluminescence images of zircon grains separated from the Penzance granite, and analysed with SHRIMP and/or LA-SS-ICPMS. The location of the spots are indicated within each grain as well as the name (and $^{207}Pb/^{206}Pb$ age and discordance for SHRIMP spots). The zircons exhibit cavities, fractures, disruption of the original zoning and/or development of dark CL areas.

Figure 7: Backscatter electron images of four monazite grains separated from the Penzance granite, and analysed with SHRIMP. The location of the spots are indicated within each grain as well as the name, $^{207}Pb/^{206}Pb$ ages and discordance. Most crystals present visible regular euhedral zoning, typical of magmatic monazite.

Figure 8: $\varepsilon Hf_{(i)}$ (CHUR) vs. $^{207}Pb/^{206}Pb$ age (Ma) plot for zircon from the Penzance granite, the volcanic sequence at Bentley and zircons from other magmatic rocks within the Kurnalpi Terrane (Wyche et al., 2012). The errors for $\varepsilon Hf_{(i)}$ are 1σ. The zircon data from this study are plotted with the interpreted $^{207}Pb/^{206}Pb$ magmatic age for each sample, which is also used in the calculation of the $\varepsilon Hf_{(i)}$. The thick black line labelled DM represents εHf of depleted mantle over time.

Figure 9: MREE and HREE patterns for zircon from the Penzance granite and the volcanic sequence at Bentley, normalized to chondrite (Anders and Grevesse, 1989). The lower graph is a compilation of the four results.

Figure 10: Graph of probability density, assuming a normal distribution, for the zircon $^{207}Pb/^{206}Pb$ mean ages obtained in this study and the previous age from Nelson (1995), with the mean age indicated by a dashed line for each sample. Each age is represented both by the probability plot and by a graph bar. In both cases, the different shades represent 1σ or 2σ for each age, as indicated in the legend. The thick red line marks the maximum age of the mineralisation. The unpublished TIMS age of the footwall rhyolite (unit I) (Das, 2018) is represented only in bar graph form.

Figure 11: Zr vs Y plot for the volcanic rocks that host the Jaguar deposit (Belford et al., 2015) and two samples from the Penzance granite from Geoscience Australia's OZCHEM database (Sedgmen et al., 2007). The filled square represents a sample collected from the same quarry that was sampled for the geochemical studies (Sample id 96969076). The roman numerals indicates the stratigraphical subdivisions from this study and their correspondence to the facies described by Belford et al. (2015). The boundaries and indicated Zr/Y ratios that define tholeiitic, transitional and calc-alkaline fields are from Barrett and MacLean (1994).

- The Teutonic Bore volcanics are broadly coeval to the Penzance granite
- The age of the Penzance granite is ca. 2682 Ma
- The Jaguar volcanics and the ore at the Teutonic Bore camp are ≤ ca. 2693 Ma
- The Penzance granite possibly supplied heat and metals to the mineralisation
- Exploration in the EGS should focus on fluid pathways of HFSE-enriched granites

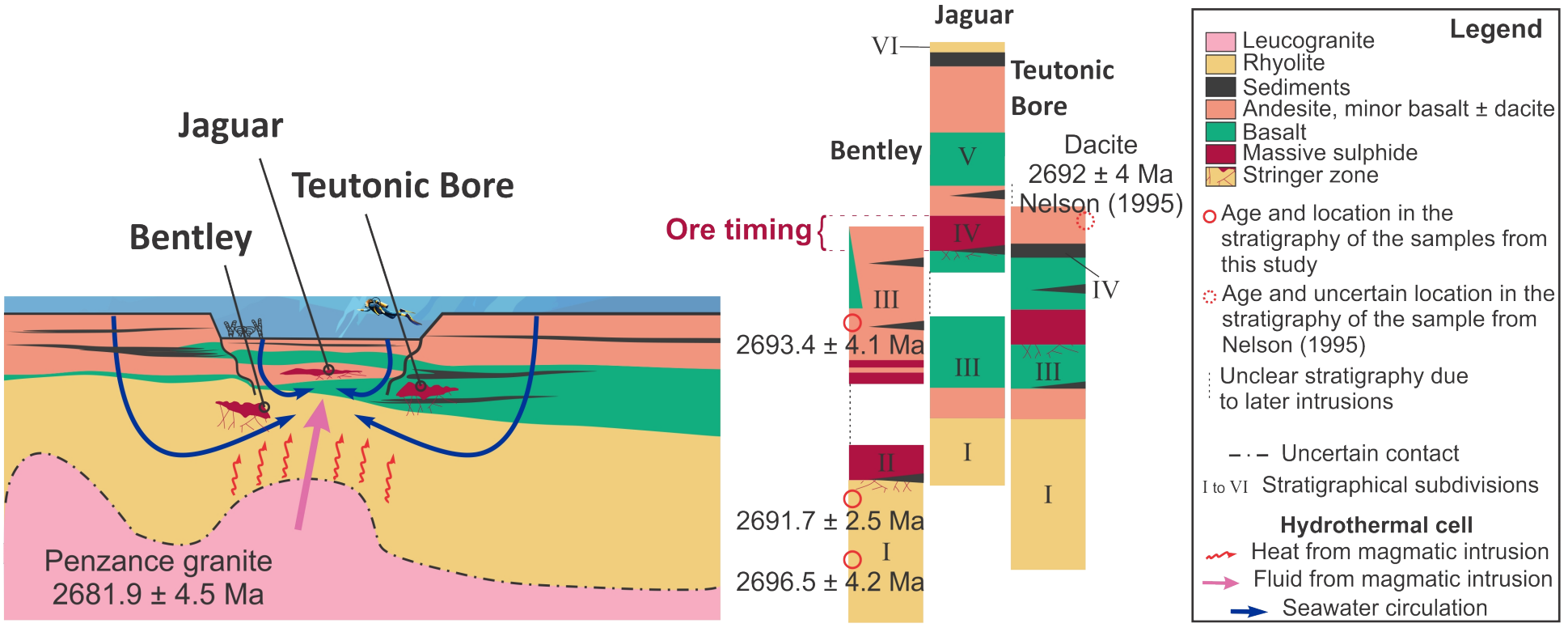
Jaguar
Teutonic Bore
Bentley
Penzance granite
2681.9 ± 4.5 Ma
Jaguar
VI
Teutonic
Bore
Bentley
V
Dacite
2692 ± 4 Ma
Nelson (1995)
Ore timing
IV
IV
III
2693.4 ± 4.1 Ma
III
III
II
I
I
2691.7 ± 2.5 Ma
I
2696.5 ± 4.2 Ma
Legend
Leucogranite
Rhyolite
Sediments
Andesite, minor basalt ± dacite
Basalt
Massive sulphide
Stringer zone
Age and location in the stratigraphy of the samples from this study
Age and uncertain location in the stratigraphy of the sample from Nelson (1995)
Unclear stratigraphy due to later intrusions
Uncertain contact
I to VI Stratigraphical subdivisions
Hydrothermal cell
Heat from magmatic intrusion
Fluid from magmatic intrusion
Seawater circulation

The 4D evolution of the Teutonic Bore Camp VHMS deposits, Yilgarn Craton, Western Australia

Vitor R. Barrote[1,2,3], Neal J. McNaughton[1], Svetlana G. Tessalina[1], Noreen J. Evans[1,2], Cristina Talavera[1,4], Jian-Wei Zi[1,5], Bradley J. McDonald[1,2]

1- John de Laeter Centre and The Institute for Geoscience Research (TIGeR), Curtin University, Kent St, Bentley, WA 6102, Australia

2- School of Earth and Planetary Sciences, Curtin University, Kent St, Bentley, WA 6102, Australia

3- School of Earth, Atmosphere and Environment, Monash University, Clayton, Victoria 3800, Australia

4- School of Geosciences, University of Edinburgh, The King's Building, James Hutton Road, EH9 3FE, Edinburgh, UK

5- State Key Lab of Geological Processes and Mineral Resources, China University of Geosciences

Declarations of interest: none

ABSTRACT

The Teutonic Bore Camp, comprised of the Teutonic Bore, Jaguar and Bentley deposits, is one of the most significant volcanic-hosted massive sulphide (VHMS) camps in Western Australia. Despite being extensively studied, only recently there have been advances in the understanding of the mechanism that drove the formation of mineralisation. It has been recognized by recent studies that the volcanic-hosted deposits from the Teutonic Bore Camp represent replacement-type VHMS systems, with significant input of fluids and metals from a magmatic source. This paper tests the existing hypothesis that the nearby Penzance granite acted as the metals source and/or thermal engine driving the development of these ore deposits.

New age constraints on the formation of the host volcanic sequence at the Bentley deposit and the crystallization of the Penzance granite allows for the construction of a 4D evolutionary model for the ore system. A new U-Pb SHRIMP monazite age of 2681.9 ± 4.5 Ma indicates that the Penzance granite post-dates the host stratigraphy at Bentley (ca. 2693 Ma) and is probably coeval with mineralisation. All zircons (Penzance, Bentley units I and III) have very similar $\varepsilon Hf_{(i)}$, with most values between -1 and +6, slightly higher than the $\varepsilon Hf_{(i)}$ of zircons from other granites and volcanics within the Kurnalpi Terrain, and indicative of juvenile sources. The mean Th/U ratios are ~0.7 and ~0.6 for the Penzance and Bentley zircons, respectively. All zircons have similar $Ce/Nd_{(CN)}$ ratios. The chemical similarities between the zircons from the granite and the volcanic rocks at Bentley support a shared magmatic source between the Penzance and the Teutonic Bore Camp sequence. The Penzance granite is the likely source of heat, and potentially metals, which drove the VHMS mineralisation at the Teutonic Bore Camp.

Keywords: Penzance; Teutonic Bore; Volcanic-hosted massive sulphide; Archean; Geochronology; 4D modelling

1 INTRODUCTION

Using an extensive database of compiled whole-rock geochemistry and U-Pb geochronology, Hollis et al (2015) proposed a link between VHMS mineralisation and the emplacement of HFSE-enriched syn-volcanic intrusions, throughout the Archean Yilgarn Craton, including the Eastern Goldfield Superterrane. Despite the apparent geographical and broadly coeval association between VHMS ores and HFSE-enriched intrusions, the identification of a genetic link would benefit from further geochronological and isotopic evidence.

The number of significant VHMS occurrences in the Yilgarn Craton is small compared to other Archean terrains with similar characteristics such as the Superior Province of Canada

(Hollis et al., 2015). Previous studies suggested that this could be due to under-exploration and the use of techniques inappropriate for mineral prospecting in the Yilgarn Craton (Butt et al., 2017; Ellis, 2004; Hollis et al., 2017, 2015; McConachy et al., 2004). Unlike classic VHMS systems, replacement-type VHMS systems, such as those in the Eastern Goldfield Superterrane, do not precipitate onto the seafloor and although some stratigraphic control can be observed within replacement-type mineralisation, it is not an inevitable feature (Doyle and Allen, 2003).

Historically, exploration for VHMS occurrences within the Teutonic Bore area was focused on key stratigraphic horizons. However, the known deposits formed at different stratigraphic positions and show significant differences in the geometry of mineralisation, compared to Teutonic Bore (Chen et al., 2015; Parker et al., 2017). This led to a significant time gap between the discoveries of the Teutonic Bore deposit in 1976, and the Jaguar and Bentley deposits in 2004 and 2008, respectively (Ellis, 2004; Parker et al., 2017).

To better understand this lack of stratigraphic control on the position of orebodies at the Teutonic Bore Camp, and a possible link between high-field-strength-elements (HFSE)-enriched granite emplacement and ore precipitation, this work re-examines and expands the database of geochronology and isotopic/geochemical fingerprints for the igneous rock units. This includes re-assessment of the geochronological data from the nearby HFSE-enriched granite, the Penzance granite (Champion and Cassidy, 2002; Geoscience Australia, 2019), and the volcanic sequence from the Teutonic Bore Camp (Nelson, 1995), with additional U-Pb Sensitive High-Resolution Ion Microprobe (SHRIMP) dating of zircon and monazite.

These geochronological studies are complemented by zircon Hf-isotope and trace element analyses from the Bentley volcanic sequence and Penzance granite, and compilation of detailed stratigraphy, whole-rock geochemistry and sulphur isotope data from previous studies (Belford et al., 2015; Chen et al., 2015; Das, 2018; Isaac, 2015; Sedgmen et al., 2007). The present work combines the improved geochronological constrains presented here to the current 3D

understanding of the geological processes at place, to develop a 4D evolutionary model of the deposits at the Teutonic Bore Camp.

Reliable and precise ages for magmatism and ore-hosting volcanism, combined with traditional and isotopic geochemistry, allows testing of the hypothesis of a genetic relationship between the HFSE-rich Penzance granite and the Teutonic Bore Camp deposits. The results could have implications for future exploration for Precambrian VHMS deposits, not only in the well-established Teutonic Bore Camp, but also in g*reenfields* throughout the Eastern Goldfield Superterrane and, potentially, elsewhere in the Yilgarn Craton.

2 GEOLOGICAL BACKGROUND

2.1 Geology of the Teutonic Bore Camp

The Teutonic Bore, Jaguar and Bentley VHMS deposits, along with several other smaller occurrences, form the Teutonic Bore Camp (Independence Group NL (IGO), 2015). The Teutonic Bore Camp is located near the town of Leonora, within the Kurnalpi Terrane of the Eastern Goldfield Superterrane, Yilgarn Craton (Figure 1). The deposits in the Teutonic Bore Camp are hosted by the Teutonic Bore volcanic complex, which comprises pillow basalt, overlain and interlayered with volcanoclastic units, coherent rhyolite, andesite and thin sedimentary units (Belford et al., 2015; Parker et al., 2017 and references therein). The prefix "meta" is assumed but omitted when addressing the Archean stratigraphic sequence of the Yilgarn Craton, because all rocks are metamorphosed to some extent (Czarnota et al., 2010).

The volcanic stratigraphy and the distribution of the three deposits, as well as other known uneconomic ore bodies, have a NW-SE trend (Figure 1). This trend coincides with the general alignment of regional structures, such as the fault that bounds the Teutonic Bore volcanic complex to the west (Hallberg and Thompson, 1985; Parker et al., 2017).

The stratigraphy at the Teutonic Bore Camp comprises a predominantly laterally continuous lithofacies association between the three deposits (Figure 2A). Therefore, the volcanic sequence that hosts the mineralisation can be broadly subdivided in six units as follow from bottom to top (Figure 2B; Belford et al., 2015; Parker et al., 2017):

I. Footwall Rhyolite: from 200 m to over 1 km thick. Mainly coherent, either massive or flow-banded, with minor breccia (Parker et al., 2017), and with calc-alkaline to transitional magmatic affinity (Belford et al., 2015). This package is footwall to all three deposits.

II. Sedimentary rocks partly derived from the rhyolite, locally coarse but grading to arenite, siltstone and shale. This is the host unit to the Bentley deposit. The thickness range from 0 to 70 m according to Parker et al. (2017)

III. Transitional to tholeiitic basalt/ transitional andesite with thickness between 30 and 170 m, with massive or pillowed habit, commonly intercalated with shale rich sediments (Parker et al., 2017). This package is host to the Teutonic Bore deposit and upper lens at Bentley (e.g.: Flying Spur, Brooklands, Comet: Independence Group NL (IGO), 2015) and overlays the lower orebody at the Bentley deposit (Arnage: Independence Group NL (IGO), 2015). Belford et al. (2015) names this unit Footwall Andesite (FA) and Footwall Basalt (FB), relative to their position to the mineralised zone at Jaguar.

IV. Upper sedimentary horizon (mineralised package from Belford et al., 2015) consists of a complex assemblage of intercalated dacite (called MPD by Belford et al., 2015), conglomerate, pumice-rich breccia, laminated sediment, laminated chert and massive sulphide (Belford et al., 2015). Unit IV marks a geochemical break in magmatic affinity, from tholeiitic/transitional of the underlying basalts/andesites to

calc-alkaline in the overlying lavas. The thickness is typically within 20 to 40 m (Parker et al., 2017).

V. Upper basalt and andesite of calc-alkaline affinity consists of massive and pillowed basalt and andesite lavas with minor volcanic breccias, and intercalated with mostly carbonaceous shales (Belford et al., 2015). The total thickness of this unit ranges between about 200 to 700 m (Parker et al., 2017).

VI. Hangingwall rhyolite: uppermost stratigraphic unit, described by Belford et al. (2015) from a single drillhole. The thickness of this unit is estimated to be between 100 to 500m according to Parker et al. (2017).

The Teutonic Bore volcanic sequence is bounded to the east by a large composite batholith (Figure 1) named the Kent Complex by Champion and Cassidy (2002) and part of the Penzance Supersuite (Hollis et al., 2015). The Penzance Supersuite consists of HFSE-enriched granites with biotite and/or amphibole in quartz and feldspar rich rocks. These granites are characterised by variably elevated total Fe, MgO, Y, LREE, Zr, coupled with low to moderate Al_2O_3, K_2O, Rb, Sr and moderate Na_2O (Champion and Cassidy, 2002).

The relationship between the Penzance granite and the volcanic sequence in the Teutonic Bore Camp area remains unclear. Earlier studies (e.g.: Hallberg and Thompson, 1985) suggest an irregular contact between the granite and the volcanic rocks, with anastomosing veins of granitoid extending into adjacent extrusive rocks and a number of xenoliths of volcanic rocks within the intrusive granite. The Penzance granite is one of several HFSE-enriched intrusions in the Yilgarn Craton that occurs in close proximity to VHMS deposits or occurrences hosted by equally HFSE-enriched volcanics (Hollis et al., 2015).

The Jaguar deposit was classified as a replacement-type VHMS deposit by Belford (2010). This classification relied on evidence including replacement front texture, absence of chimney structures, and rapid emplacement of the host volcanic sequence, according to the criteria

proposed by Doyle and Allen (2003). Later studies (Chen et al., 2015; Das, 2018; Parker et al., 2017) have identified similar textures in Bentley and other smaller occurrences and, consequently, the replacement-type VHMS model is accepted within the Teutonic Bore Camp.

Despite the predominance of sub-seafloor replacement processes, Belford (2010) observed features that indicate possible above seafloor activity. The development of thin beds of translucent chert with colloform intergrowths of chert and sulphide is interpreted as products of a waning hydrothermal system that had vented fluid to the sediment–water interface and deposited precipitates onto the seafloor (Belford et al., 2015). Massive sulphides conformably overlain by, and gradational upwards into, narrow beds of laminated chert intercalated with finely-bedded sulphide-rich mudstone, support the idea of a progressive disruption of the mineral activity and indicate that some sulphide precipitation might have taken place very near or at seafloor (Belford et al., 2015).

The occurrence of massive sulphide clasts in the surrounding breccias and conglomerates, which were the result of rapid erosion and mass flow, indicates that the sulphide body was formed contemporaneously with the deposition of the upper sedimentary horizon (IV) (Belford et al., 2015). Similar features have not been observed in either the Bentley or the Teutonic Bore deposits.

2.2 Geochronology of the Teutonic Bore sequence and the Penzance granite

The SHRIMP zircon age of 2692 ± 4 Ma (Nelson, 1995) is the only published age for the volcanic sequence at the Teutonic Bore Camp and comes from a porphyric dacite with unclear stratigraphic position (Belford et al., 2015). Additionally, Das (2018) reported an ID-TIMS U-Pb age of 2692 ± 1.5 Ma for a sample of coherent Footwall Rhyolite (unit IV) from Jaguar. These analysis remain unpublished and no data table or sample characterization is provided by Das (2018).

The reported ages for the Penzance granite are 2679 ± 8Ma (Champion and Cassidy, 2002) and 2686 ± 9 Ma (Geoscience Australia, 2019, sample ID 96969076). The two ages are derived from the same analyses and calculated from a single dataset for sample ID 96969076. No explanation is provided by either references as to the reason behind the difference in age calculation from a single set of analysis.

3 SAMPLES AND METHODS

3.1 Penzance samples

Samples from the Penzance granite were collected from three different positions within the same quarry (Lat. -28.264050, Long. 121.077888, Penzance Quarry in Figure 1). They were collected from the same quarry as sample ID 96969076 from the Geochron Delivery database of Geoscience Australia (2019). Each one of the three samples was processed separately and treated as different samples, the analyses were combined only in the data processing phase of each technique.

3.2 Bentley samples

Two samples were collected from different positions within the footwall rhyolite (unit I) in the Bentley deposit. Sample 15BUDD78 – 111.60 m was collected from drillhole 15BUDD78 at 111.60 meters depth, from a distal position to the ore. Sample 15BUDD137 – 398.60 m was collected from a higher stratigraphic position within the sequence, a stringer zone to the lower massive sulphide lens, from a different drillhole (15BUDD137).

Two samples (15BUDD120 - 228.42 and 15BUDD120 - 226.04) of the transitional andesite (unit III), were collected from a single drillhole (15BUDD120), within two meters of each other. The transitional andesite at the sampled point is hangingwall to the lower lens (Arnage), but it is in the stringer zone for the upper lens, marked by the occurrence of disseminated sulphides.

3.3 Analytical techniques

Zircon and Monazites were analysed on the SHRIMP II at the John de Laeter Centre, Curtin University (JdLC). Additionally, Zircon Lu–Hf isotopes and rare earth element (REE) abundances were measured over two analytical sessions using laser ablation split stream inductively coupled plasma mass spectrometry (LA-SS-ICPMS). The analyses were conducted in zircons from the same samples that were analysed by SHRIMP, but not necessarily on the same grain or over the same spot as the SHRIMP analysis. Detailed description of the conditions and procedures are provided in Supplementary Material 1.

4 RESULTS

4.1 U-Pb SHRIMP Zircon dating

4.1.1 Footwall rhyolite (unit I) – Bentley Footwall

Fourteen analyses on 14 zircons from sample 15BUDD78 – 111.60 m were performed (Supplementary Material 2). Using only analyses within 3% of concordant yields a mean $^{207}Pb/^{206}Pb$ age of 2696.5 ± 4.2 Ma (95% c.l., n=12; mean square weighted deviation, MSWD=1.04, Figure 3). The average and range of Th/U ratio from the most concordant SHRIMP analyses for this sample are 0.60 and 0.45-0.72, respectively.

A second sample from unit I was dated, twenty-seven analyses from 27 zircons from sample 15BUDD137 – 398.60 m were collected (Supplementary Material 2). The mean $^{207}Pb/^{206}Pb$ age obtained for analyses within 4% of concordant and with <0.3% common Pb was 2691.7 ± 2.5 Ma (95% c.l.; n=25; MSWD=0.95, Figure 3). The average and range of Th/U ratio from the most concordant SHRIMP analyses are 0.63 and 0.41-0.84, respectively.

The CL images of zircons from the two unit I, footwall rhyolite samples show grains with continuous oscillatory zoning and no discernible core and/or rims, with sizes ranging from about 50 to 100 μm (Figure 4). Their morphologies, Th/U and ages are indistinguishable, and

combining the most concordant data, the resulting age of 2692.9 ± 2.1 Ma (95% cl; n=37; MSWD=1.05) is our best estimate of the age of the footwall rhyolite at Bentley.

4.1.2 Transitional andesite (unit III) – Bentley Hangingwall

The samples from the transitional andesite were treated as two separate samples for the geochronology portion of this study. However, these samples were taken 2 meters apart, from the same drillcore (15BUDD120), and were within the same stratigraphic facies. The CL images show zircons with continuous oscillatory zoning, and ranging from 15 to 30 μm in diameter (Figure 5).

Sample 15BUDD120 – 226.04 m yielded 24 dates from 20 zircons. Considering only the 13 results with <5% discordance (Supplementary Material 2), the MSWD is 2.7 and indicates an age spread not consistent with a single age population. Omitting the three youngest ages as statistical outliers probably influenced by diffusional Pb-loss, the remaining population yields a mean age of 2693.2 ± 5.8 Ma (95% cl; n= 10; MSWD=0.88, Figure 3). The average and range of Th/U from the SHRIMP analyses of the more concordant zircons from this sample is 0.90 and 0.39-1.55, respectively.

Sample 15BUDD120 – 228.42 has 18 dates from 16 grains. The ages <5% discordant and <0.1% common Pb yield a mean $^{207}Pb/^{206}Pb$ age of 2693.6 ± 6.0 Ma (95% cl, n=9; MSWD=0.24, Figure 3; Supplementary Material 2). The average and range of Th/U of the more concordant zircons is 0.95 and 0.73-1.31, respectively.

The ages obtained for the two adjacent samples from the same stratigraphical facies agree within error. Hence, the data can be combined to obtain a mean $^{207}Pb/^{206}Pb$ age for the Transitional Andesite (unit III) of 2693.4 ± 4.1 Ma (95% c.l., n=19; MSWD=0.55). The average Th/U from the zircons used in this mean age calculation was 0.92.

4.1.3 Penzance granite

The CL imaging of abundant zircons from all three samples collected from different locations in a single quarry of the Penzance granite displays textures typical of metamict zircons (Figure 6). These include cavities, fractures, disruption of the original zoning and development of dark CL areas (Corfu, 2003; Kılıç, 2016).

Even when targeting zircon grains seemingly less affected by metamictisation, twenty-seven analysis were aborted throughout a single analytical session due to the unacceptably high ^{204}Pb content. Of the twenty-four analysis which were not aborted, only nine were <5% discordant and had less than 1% common Pb (Figure 6, Supplementary Material 2). The U and Th contents of completed analyses (average of ~580 and ~400 ppm, respectively) were commensurate with the observed metamictisation. The nine near concordant analysis have scattered ages typical of metamict zircons, and only one of the ages is within error of the previously reported age (Geoscience Australia, 2019). We conclude that no reliable age could be calculated from these zircon data. The average and range of Th/U from the completed SHRIMP analyses was 0.72 and 0.52-1.46, respectively.

4.2 U-Pb SHRIMP monazite dating of the Penzance granite

A significant number of the monazite grains were separated from the three Penzance granite samples. They have euhedral zoning textures on BSE images (Figure 7), which indicates magmatic crystallization. Recent studies (e.g.: Piechocka et al., 2017) have demonstrated the increased reliability of magmatic monazite as a geochronometer for igneous rocks with unreliable zircon age data, when subsequent metamorphic conditions remained under the Pb closure temperature of monazite. Monazite contains high U and Th and incorporates minor common Pb and, unlike zircon, is largely immune to metamictisation and radiogenic Pb loss at low temperatures (Piechocka et al., 2017).

A total of 38 of 56 analysis from 18 grains with low common Pb (f206 <0.5%) and low discordance (≤5%) (Table 1) yield a mean $^{207}Pb/^{206}Pb$ age of 2681.9 ± 4.5 Ma (95% c1; MSWD = 1.4; Figure 3). The slightly high MSWD indicates the possibility of scatter from a single-age population. However, in the absence of any skewness in the age probability plot (not shown), anomalous Th-U chemistry or other evidence for either inheritance or Pb-loss, and given the amount of data collected (n=56) and used (n=38), this is considered to be the age of these igneous monazite.

4.3 HF-isotopes in zircon

4.3.1 Teutonic Bore volcanics

Twenty-five zircon grains from sample 15BUDD78 – 111.60 m of the footwall rhyolite (unit I) were analysed for Lu–Hf by LA-SS-ICP-MS (Supplementary Material 3, mount N18-15D, sample B78,). The calculated $\varepsilon Hf_{(i)}$, based on the interpreted SHRIMP $^{207}Pb/^{206}Pb$ age (2692.9Ma), plot in a homogeneous population with values ranging between +2.3 and +5.6 (Figure 8), and a mean of 3.7 ± 0.5 (MSWD = 0.47, n = 25). The low MSWD value partly reflects the relatively large $\varepsilon Hf_{(i)}$ errors on individual analyses.

Twenty-nine Lu–Hf analysis (Supplementary Material 3, mount N18-15C, sample B137) were conducted on zircons from sample 15BUDD137 – 398.60 m of the same footwall rhyolite (unit I), and, once again, the $\varepsilon Hf_{(i)}$ is calculated based on the interpreted SHRIMP $^{207}Pb/^{206}Pb$ age for emplacement. $\varepsilon Hf_{(i)}$ values range between -0.6 and +5.2 with a mean of 2.9 ± 0.5 (MSWD = 0.90, n = 29, Figure 8). Combining the $\varepsilon Hf_{(i)}$ data for the both footwall rhyolite samples (unit I) yields a value of 3.27 ± 0.33 (MSWD = 0.79, n = 54).

Sixteen Lu–Hf analysis (Supplementary Material 3, B37) were conducted on zircon from both samples of transitional andesite (unit III) and the mean age of the combined SHRIMP analyses of 2693.4 Ma was used to calculate $\varepsilon Hf_{(i)}$ which showed considerable scatter and ranged between -11.7 and +8.6 with significant errors on individual analyses (Supplementary

Material 3). The lower precision is a result of the smaller spot-size necessary for the small zircons from these samples. The mean $\varepsilon Hf_{(i)}$ for the transitional andesite (unit III) is 2.6 ± 1.8 (MSWD = 1.05, n = 16, Figure 8).

4.3.2 Penzance granite

Recent studies show that the Lu–Hf system remains relatively undisturbed within metamic zircon that do not undergo significant later alteration (Lenting et al., 2010). Thirty-four Lu–Hf analyses on zircon from the Penzance granite (Supplementary Material 3, N18-06) show a range of $\varepsilon Hf_{(i)}$ between -1.5 to +4.7 with mean value of 2.17 ± 0.45 (MSWD = 1.15, n = 34). The $\varepsilon Hf_{(i)}$ values were calculated based on the SHRIMP monazite ages presented herein.

4.4 Trace elements in zircon

Selected trace elements were measured via LA-SS-ICP-MS (Supplementary Material 4). Figure 9 illustrates patterns for selected REEs normalized to chondrite (Anders and Grevesse, 1989) for the two samples from the footwall rhyolite (unit I), the combined samples of andesite (unit III) and the Penzance granite.

The zircons from the footwall rhyolite (unit I) and the andesite (unit III) have similar MREE and HREE content (Figure 9). The mean Yb/Dy ratio is 4.15 ± 0.85 and 4.45 ± 0.68 (1σ) for the rhyolite and andesite, respectively. The Ce anomaly is estimated by the $Ce/Nd_{(CN)}$ ratio (Loucks et al., 2018) to be positive in both rock types (Supplementary Material 4), with mean $Ce/Nd_{(CN)}$ of 1.04 ± 0.58 and 1.30 ± 0.75 (1σ) for the rhyolite and andesite, respectively. The zircons from the Penzance granite show a mean $Ce/Nd_{(CN)}$ of 0.92 ± 0.23 (1δ), indicating a positive Ce anomaly, and Yb/Dy ratio of 2.5 ± 0.67 (1σ).

5 DISCUSSION

5.1 Age constrains on the Penzance granite

Hollis et al. (2015) proposed a link between VHMS mineralisation at the Teutonic Bore Camp and the emplacement of the HFSE-enriched Penzance granite, based on geochemical similarities, the proximity and broad synchronicity between the intrusive magmatic activity and the volcanism of the host sequence. These observations were underpinned by a U-Pb zircon age for the volcanism (2692 ± 4 Ma; Nelson, 1995) and the age reported by Champion and Cassidy (2002) of 2679 ± 8 Ma, for the Kent Complex of the Penzance Supersuite. This latter age was obtained by SHRIMP U-Pb zircon dating of sample ID 96969076 of Geoscience Australia's database, after L.Black, AGSO (unpublished) in Champion and Cassidy (2002).

Champion and Cassidy (2002) reported the age but not the data table. However, the geochronological data, as well as location and description for sample ID 96969076, are available from Geoscience Australia's Geochron Delivery database (Geoscience Australia, 2019). The reported age for this sample is 2686 ± 9 Ma with MSWD = 1.6 and probability = 0.044 (Geoscience Australia, 2019), which is within error of the age reported by Champion and Cassidy (2002), but not identical.

We have reprocessed the data available from Geochron Delivery for sample 96969076 and obtained an identical age of 2686 ± 9 Ma, MSWD = 1.6 from 21 analysis. However, given the scatter inferred by the high MSWD, we have filtered the data by only considering analysis with common Pb <0.3%, deriving a more statistically robust age of 2682 ± 9 Ma (n=12; MSWD = 1.3). More importantly, only four zircons were recovered from sample 96969076 and the 21 analyses and calculated age is based on analyses from only three grains, of which one is a xenocryst. Each of our three samples collected from the same quarry had hundreds of zircon grains, and after hand-picking the clearest (least metamict) zircons and analysing the best areas based on CL-SE imaging, we only detected one analysis in the relevant time interval, and it

was 7% discordant. In view of this discrepancy, we searched for other datable minerals in the Penzance granite and identified igneous monazite. The monazite age of 2681.9 ± 4.5 Ma discussed above is considered to be a statistically valid age of magma crystallization for the Penzance granite, and supersedes the previous zircon age(s).

5.2 Geochronological associations

The relative timing of ore formation in the Teutonic Bore Camp is well constrained within the stratigraphic sequence at Jaguar, where substantial evidence of seafloor precipitation indicate coeval mineralisation to the development of the upper sedimentary package (unit IV). Such evidence is absent from Bentley and the Teutonic Bore deposit, which indicates that they were formed at greater depths, probably by replacement of a slightly older stratigraphy (see Figure 2A).

The syn-ore nature of the upper sedimentary package (unit IV) at Jaguar, the deposit hosted within the youngest stratigraphic level in the Teutonic Bore Camp, indicates that the hangingwall sequence at Jaguar post-dates ore formation and could provide a potential minimum mineralisation age. Attempts to date this sequence have proven unsuccessful to date (Das, 2018). The footwall in all three deposits, as well as the hangingwall immediately above the orebodies of the Bentley and the Teutonic Bore deposits, pre-date the mineralisation and represent a maximum age of ore formation.

The ages obtained in this study for the footwall rhyolite (unit I - 2691.7 ± 2.5 Ma and 2696.5 ± 4.3 Ma) and the transitional andesite (unit III - 2693.4 ± 4.1 Ma) suggest that mineralisation at the Teutonic Bore Camp is younger than c.a. 2694 Ma (Figure 10). The unpublished TIMS age for the footwall rhyolite sequence (unit I) of 2692.6 ± 1.5 Ma (Das, 2018) is indistinguishable from the SHRIMP age presented here for the pre-ore volcanic sequence at the Teutonic Bore Camp. Similarly, the previous SHRIMP age for the Teutonic Bore Camp sequence (2692 ± 4 Ma; (Nelson, 1995) is similar to the age determined in this study (Figure

10). Therefore, although poorly constrained in the stratigraphy, it is likely that the porphyritic dacite dated by Nelson (1995) is part of the pre-ore stratigraphy (units I, II, or III).

The ages for the footwall rhyolite (unit I) of 2696.5 ± 4.3 Ma and 2691.7 ± 2.5 Ma are within error of each other, when considering a 95% confidence interval. However, considering the normal distribution tendency of single-population ages obtained from multiple grains (Figure 10; Schoene et al., 2013), it is probable that these could also represent a long duration of volcanic activity during the development of this stratigraphic facies.

The ages for the footwall rhyolite (unit I) and the Penzance granite (2681.9 ± 4.5 Ma) do not overlap (Figure 10) at the 95% confidence interval and are not, therefore, coeval. Furthermore, the porphyritic dacite from Nelson (1995) and the transitional andesite (unit III) do not overlap the age of the Penzance (Figure 10) at a 95% confidence interval. We infer that these rocks pre-date the mineralisation and the syn-ore stratigraphy.

5.3 Geochemical correlations

5.3.1 Whole-rock geochemistry

Hollis et al. (2015) described similarities in whole-rock REE distribution between the Penzance granite (Kent Complex) and the felsic volcanics that host the mineralisation at Jaguar (footwall rhyolite – unit I). Based on these observations and the HFSE enrichment of both rock types they suggested a possible genetic link between these rocks, proposing that the footwall volcanic sequence at Jaguar would be the extrusive equivalent to the Penzance granite.

The geochronological results presented here indicate that the crystallization of the Penzance granite is not coeval to the formation of the footwall rhyolite (unit I) or the transitional andesite (unit III) at Bentley. However, these processes occur within a ~12 M.y. interval. Given the chemical similarities between these rock types and their proximity in age it is conceivable that they are both the product of a single magmatic system or had a common source.

Additionally, based on whole-rock geochemistry observations, other stratigraphic facies within the younger, syn-ore, portion of the volcanic sequence at the Teutonic Bore Camp are alternative candidates to be the extrusive correspondent to the Penzance granite.

The dacite that can be observed at the sedimentary-volcanic package of the upper sedimentary horizon (unit IV) in the Jaguar deposit (MPD from Belford et al., 2015) has Y/Zr ratios that indicates a tholeiitic affinity (Belford et al., 2015), which is also the case for the Penzance granite (ID 96969076, sampled from the same locality of the geochronological study; Sedgmen et al., 2007) (Figure 11). Furthermore, the MPD dacite yields a La/Yb_{CN} ratio of 3.4 – 5.5 (Belford, 2010), which indicates a significant LREE/HREE enrichment, equal to what is indicated by whole-rock REE content for the Penzance granite (Hollis et al., 2015).

5.3.2 Zircon geochemistry

The Hf-isotopes corroborate Hollis et al. (2015)'s hypothesis of a genetic link between the Teutonic Bore Camp volcanic sequence and the Penzance granite. All zircons (Penzance, units I and III) have very similar $\varepsilon Hf_{(i)}$, with most values between -1 and +6 (Figure 8). The $\varepsilon Hf_{(i)}$ values show little contribution from evolved sources (Figure 8). Indeed, Nd and Pb isotopes indicate that the Teutonic Bore Camp is located within a more juvenile zone of the Yilgarn craton, the Teutonic zone (Huston et al., 2014). The $\varepsilon Hf_{(i)}$ for the zircons from the Penzance granite and the volcanic rocks from the Teutonic Bore Camp plot above the CHUR line (Figure 8), indicating a juvenile depleted mantle source component. These $\varepsilon Hf_{(i)}$ are slightly higher than the $\varepsilon Hf_{(i)}$ of zircons from other granites and volcanics within the Kurnalpi Terrain (Isaac, 2015; Wyche et al., 2012).

According to Kirkland et al. (2015), parental magma composition is one of four factors that may contribute to variations in the Th/U of a zircon crystal.Therefore, the similar Th/U ratios (Supplementary Material 2) of the Penzance (~0.7) and Bentley zircons (Unit I: ~0.6) also suggest they could have a shared magma source. Furthermore, all zircons have similar

$Ce/Nd_{(CN)}$ ratios (Supplementary Material 4), which indicates comparable redox conditions, as this ratio is a proxy for the Ce anomaly (Loucks et al., 2018).

The zircons from the Penzance granite have higher overall REE content and MREE/HREE enrichment (indicated by the Yb/Dy ratio), when compared to the Bentley units I and III zircons (Supplementary Material 4). These chemical differences indicate that the Penzance granite is more fractionated but do not resolve whether this is the result of igneous differentiation from a common magma or magma production from a common source. The ~12 M.y. interval between the units I and III volcanics, and the Penzance granite suggests the latter.

5.4 Contribution to the 4D evolutionary model of the Teutonic Bore Camp ore

The 4D evolutionary model of the Teutonic Bore Camp is achieved by the addition of the time dimension to the current understanding of the geological evolution of the deposits, including stratigraphy and geochemistry (Figure 2; Belford, 2010; Belford et al., 2015; Chen et al., 2015; Das, 2018; Hallberg and Thompson, 1985; Macklin, 2010; Parker et al., 2017). The geochronology data presented in this study constrain in time several processes within the Teutonic Bore Camp, including the intrusion of the Penzance granite, which could be linked to the development of the mineral system.

Similarities in zircon chemistry (i.e.: $\square Hf_{(i)}$ and Th/U ratio; see section 5.3: Geochemical correlations) complemented by the geochemical correspondences between the Penzance granite and the Teutonic Bore volcanics (i.e.: HFSE-enrichment and REE pattern, see section 5.3: Geochemical correlations), suggest a genetic association between the intrusive granite and the extrusive rocks that constitute the Teutonic Bore Camp host sequence.

Irregular contact between the Penzance granite and the volcanic sequence, as well as, the recognition of intrusive veins of granitoid within the volcanics, and xenoliths of volcanic rocks within the granite (Hallberg and Thompson, 1985) indicate that the Penzance intrudes the volcanic Teutonic Bore sequence and that their proximity is not the result of subsequent

tectonic processes. Considering the close geographic position of the granite and the ore-bearing volcanic sequence (Figure 1), their shared geochemical features and broad synchronicity, it is possible that the Penzance granite was involved in the process that generated the VHMS mineralisation at the Teutonic Bore Camp.

Magmatic-hydrothermal contribution of metals is not necessary in the development of VHMS deposits (Huston et al., 2011) and syn-ore intrusions do not always directly supply metal to the system, but rather act as a heating source, driving hydrothermal circulation that leaches metals from the country host rock (Lode et al., 2017). However, in a number of cases there is evidence of a significant contribution of metals and/or volatiles from the magmatic source, in addition to the supply of heat (e.g.: Chen et al., 2015; Lode et al., 2017; Yang and Scott, 1996).

Chen et al. (2015) used S-isotopes as a proxy for the hydrothermal fluid composition in the Teutonic Bore Camp and interpreted that the supply of sulphur to the hydrothermal ore fluid was the result of a mixture between seawater and a hydrothermal fluid of magmatic origin. These authors did not find compelling evidence for leaching of sulphur from the host sequence into the ore fluid in the Teutonic Bore Camp. Therefore, the Penzance granite is a strong candidate to have acted as the probable magmatic source of sulphur to the mineralisation, and possibly, metals.

5.5 Exploration strategies

Our observations show that the HFSE-enriched Penzance granite probably played a fundamental role in the supply of metals and heat that culminated in the development of the replacement-type VHMS deposits of the Teutonic Bore Camp. Therefore, future exploration efforts within the camp should focus on fluid pathways from similar granites. The emphasis should be on mapping syn- or pre-intrusive structures that could facilitate fluid flow from the granite to the host sequence. Fertile zones are likely to be discovered where these fluid paths

find the appropriate conditions for metal precipitation, which has been suggested by previous studies to be sediment-rich horizons (Parker et al., 2017) and/or depositional breaks (Belford et al., 2015).

This paper supports conclusions proposed by Hollis et al. (2015), of a connection between HFSE-enriched granites and VHMS (± base metals) deposits within the Yilgarn Craton. Following the identification of fertile terrains, populated with HFSE-enriched granites, *greenfield* exploration campaigns should employ a multi-disciplinary approach to test the processes involved in the formation of an ore deposit. The development of 4D models (i.e. constrain in time of 3D geological processes) allows for a better understanding of the timing and nature of the magmatic and stratigraphical processes necessary for the development of such ore deposits. This is particular true in Archean replacement-type VHMS deposits, where the syn-volcanic timing of the mineralisation is not always clear (e.g. Barrote et al., 2019)

6 CONCLUSIONS

- Three mined VHMS orebodies in the Teutonic Bore Camp (Teutonic Bore deposit, Jaguar and Bentley) formed at different stratigraphic levels.
- Jaguar formed coeval with its host sequence, whereas the ore in Teutonic Bore and Bentley replaces slightly older stratigraphy.
- The age of the host sequence at the stratigraphic level of the Bentley deposit is ca. 2693 Ma.
- The age of the Teutonic Bore Camp mineralisation is possibly coeval to the intrusion of the Penzance granite at ca. 2682 Ma.
- Monazite has been shown to be a more reliable chronometer than high-U-Th zircons in the HFSE-enriched Penzance granite.

- The Penzance granite possibly acted as the source of heat and potentially fluid/metals to the ore formation at the Teutonic Bore Camp.
- VHMS exploration in the Yilgarn Craton should focus in finding fluid pathways between HFSE-enriched intrusives and potential host sequences to orebodies.

7 ACKNOWLEGMENTS

The authors acknowledge: Dr Steve Bereford and Mr. Kyle Hodges from IGO for their wisdom, access to samples, drill core and internal data; Thermo Fisher, GSWA and MRIWA for financial support; and the John de Laeter Centre (JdLC) for the facilities, scientific and technical assistance. We thank Dr. Haoyang Zhou, Dr. Nicolas Thebaud and an anonymous reviewer whose comments helped improve and clarify this manuscript. JdLC facilities are supported by a university-government consortium, ARC and AuScope via NCRIS. GeoHistory Facility instruments in the John de Laeter Centre, Curtin University were funded via an Australian Geophysical Observing System grant provided to AuScope Pty Ltd. by the AQ44 Australian Education Investment Fund program. The NPII multi-collector was obtained via funding from the Australian Research Council LIEF program (LE150100013).

8 BIBLIOGRAPHY

Anders, E., Grevesse, N., 1989. Abundances of the elements: Meteoritic and solar. Geochim. Cosmochim. Acta 53, 197–214. https://doi.org/10.1016/0016-7037(89)90286-X

Barrett, T.J., MacLean, W.H., 1994. Chemostratigraphy and hydrothermal alterationin exploration for VHMS deposits in greenstones and younger volcanic rocks., in: Lentz, D.R. (Ed.), Alteration and Alteration Processes Associated with Ore-Forming Systems, Short Course Notes / Geological Association of Canada. Geological Assoc. of Canada, St.John's, Newfoundland, pp. 433–467.

Barrote, V., Tessalina, S., McNaughton, N., Jourdan, F., Hollis, S.P., Ware, B., Zi, J.-W., 2020. 4D history of the Nimbus VHMS ore deposit in the Yilgarn Craton, Western Australia. Precambrian Research 337, 105536. https://doi.org/10.1016/j.precamres.2019.105536

Belford, S.M., 2010. Genetic and chemical characterisation of the host succession to the archean Jaguar VHMS deposit. (Doctoral dissertation). University of Tasmania, UTAS, Hobart, Tasmania, Australia.

Belford, S.M., Davidson, G.J., McPhie, J., Large, R.R., 2015. Architecture of the Neoarchaean Jaguar VHMS deposit, Western Australia: Implications for prospectivity and the

presence of depositional breaks. Precambrian Res. 260, 136–160. https://doi.org/10.1016/j.precamres.2014.12.019

Butt, C.R.M., Anand, R.R., Smith, R.E., 2017. Geology of the Australian regolith, in: Phillips, G.N. (Ed.), Australian Ore Deposits. The Australian Institute of Mining and Metallurgy, Melbourne, pp. 27–34.

Champion, D.C., Cassidy, K.F., 2002. Granites of the Northern Eastern Goldfields: their Distribution, Age, Geochemistry, Petrogenesis, Relationship with Mineralisation, and Implications for Tectonic Environment, AMIRA P482/MERIWAM281-Yilgarn Granitoids. AMIRA P482/MERIWAM281-Yilgarn Granitoids.

Chen, M., Campbell, I.H., Xue, Y., Tian, W., Ireland, T.R., Holden, P., Cas, R.A.F., Hayman, P.C., Das, R., 2015. Multiple Sulfur Isotope Analyses Support a Magmatic Model for the Volcanogenic Massive Sulfide Deposits of the Teutonic Bore Volcanic Complex, Yilgarn Craton, Western Australia. Econ. Geol. 110, 1411–1423. https://doi.org/10.2113/econgeo.110.6.1411

Corfu, F., 2003. Atlas of Zircon Textures. Rev. Mineral. Geochem. 53, 469–500. https://doi.org/10.2113/0530469

Czarnota, K., Champion, D.C., Goscombe, B., Blewett, R.S., Cassidy, K.F., Henson, P.A., Groenewald, P.B., 2010. Geodynamics of the eastern Yilgarn Craton. Precambrian Res. 183, 175–202. https://doi.org/10.1016/j.precamres.2010.08.004

Das, R., 2018. Understanding the Palaeovolcanological and Palaeoenvironmental setting of Archaean VMS Deposit: Stratigraphic Architecture and Volcanology of the Archaean VMS host rock succession of the Teutonic Bore, Jaguar and Bentley Mine corridor, Eastern Goldfields Province, Western Australia (Master thesis). Melbourne University, Melbourne.

Doyle, M.G., Allen, R.L., 2003. Subsea-floor replacement in volcanic-hosted massive sulfide deposits. Ore Geol. Rev. 23, 183–222. https://doi.org/10.1016/S0169-1368(03)00035-0

Ellis, P., 2004. Geology and mineralisation of the Jaguar copper-zinc deposit, Western Australia, in: McConachy, T.F., McInnes, B.I.A. (Eds.), Copper-Zinc Massive Sulphide Deposits in Western Australia. CSIRO Exploration and Mining, Melbourne, pp. 39–46.

Geoscience Australia, 2019. Geochron Delivery Database. Accessed June 2019. http://www.ga.gov.au/geochron-sapub-web/geochronology/shrimp/search.htm.

GeoVIEW.WA, 2016. 1:500 000 State interpreted bedrock geology polygons, 2016.

Hallberg, J.A., Thompson, J.F.H., 1985. Geologic setting of the Teutonic Bore massive sulfide deposit, Archean Yilgarn Block, Western Australia. Econ. Geol. 80, 1953–1964. https://doi.org/10.2113/gsecongeo.80.7.1953

Hollis, S.P., Mole, D.R., Gillespie, P., Barnes, S.J., Tessalina, S., Cas, R.A.F., Hildrew, C., Pumphrey, A., Goodz, M.D., Caruso, S., Yeats, C.J., Verbeeten, A., Belford, S.M., Wyche, S., Martin, L.A.J., 2017. 2.7 Ga plume associated VHMS mineralization in the Eastern Goldfields Superterrane, Yilgarn Craton: Insights from the low temperature and shallow water, Ag-Zn-(Au) Nimbus deposit. Precambrian Res. 291, 119–142. https://doi.org/10.1016/j.precamres.2017.01.002

Hollis, S.P., Yeats, C.J., Wyche, S., Barnes, S.J., Ivanic, T.J., Belford, S.M., Davidson, G.J., Roache, A.J., Wingate, M.T.D., 2015. A review of volcanic-hosted massive sulfide (VHMS) mineralization in the Archaean Yilgarn Craton, Western Australia: Tectonic, stratigraphic and geochemical associations. Precambrian Res. 260, 113–135. https://doi.org/10.1016/j.precamres.2014.11.002

Huston, D.L., Champion, D.C., Cassidy, K.F., 2014. Tectonic Controls on the Endowment of Neoarchean Cratons in Volcanic-Hosted Massive Sulfide Deposits: Evidence from

Lead and Neodymium Isotopes. Econ. Geol. 109, 11–26. https://doi.org/10.2113/econgeo.109.1.11

Huston, D.L., Relvas, J.M.R.S., Gemmell, J.B., Drieberg, S., 2011. The role of granites in volcanic-hosted massive sulphide ore-forming systems: an assessment of magmatic–hydrothermal contributions. Miner. Deposita 46, 473–507. https://doi.org/10.1007/s00126-010-0322-7

Independence Group NL (IGO), 2015. Annual Report 2015 (Unpublished Annual Report). Independence Group NL (IGO), Perth, W.A.

Isaac, C., 2015. Geochemistry of the north Eastern Goldfields, Western Australia: examining the processes that produce nickel sulphide camps (Masters Thesis). The University of Western Australia, Perth, W.A.

Kirkland, C.L., Smithies, R.H., Taylor, R.J.M., Evans, N., McDonald, B., 2015. Zircon Th/U ratios in magmatic environs. Lithos 212–215, 397–414. https://doi.org/10.1016/j.lithos.2014.11.021

Kılıç, A.D., 2016. Investigation of zircon by CL (Cathodoluminescence) and Raman Spectroscopy. IOP Conf. Ser. Earth Environ. Sci. 44, 042006. https://doi.org/10.1088/1755-1315/44/4/042006

Lenting, C., Geisler, T., Gerdes, A., Kooijman, E., Scherer, E.E., Zeh, A., 2010. The behavior of the Hf isotope system in radiation-damaged zircon during experimental hydrothermal alteration. Am. Mineral. 95, 1343–1348. https://doi.org/10.2138/am.2010.3521

Lode, S., Piercey, S.J., Layne, G.D., Piercey, G., Cloutier, J., 2017. Multiple sulphur and lead sources recorded in hydrothermal exhalites associated with the Lemarchant volcanogenic massive sulphide deposit, central Newfoundland, Canada. Miner. Deposita 52, 105–128. https://doi.org/10.1007/s00126-016-0652-1

Loucks, R.R., Fiorentini, M.L., Rohrlach, B.D., 2018. Divergent T–$fO2$ paths during crystallisation of H2O-rich and H2O-poor magmas as recorded by Ce and U in zircon, with implications for TitaniQ and TitaniZ geothermometry. Contrib. Mineral. Petrol. 173. https://doi.org/10.1007/s00410-018-1529-3

Macklin, D., 2010. Alteration at the Teutonic Bore (VHMS) Deposit, Western Australia (B.Sc with honours thesis). University of Tasmania, UTAS.

McConachy, T.F., McInnes, B.I.A., Carr, G.R., 2004. Is Western Australia intrinsically impoverished in volcanogenic massive sulphide deposits, or under explored?, in: McConachy, T.F., McInnes, B.I.A. (Eds.), Copper-Zinc Massive Sulphide Deposits in Western Australia. CSIRO Exploration and Mining, Melbourne, pp. 15–32.

Nelson, D.R., 1995. Compilation of SHIRMP U-Pb zircon geochronology data, 1994, Record / Geological Survey of Western Australia. Geological Survey of Western Australia, Perth.

Parker, P., Belford, S.M., Maier, R., Lynn, S., Stewart, W., 2017. Teutonic Bore - Jaguar - Bentley volcanogenic massive sulfide field, in: Phillips, G.N. (Ed.), Australian Ore Deposits. The Australian Institute of Mining and Metallurgy, Melbourne, pp. 167–172.

Piechocka, A.M., Gregory, C.J., Zi, J.-W., Sheppard, S., Wingate, M.T.D., Rasmussen, B., 2017. Monazite trumps zircon: applying SHRIMP U–Pb geochronology to systematically evaluate emplacement ages of leucocratic, low-temperature granites in a complex Precambrian orogen. Contrib. Mineral. Petrol. 172. https://doi.org/10.1007/s00410-017-1386-5

Schoene, B., Condon, D.J., Morgan, L., McLean, N., 2013. Precision and Accuracy in Geochronology. Elements 9, 19–24. https://doi.org/10.2113/gselements.9.1.19

Sedgmen, A., Hazell, M.S., Budd, A.R., Champion, D.C., 2007. OZCHEM National Whole Rock Geochemistry Dataset.

Wyche, S., Kirkland, C.L., Riganti, A., Pawley, M.J., Belousova, E., Wingate, M.T.D., 2012. Isotopic constraints on stratigraphy in the central and eastern Yilgarn Craton, Western Australia. Aust. J. Earth Sci. 59, 657–670. https://doi.org/10.1080/08120099.2012.697677

Yang, K., Scott, S.D., 1996. Possible contribution of a metal-rich magmatic fluid to a sea-floor hydrothermal system. Nature 383, 420–423. https://doi.org/10.1038/383420a

Figure 1: Location of the Teutonic Bore Camp on a map showing the major subdivisions of the Eastern Goldfields Superterrane, Yilgarn Craton, Western Australia. The town of Leonora is indicated by a black diamond. The inset map shows the location of the three deposits (Teutonic Bore, Jaguar and Bentley) and the sampled Penzance granite on the 1:500 000 State interpreted bedrock geological map from the GSWA online database GeoVIEW.WA (2016).

Figure 2: A) Schematic geological model for the Teutonic Bore Camp showing the position of each deposit within the stratigraphic sequence and illustrating the sub-seafloor replacement feature of the VHMS mineralisation and possible relationship of the host stratigraphy and the intrusive leucogranite described by Hallberg and Thompson (1985). B) Simplified stratigraphic sequence and stratigraphical subdivisions for each of the three deposits within the Teutonic Bore Camp (Belford, 2010; Belford et al., 2015; Chen et al., 2015; Das, 2018 and complemented by this study; stratigraphic sequence modified from Hallberg and Thompson, 1985; Macklin, 2010; Parker et al., 2017). The U-Pb zircon age, drillhole and depth for the dacite are from Nelson (1995).

Figure 3: U-Pb Concordia diagram showing the SHRIMP spot analyses and mean $^{207}Pb/^{206}Pb$ ages for: A) Footwall rhyolite (unit I) – Bentley footwall zircons (sample 15BUDD78; mount N18-15D). B) Footwall rhyolite (unit I) – Bentley footwall zircons (sample 15BUDD138; mount N18-15C). C) Transitional andesite (unit III) – Bentley hangingwall zircons (sample 15BUDD120 - 226.04m; mount N19-07, 08). D) Transitional andesite (unit III) – Bentley hangingwall zircons (sample 15BUDD120 - 228.42m; mount N19-09, 10). E) Penzance granite zircons (mount N18-06, 16). F) Penzance granite monazite (mounts N18-06, N18-16). Error ellipses are ±1σ.

Figure 4: Cathodoluminescence electron microscope images of zircon grains separated from the footwall rhyolite (unit I) at the Bentley deposit, and analysed with SHRIMP and/or LA-SS-ICPMS. The location of the spots are indicated within each grain as well as the name (and $^{207}Pb/^{206}Pb$ age for SHRIMP spots).

Figure 5: Cathodoluminescence electron microscope images of zircon grains separated from the transitional andesite (unit III) at the Bentley deposit, and analysed with SHRIMP or LA-SS-ICPMS. The location of the spots are indicated within each grain as well as the name (and $^{207}Pb/^{206}Pb$ age and discordance for SHRIMP spots).

Figure 6: Cathodoluminescence images of zircon grains separated from the Penzance granite, and analysed with SHRIMP and/or LA-SS-ICPMS. The location of the spots are indicated within each grain as well as the name (and $^{207}Pb/^{206}Pb$ age and discordance for SHRIMP spots). The zircons exhibit cavities, fractures, disruption of the original zoning and/or development of dark CL areas.

Figure 7: Backscatter electron images of four monazite grains separated from the Penzance granite, and analysed with SHRIMP. The location of the spots are indicated within each grain as well as the name, $^{207}Pb/^{206}Pb$ ages and discordance. Most crystals present visible regular euhedral zoning, typical of magmatic monazite.

Figure 8: $\varepsilon Hf_{(i)}$ (CHUR) vs. $^{207}Pb/^{206}Pb$ age (Ma) plot for zircon from the Penzance granite, the volcanic sequence at Bentley and zircons from other magmatic rocks within the Kurnalpi Terrane (Wyche et al., 2012). The errors for $\varepsilon Hf_{(i)}$ are 1σ. The zircon data from this study are plotted with the interpreted $^{207}Pb/^{206}Pb$ magmatic age for each sample, which is also used in the calculation of the $\varepsilon Hf_{(i)}$. The thick black line labelled DM represents εHf of depleted mantle over time.

Figure 9: MREE and HREE patterns for zircon from the Penzance granite and the volcanic sequence at Bentley, normalized to chondrite (Anders and Grevesse, 1989). The lower graph is a compilation of the four results.

Figure 10: Graph of probability density, assuming a normal distribution, for the zircon $^{207}Pb/^{206}Pb$ mean ages obtained in this study and the previous age from Nelson (1995), with the mean age indicated by a dashed line for each sample. Each age is represented both by the probability plot and by a graph bar. In both cases, the different shades represent 1σ or 2σ for each age, as indicated in the legend. The thick red line marks the maximum age of the mineralisation. The unpublished TIMS age of the footwall rhyolite (unit I) (Das, 2018) is represented only in bar graph form.

Figure 11: Zr vs Y plot for the volcanic rocks that host the Jaguar deposit (Belford et al., 2015) and two samples from the Penzance granite from Geoscience Australia's OZCHEM database (Sedgmen et al., 2007). The filled square represents a sample collected from the same quarry that was sampled for the geochemical studies (Sample id 96969076). The roman numerals indicates the stratigraphical subdivisions from this study and their correspondence to the facies described by Belford et al. (2015). The boundaries and indicated Zr/Y ratios that define tholeiitic, transitional and calc-alkaline fields are from Barrett and MacLean (1994).

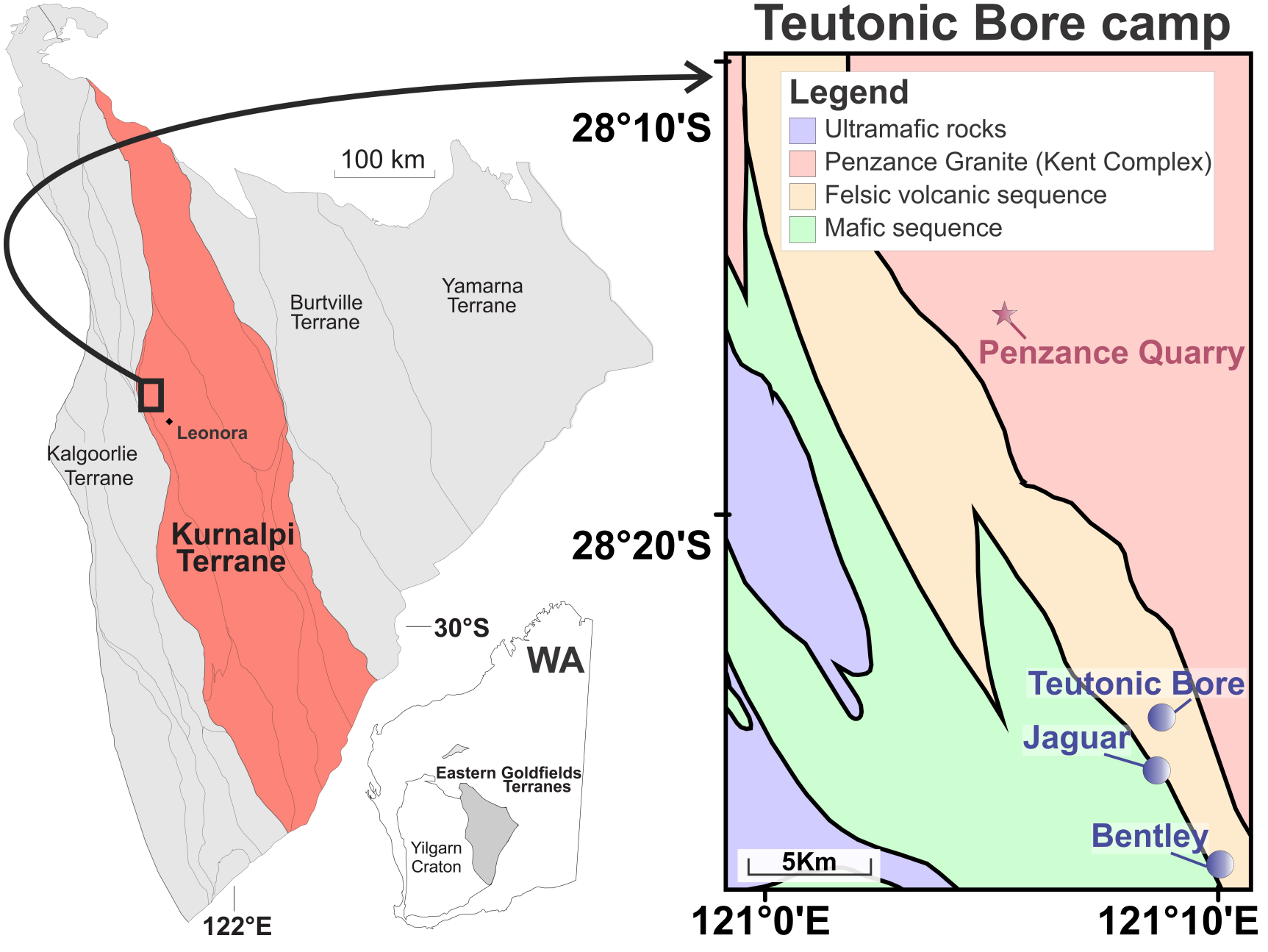
Teutonic Bore camp
Legend
Ultramafic rocks
Penzance Granite (Kent Complex)
Felsic volcanic sequence
Mafic sequence
Penzance Quarry
Teutonic Bore
Jaguar
Bentley
5Km
28°10'S
28°20'S
121°0'E
121°10'E
100 km
Burtville Terrane
Yamarna Terrane
Leonora
Kalgoorlie Terrane
Kurnalpi Terrane
30°S
WA
Eastern Goldfields Terranes
Yilgarn Craton
122°E

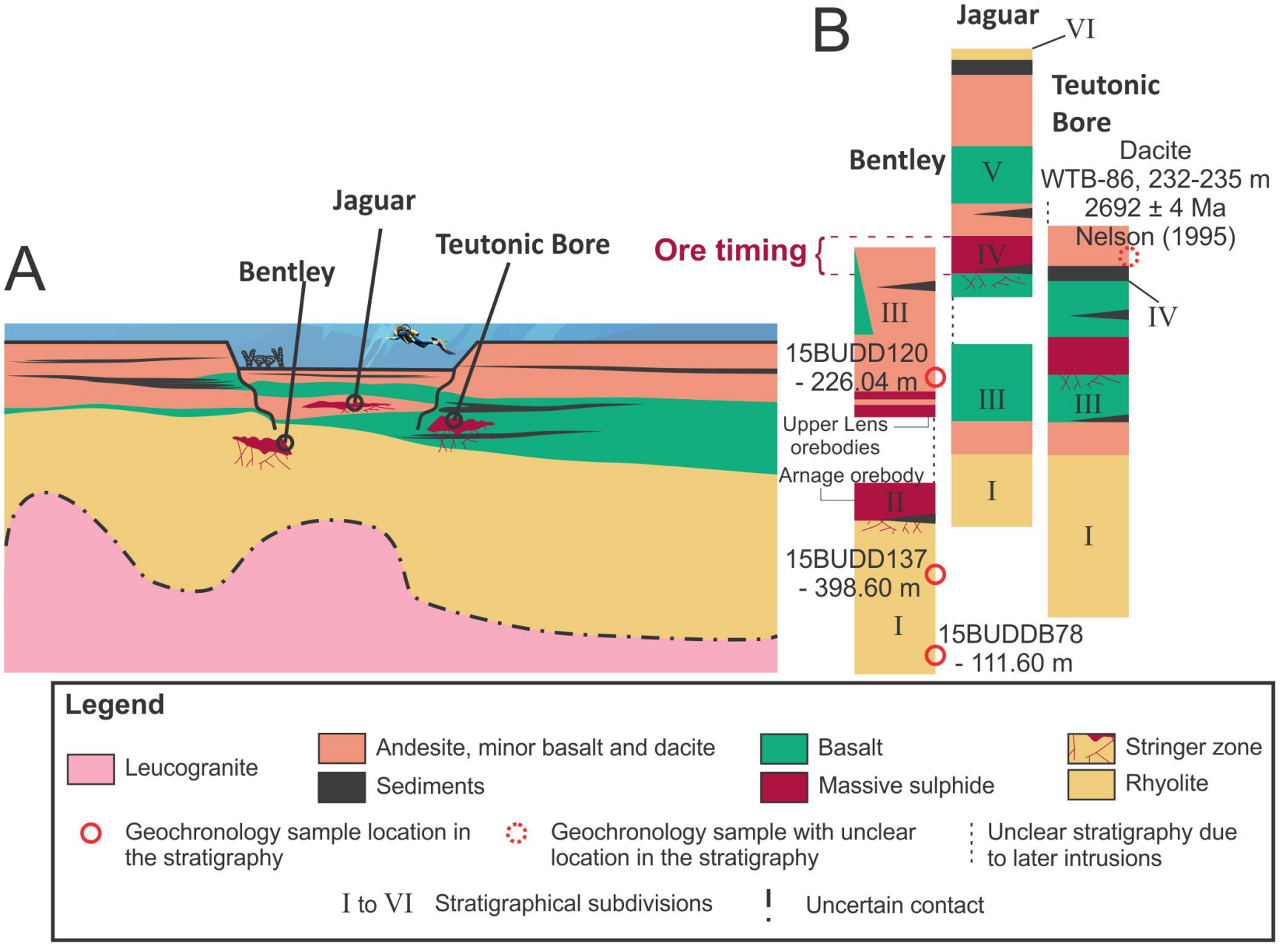
A
Bentley
Jaguar
Teutonic Bore
B
Jaguar
VI
Teutonic
Bore
Bentley
V
Dacite
WTB-86, 232-235 m
2692 ± 4 Ma
Nelson (1995)
Ore timing
IV
III
IV
15BUDD120
- 226.04 m
III
III
Upper Lens
orebodies
Arnage orebody
II
I
I
15BUDD137
- 398.60 m
I
15BUDDB78
- 111.60 m
Legend
Leucogranite
Andesite, minor basalt and dacite
Sediments
Basalt
Massive sulphide
Stringer zone
Rhyolite
Geochronology sample location in the stratigraphy
Geochronology sample with unclear location in the stratigraphy
Unclear stratigraphy due to later intrusions
I to VI Stratigraphical subdivisions
Uncertain contact

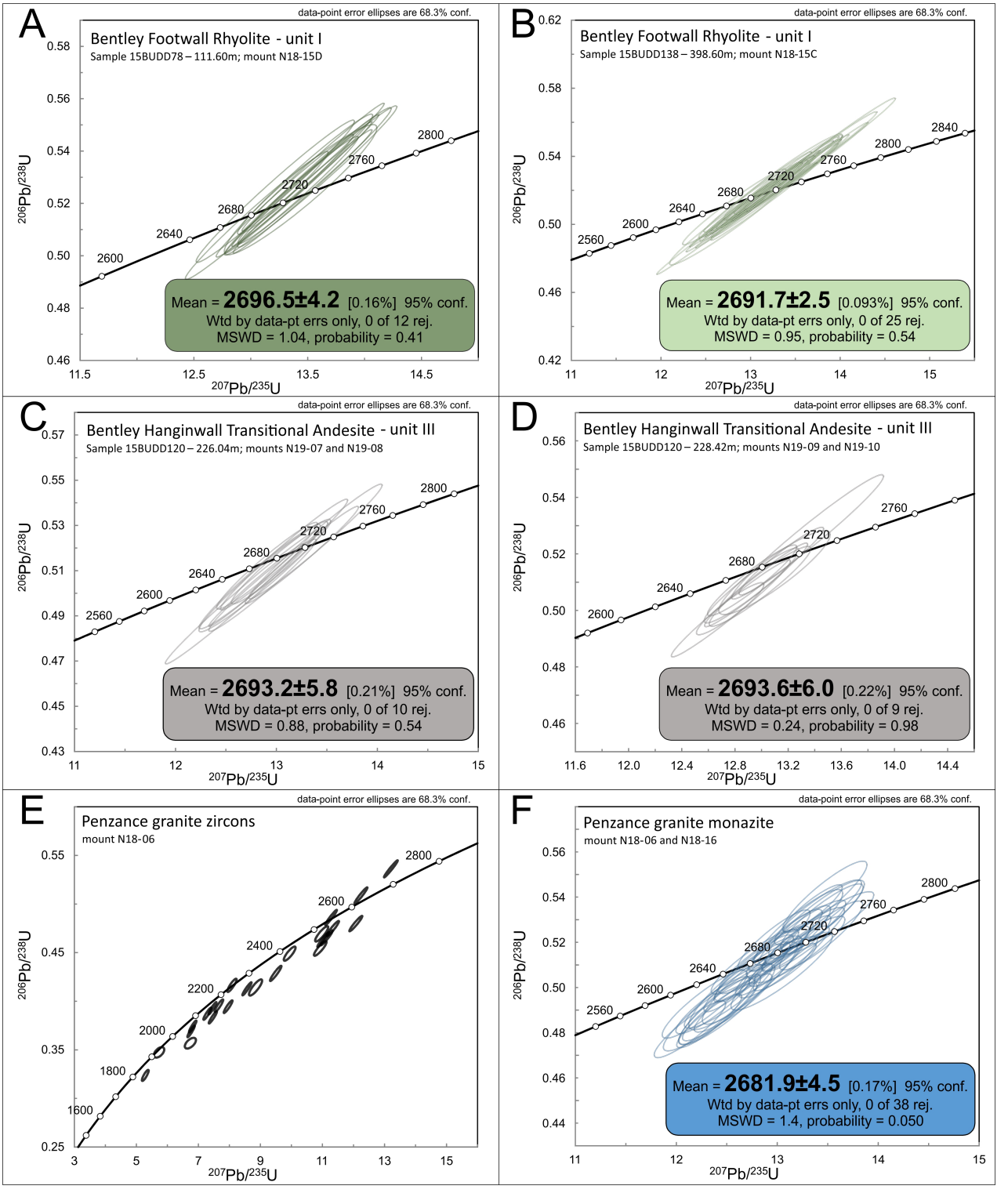
A
data-point error ellipses are 68.3% conf.
Bentley Footwall Rhyolite - unit I
Sample 15BUDD78 – 111.60m; mount N18-15D
Mean = 2696.5±4.2 [0.16%] 95% conf.
Wtd by data-pt errs only, 0 of 12 rej.
MSWD = 1.04, probability = 0.41
B
data-point error ellipses are 68.3% conf.
Bentley Footwall Rhyolite - unit I
Sample 15BUDD138 – 398.60m; mount N18-15C
Mean = 2691.7±2.5 [0.093%] 95% conf.
Wtd by data-pt errs only, 0 of 25 rej.
MSWD = 0.95, probability = 0.54
C
data-point error ellipses are 68.3% conf.
Bentley Hanginwall Transitional Andesite - unit III
Sample 15BUDD120 – 226.04m; mounts N19-07 and N19-08
Mean = 2693.2±5.8 [0.21%] 95% conf.
Wtd by data-pt errs only, 0 of 10 rej.
MSWD = 0.88, probability = 0.54
D
data-point error ellipses are 68.3% conf.
Bentley Hanginwall Transitional Andesite - unit III
Sample 15BUDD120 – 228.42m; mounts N19-09 and N19-10
Mean = 2693.6±6.0 [0.22%] 95% conf.
Wtd by data-pt errs only, 0 of 9 rej.
MSWD = 0.24, probability = 0.98
E
data-point error ellipses are 68.3% conf.
Penzance granite zircons
mount N18-06
F
data-point error ellipses are 68.3% conf.
Penzance granite monazite
mount N18-06 and N18-16
Mean = 2681.9±4.5 [0.17%] 95% conf.
Wtd by data-pt errs only, 0 of 38 rej.
MSWD = 1.4, probability = 0.050
206Pb/238U
207Pb/235U

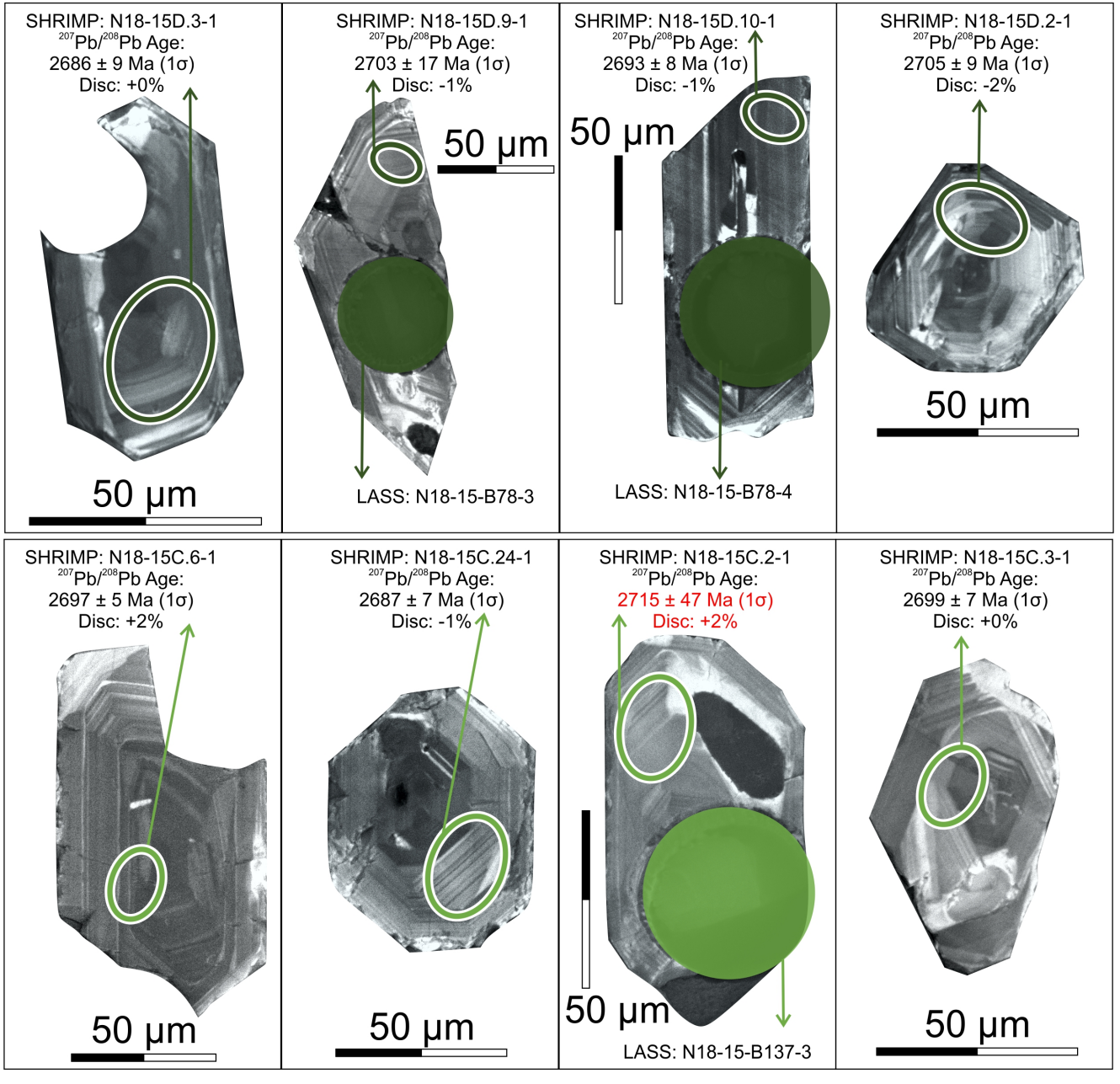
SHRIMP: N18-15D.3-1
$^{207}Pb/^{208}Pb$ Age:
2686 ± 9 Ma (1σ)
Disc: +0%
50 µm
SHRIMP: N18-15D.9-1
$^{207}Pb/^{208}Pb$ Age:
2703 ± 17 Ma (1σ)
Disc: -1%
50 µm
LASS: N18-15-B78-3
SHRIMP: N18-15D.10-1
$^{207}Pb/^{208}Pb$ Age:
2693 ± 8 Ma (1σ)
Disc: -1%
50 µm
LASS: N18-15-B78-4
SHRIMP: N18-15D.2-1
$^{207}Pb/^{208}Pb$ Age:
2705 ± 9 Ma (1σ)
Disc: -2%
50 µm
SHRIMP: N18-15C.6-1
$^{207}Pb/^{208}Pb$ Age:
2697 ± 5 Ma (1σ)
Disc: +2%
50 µm
SHRIMP: N18-15C.24-1
$^{207}Pb/^{208}Pb$ Age:
2687 ± 7 Ma (1σ)
Disc: -1%
50 µm
SHRIMP: N18-15C.2-1
$^{207}Pb/^{208}Pb$ Age:
2715 ± 47 Ma (1σ)
Disc: +2%
50 µm
LASS: N18-15-B137-3
SHRIMP: N18-15C.3-1
$^{207}Pb/^{208}Pb$ Age:
2699 ± 7 Ma (1σ)
Disc: +0%
50 µm

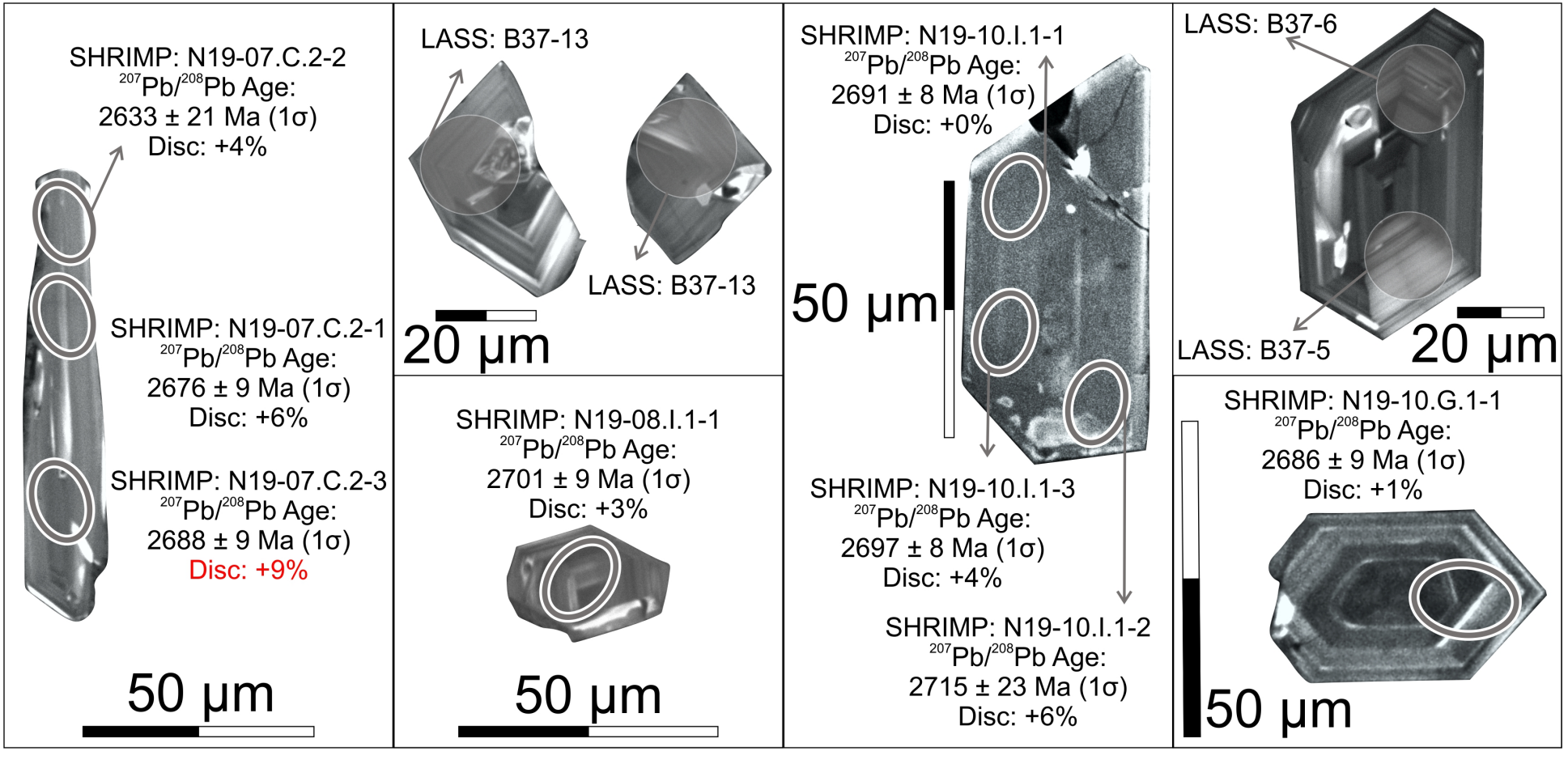
SHRIMP: N19-07.C.2-2
207Pb/208Pb Age:
2633 ± 21 Ma (1σ)
Disc: +4%
SHRIMP: N19-07.C.2-1
207Pb/208Pb Age:
2676 ± 9 Ma (1σ)
Disc: +6%
SHRIMP: N19-07.C.2-3
207Pb/208Pb Age:
2688 ± 9 Ma (1σ)
Disc: +9%
50 µm
LASS: B37-13
LASS: B37-13
20 µm
SHRIMP: N19-08.I.1-1
207Pb/208Pb Age:
2701 ± 9 Ma (1σ)
Disc: +3%
50 µm
SHRIMP: N19-10.I.1-1
207Pb/208Pb Age:
2691 ± 8 Ma (1σ)
Disc: +0%
50 µm
SHRIMP: N19-10.I.1-3
207Pb/208Pb Age:
2697 ± 8 Ma (1σ)
Disc: +4%
SHRIMP: N19-10.I.1-2
207Pb/208Pb Age:
2715 ± 23 Ma (1σ)
Disc: +6%
LASS: B37-6
LASS: B37-5
20 µm
SHRIMP: N19-10.G.1-1
207Pb/208Pb Age:
2686 ± 9 Ma (1σ)
Disc: +1%
50 µm

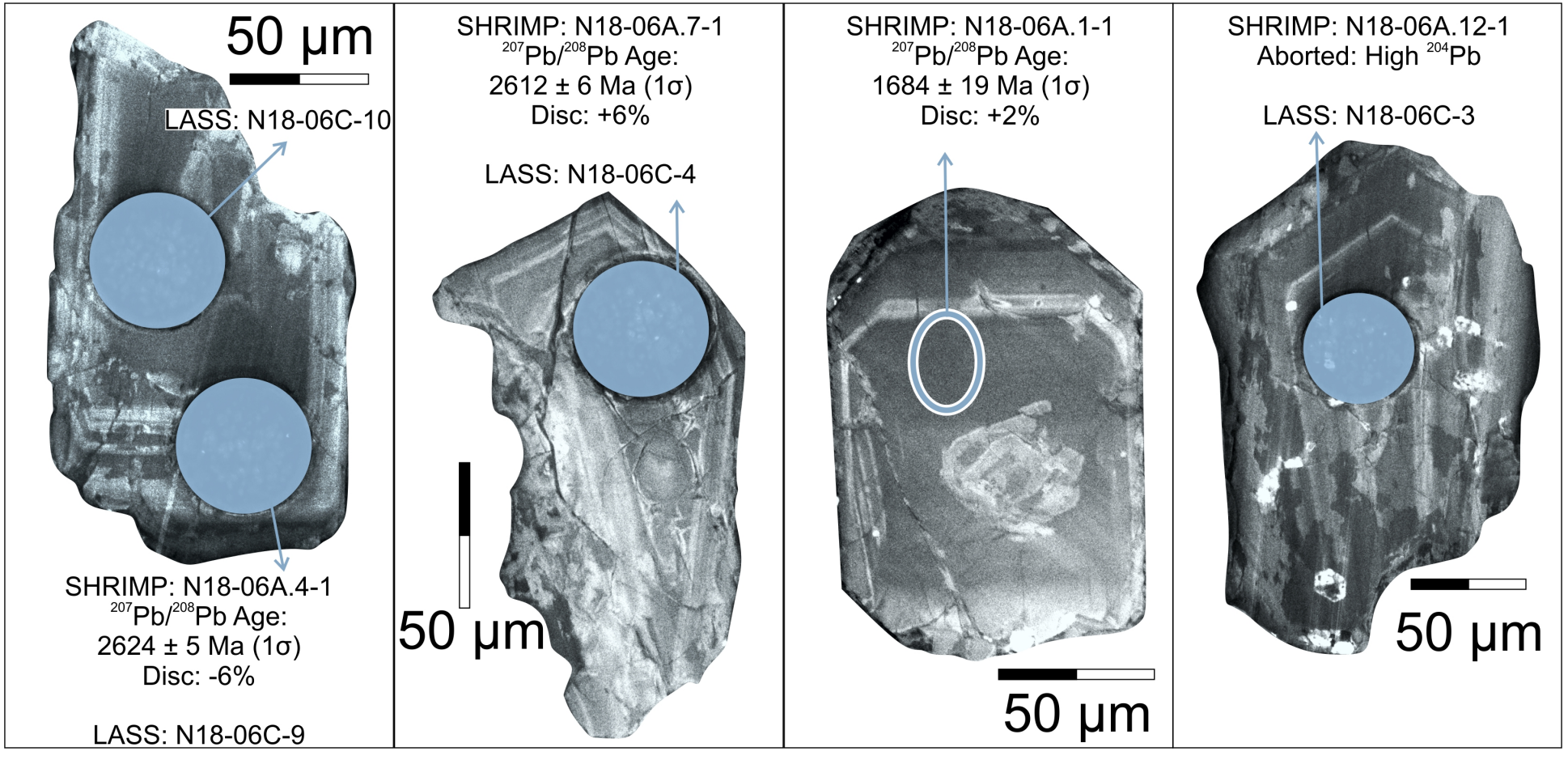
50 µm
LASS: N18-06C-10
SHRIMP: N18-06A.4-1
$^{207}Pb/^{208}Pb$ Age:
2624 ± 5 Ma (1σ)
Disc: -6%
LASS: N18-06C-9
SHRIMP: N18-06A.7-1
$^{207}Pb/^{208}Pb$ Age:
2612 ± 6 Ma (1σ)
Disc: +6%
LASS: N18-06C-4
50 µm
SHRIMP: N18-06A.1-1
$^{207}Pb/^{208}Pb$ Age:
1684 ± 19 Ma (1σ)
Disc: +2%
50 µm
SHRIMP: N18-06A.12-1
Aborted: High ^{204}Pb
LASS: N18-06C-3
50 µm

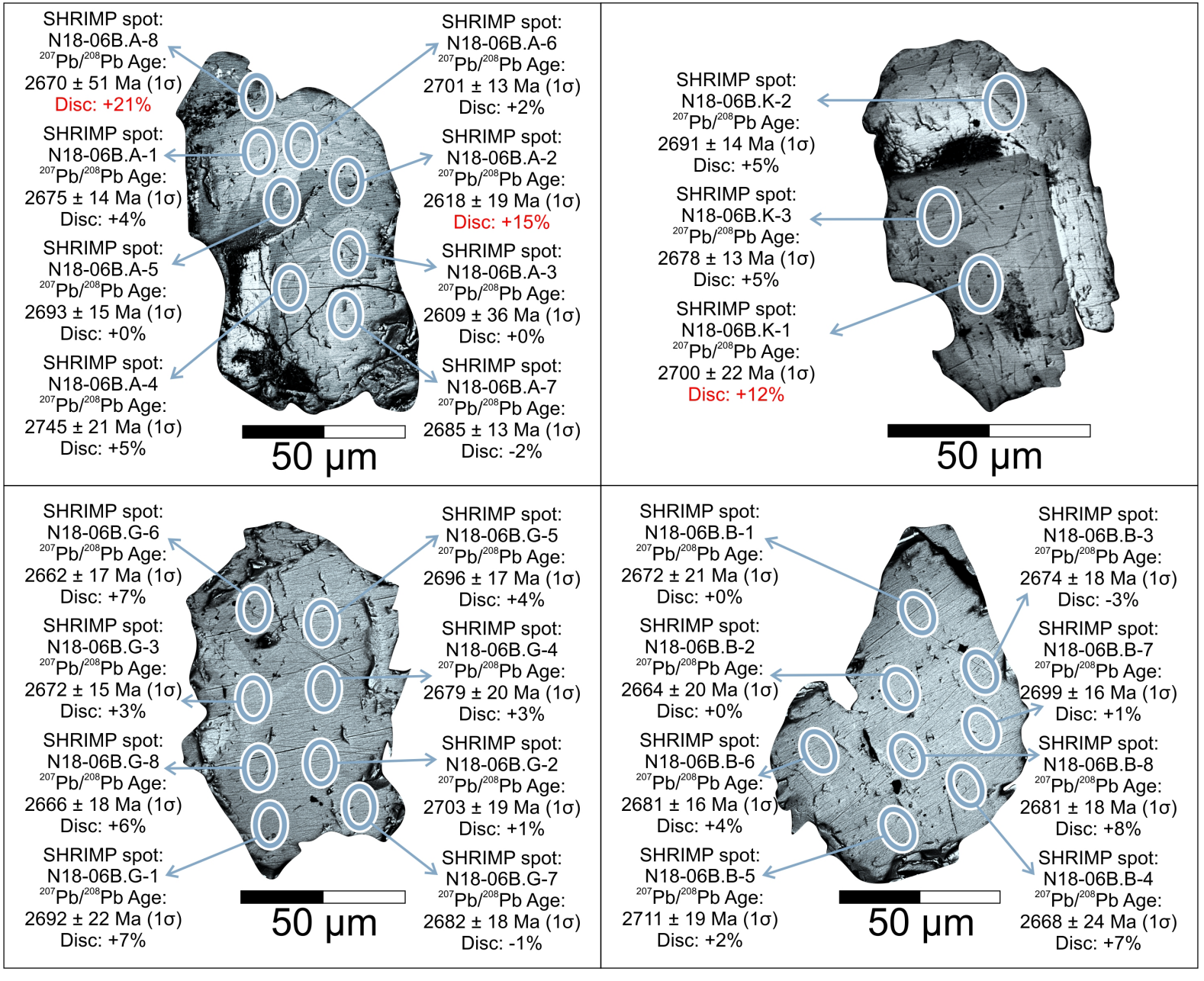
SHRIMP spot:
N18-06B.A-8
$^{207}Pb/^{208}Pb$ Age:
2670 ± 51 Ma (1σ)
Disc: +21%
SHRIMP spot:
N18-06B.A-1
$^{207}Pb/^{208}Pb$ Age:
2675 ± 14 Ma (1σ)
Disc: +4%
SHRIMP spot:
N18-06B.A-5
$^{207}Pb/^{208}Pb$ Age:
2693 ± 15 Ma (1σ)
Disc: +0%
SHRIMP spot:
N18-06B.A-4
$^{207}Pb/^{208}Pb$ Age:
2745 ± 21 Ma (1σ)
Disc: +5%
SHRIMP spot:
N18-06B.A-6
$^{207}Pb/^{208}Pb$ Age:
2701 ± 13 Ma (1σ)
Disc: +2%
SHRIMP spot:
N18-06B.A-2
$^{207}Pb/^{208}Pb$ Age:
2618 ± 19 Ma (1σ)
Disc: +15%
SHRIMP spot:
N18-06B.A-3
$^{207}Pb/^{208}Pb$ Age:
2609 ± 36 Ma (1σ)
Disc: +0%
SHRIMP spot:
N18-06B.A-7
$^{207}Pb/^{208}Pb$ Age:
2685 ± 13 Ma (1σ)
Disc: -2%
50 µm
SHRIMP spot:
N18-06B.K-2
$^{207}Pb/^{208}Pb$ Age:
2691 ± 14 Ma (1σ)
Disc: +5%
SHRIMP spot:
N18-06B.K-3
$^{207}Pb/^{208}Pb$ Age:
2678 ± 13 Ma (1σ)
Disc: +5%
SHRIMP spot:
N18-06B.K-1
$^{207}Pb/^{208}Pb$ Age:
2700 ± 22 Ma (1σ)
Disc: +12%
50 µm
SHRIMP spot:
N18-06B.G-6
$^{207}Pb/^{208}Pb$ Age:
2662 ± 17 Ma (1σ)
Disc: +7%
SHRIMP spot:
N18-06B.G-3
$^{207}Pb/^{208}Pb$ Age:
2672 ± 15 Ma (1σ)
Disc: +3%
SHRIMP spot:
N18-06B.G-8
$^{207}Pb/^{208}Pb$ Age:
2666 ± 18 Ma (1σ)
Disc: +6%
SHRIMP spot:
N18-06B.G-1
$^{207}Pb/^{208}Pb$ Age:
2692 ± 22 Ma (1σ)
Disc: +7%
SHRIMP spot:
N18-06B.G-5
$^{207}Pb/^{208}Pb$ Age:
2696 ± 17 Ma (1σ)
Disc: +4%
SHRIMP spot:
N18-06B.G-4
$^{207}Pb/^{208}Pb$ Age:
2679 ± 20 Ma (1σ)
Disc: +3%
SHRIMP spot:
N18-06B.G-2
$^{207}Pb/^{208}Pb$ Age:
2703 ± 19 Ma (1σ)
Disc: +1%
SHRIMP spot:
N18-06B.G-7
$^{207}Pb/^{208}Pb$ Age:
2682 ± 18 Ma (1σ)
Disc: -1%
50 µm
SHRIMP spot:
N18-06B.B-1
$^{207}Pb/^{208}Pb$ Age:
2672 ± 21 Ma (1σ)
Disc: +0%
SHRIMP spot:
N18-06B.B-2
$^{207}Pb/^{208}Pb$ Age:
2664 ± 20 Ma (1σ)
Disc: +0%
SHRIMP spot:
N18-06B.B-6
$^{207}Pb/^{208}Pb$ Age:
2681 ± 16 Ma (1σ)
Disc: +4%
SHRIMP spot:
N18-06B.B-5
$^{207}Pb/^{208}Pb$ Age:
2711 ± 19 Ma (1σ)
Disc: +2%
SHRIMP spot:
N18-06B.B-3
$^{207}Pb/^{208}Pb$ Age:
2674 ± 18 Ma (1σ)
Disc: -3%
SHRIMP spot:
N18-06B.B-7
$^{207}Pb/^{208}Pb$ Age:
2699 ± 16 Ma (1σ)
Disc: +1%
SHRIMP spot:
N18-06B.B-8
$^{207}Pb/^{208}Pb$ Age:
2681 ± 18 Ma (1σ)
Disc: +8%
SHRIMP spot:
N18-06B.B-4
$^{207}Pb/^{208}Pb$ Age:
2668 ± 24 Ma (1σ)
Disc: +7%
50 µm

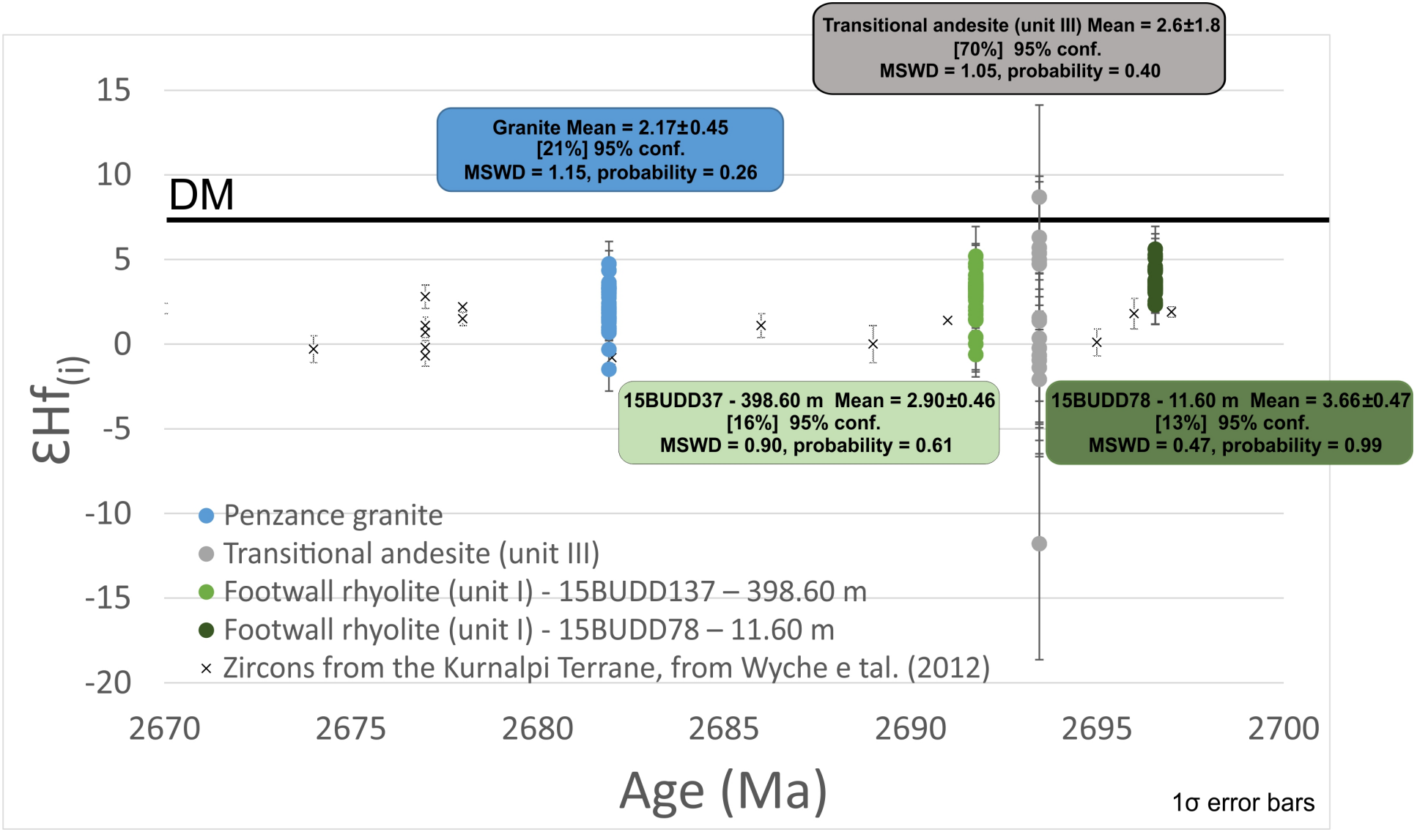
Transitional andesite (unit III) Mean = 2.6±1.8
[70%] 95% conf.
MSWD = 1.05, probability = 0.40
Granite Mean = 2.17±0.45
[21%] 95% conf.
MSWD = 1.15, probability = 0.26
DM
15BUDD37 - 398.60 m Mean = 2.90±0.46
[16%] 95% conf.
MSWD = 0.90, probability = 0.61
15BUDD78 - 11.60 m Mean = 3.66±0.47
[13%] 95% conf.
MSWD = 0.47, probability = 0.99
εHf(i)
15
10
5
0
-5
-10
-15
-20
Penzance granite
Transitional andesite (unit III)
Footwall rhyolite (unit I) - 15BUDD137 – 398.60 m
Footwall rhyolite (unit I) - 15BUDD78 – 11.60 m
Zircons from the Kurnalpi Terrane, from Wyche e tal. (2012)
2670
2675
2680
2685
2690
2695
2700
Age (Ma)
1σ error bars

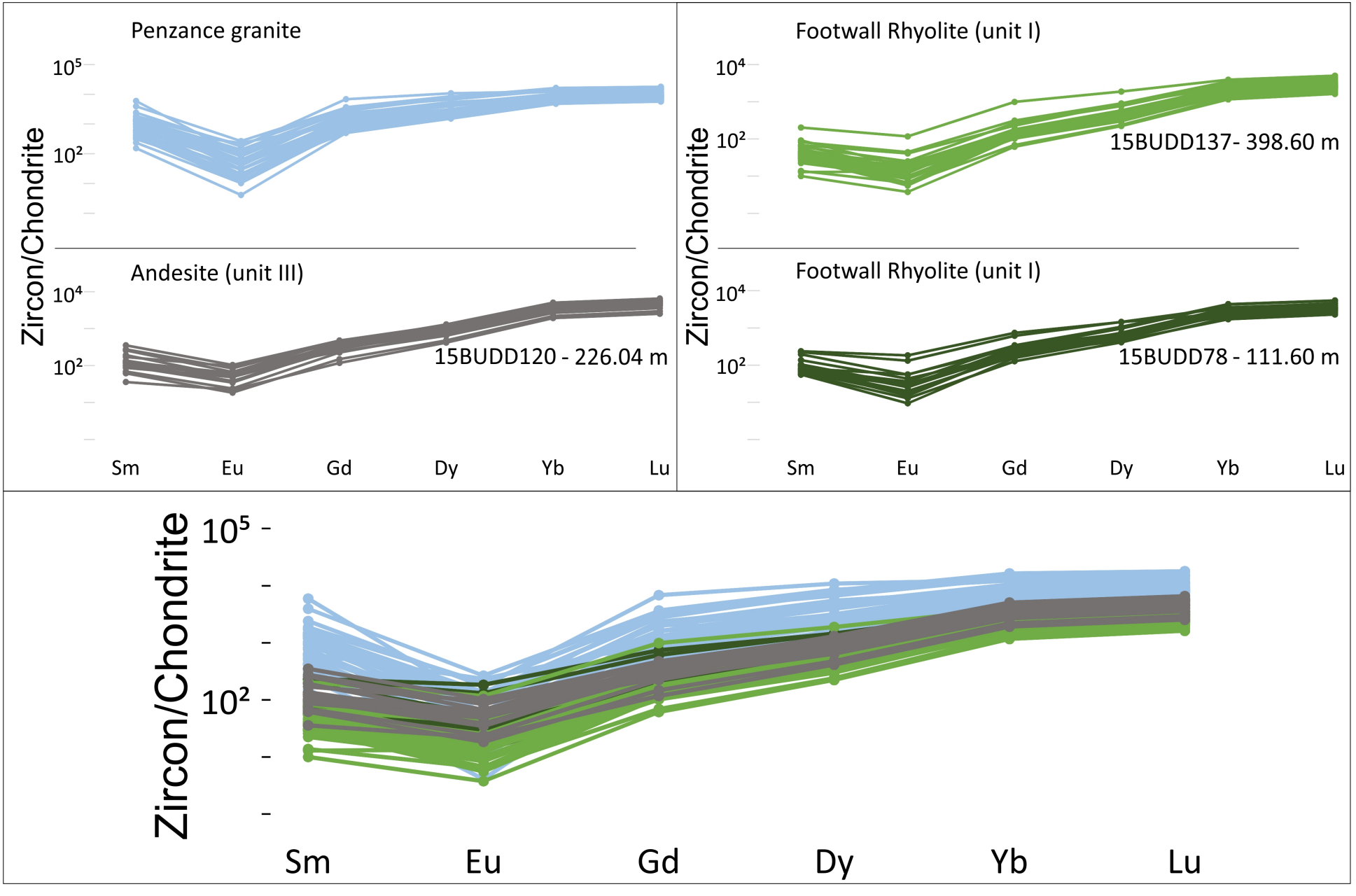
Penzance granite
Zircon/Chondrite
10^5
10^2
Andesite (unit III)
10^4
10^2
15BUDD120 - 226.04 m
Sm
Eu
Gd
Dy
Yb
Lu
Footwall Rhyolite (unit I)
10^4
10^2
15BUDD137- 398.60 m
Footwall Rhyolite (unit I)
10^4
10^2
15BUDD78 - 111.60 m
Zircon/Chondrite
10^5
10^2
Sm
Eu
Gd
Dy
Yb
Lu

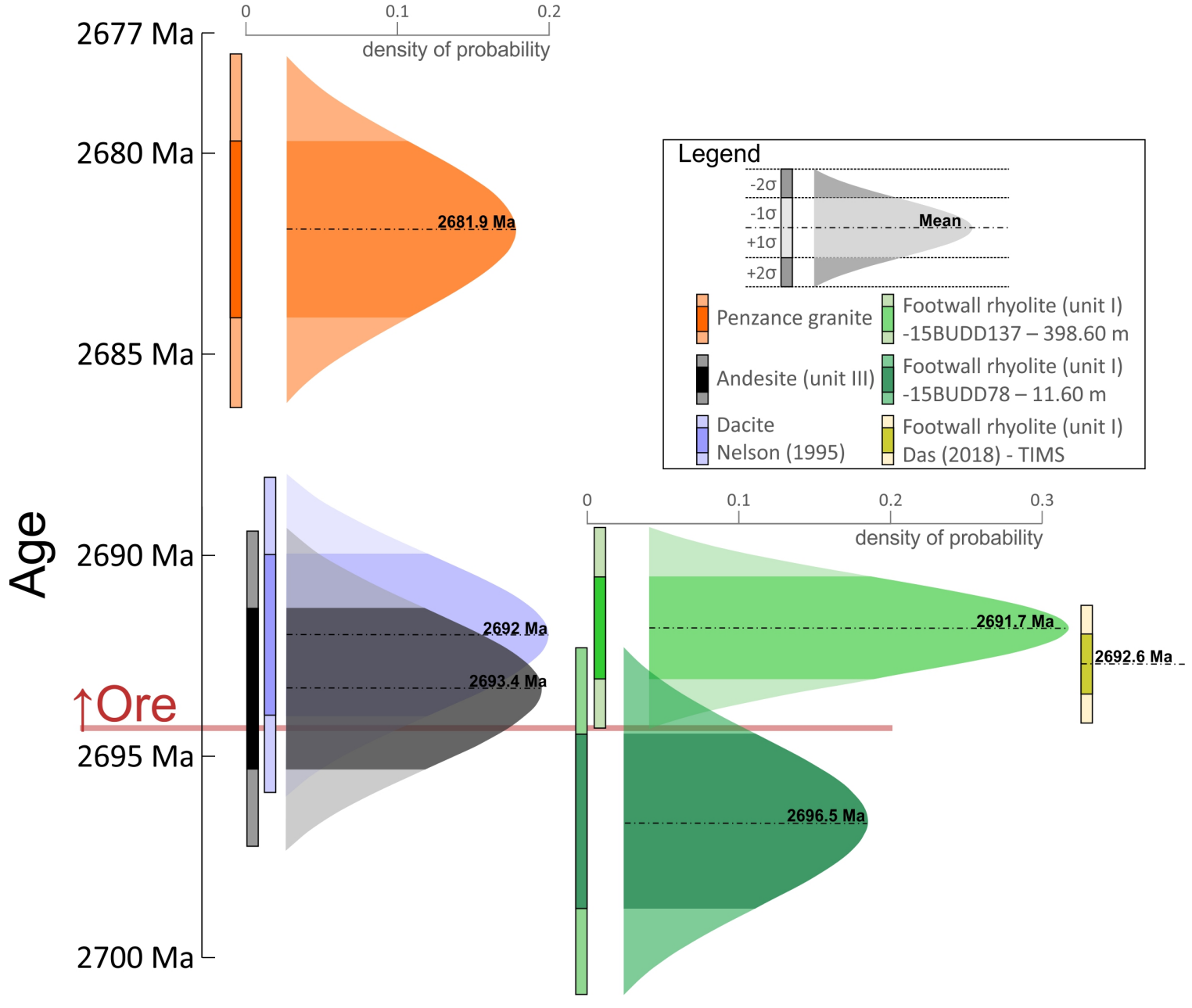
0
0.1
0.2
density of probability
2677 Ma
2680 Ma
2685 Ma
2690 Ma
2695 Ma
2700 Ma
Age
2681.9 Ma
Legend
-2σ
-1σ
+1σ
+2σ
Mean
Penzance granite
Andesite (unit III)
Dacite
Nelson (1995)
Footwall rhyolite (unit I)
-15BUDD137 – 398.60 m
Footwall rhyolite (unit I)
-15BUDD78 – 11.60 m
Footwall rhyolite (unit I)
Das (2018) - TIMS
0
0.1
0.2
0.3
density of probability
2692 Ma
2693.4 Ma
↑Ore
2691.7 Ma
2692.6 Ma
2696.5 Ma

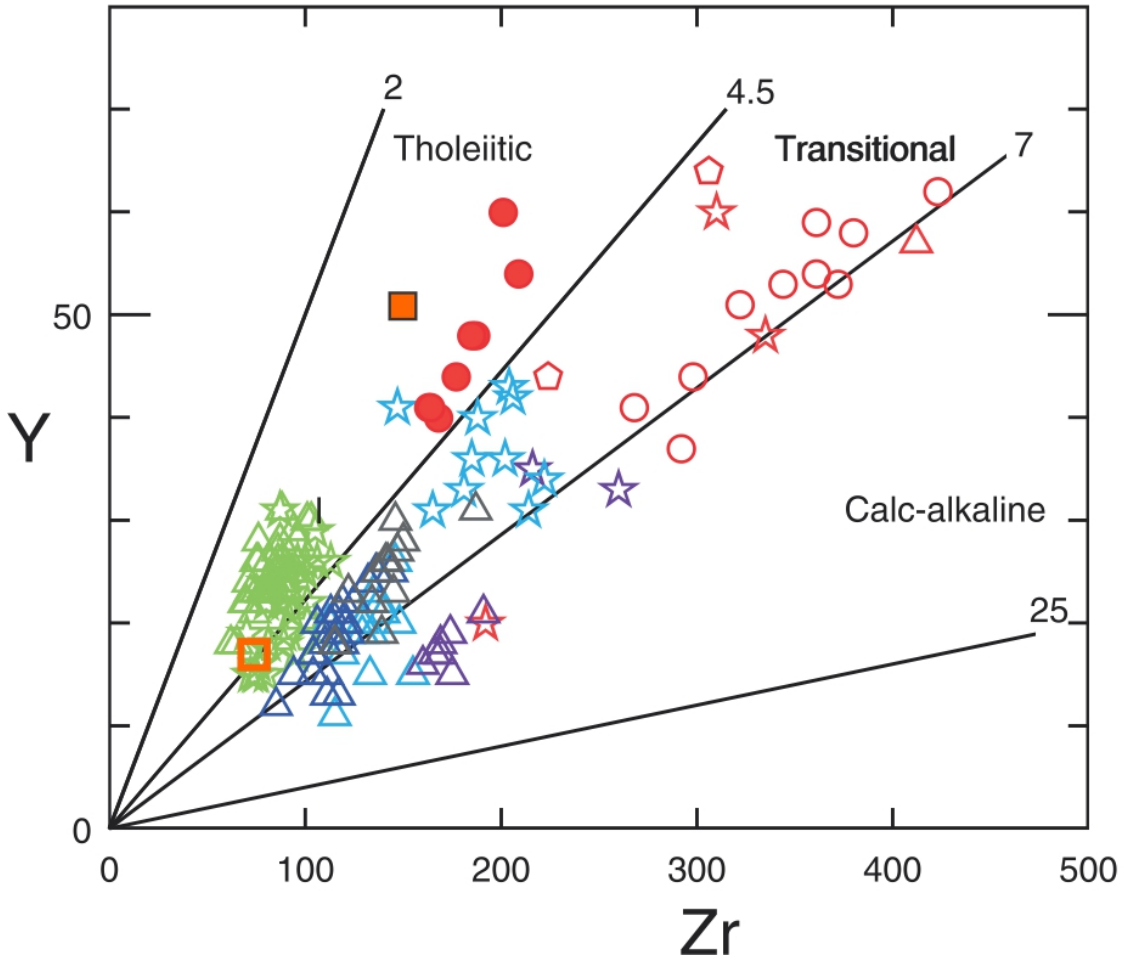

OZCHEM

- Penzance (Kent) granite (96969076)* Zr/Y = 2.9
- Penzance granite (92969084)* Zr/Y = 4.6

Belford et al. (2015)

- hangingwall upper rhyolite
- hangingwall upper andesite

unit VI

- hangingwall basalt
- hangingwall andesite 3
- hangingwall andesite 2
- hangingwall andesite 1

unit V

- mineralized package felsics (thol)
- mineralized package felsics (trans)
- mineralized package felsics (calc-alk)

unit IV

- footwall basalts
- footwall andesites

unit III

- footwall felsics
- deep footwall andesite

unit I

Declaration of conflict of interests

 The authors declare that they have no known competing financial interests or personal relationships that could have appeared to influence the work reported in this paper.

☐The authors declare the following financial interests/personal relationships which may be considered as potential competing interests:

Vitor Rodrigues Barrote

SUPPLEMENTARY MATERIAL 1

1.1 SHRIMP U-Pb dating of Zircon and Monazite

1.1.1 Mount preparation

Zircon and monazite grains were separated from crushed rock samples using a Frantz magnetic separator and heavy liquids (methylene iodide). Grains were handpicked, mounted in epoxy resin discs and polished to expose their interiors. The zircon crystals were characterized by cathodoluminescence (CL) imaging, and monazite crystals by back-scattered electron (BSE) microscopy using the Mira3, at the Microscopy and Microanalysis Facility, John de Laeter Centre, Curtin University. The epoxy mounts were carbon coated for SEM imaging and Au-coated before each SHRIMP analytical session.

Polished thin sections prepared from samples of transitional andesite (unit III) were examined to identify suitable zircon grains for SHRIMP geochronology using the Tescan Integrated Mineral Analyzer (TIMA GM) and back-scattered electron (BSE) microscopy using the Mira3, at the Microscopy and Microanalysis Facility, John de Laeter Centre, Curtin University. Portions of the thin sections containing grains large enough (>15 μm) for ion microprobe analysis were drilled out, in ~3 mm plugs, and cast in 25 mm epoxy mounts. The reference materials were in a separate mount that was cleaned and Au-coated with the sample mounts before each SHRIMP analytical session.

1.1.2 Zircon

Selected areas of the imaged zircon were analysed on the SHRIMP II at the John de Laeter Centre, Curtin University (JdLC). The analytical procedures for the Curtin consortium SHRIMP II have been described by de Laeter and Kennedy (1998) and Kennedy and de Laeter (1994) and are similar to those described by Compston et al. (1984) and Williams (1998). For the larger zircons in grain mounts, a 20-25 μm elliptical spot was used, with a mass-filtered O_2^--

primary beam of ~2.8-3.0 nA, whereas a 10-12 μm spot of ~0.5 nA was used on the smaller zircons in polished thin sections. Data for each spot was collected in sets of six scans on the zircons through the mass range of $^{196}Zr2O^{+}$, $^{204}Pb^{+}$, Background, $^{206}Pb^{+}$, $^{207}Pb^{+}$, $^{208}Pb^{+}$, $^{238}U^{+}$, $^{248}ThO^{+}$ and $^{254}UO^{+}$. The $^{206}Pb/^{238}U$ age standard and U-content standard used was M257 (561.3 Ma and 840 ppm U; Nasdala et al., 2008) while OGC zircon was utilized as the $^{207}Pb/^{206}Pb$ standard, to monitor instrument induced mass fractionation (3465.4 ± 0.6 Ma; Stern et al., 2009). The $^{207}Pb/^{206}Pb$ dates obtained on OGC zircons during the SHRIMP sessions matched the $^{207}Pb/^{206}Pb$ standard age within uncertainty and no fractionation correction was warranted. The common Pb correction was based on the measured ^{204}Pb-content (Compston et al., 1984). The correction formula for Pb/U fractionation is $^{206}Pb^{+}/^{238}U^{+}$ = a $(^{254}UO^{+}/^{238}U^{+})^{b}$ (Claoué-Long et al., 1995) using the parameter values of Black et al. (2003). The constant "a" is determined empirically from analyses of the standard during each analytical session. The programs SQUID II and Isoplot (Ludwig, 2011, 2009) were used for data processing.

1.1.3 Monazite

The U–Th–Pb analyses were performed using the high spatial-resolution capability of the SHRIMP II at the JdLC. Monazite was analysed in two analytical sessions. Grains were analysed using a 30 μm Köhler aperture, ~0.3 nA primary ion beam (O_2^-) and a ~10 μm analysis spot. Energy filtering was not applied, and the post-collector retardation lens was activated to reduce stray ion arrivals. The mass resolution (M/ΔM at 1% peak height) was >5000. French ($^{206}Pb/^{238}U$ age 514 Ma) was used as the primary Pb/U reference material, and Z2908 and Z2234 were the secondary reference materials used to monitor matrix effects (Fletcher et al., 2010). Z2908 ($^{207}Pb/^{206}Pb$ age 1796 Ma) was also analysed to monitor and correct for instrumental mass fractionation of ^{207}Pb from ^{206}Pb. SQUID II software (Ludwig, 2009) was used for initial data reduction including ^{204}Pb correction. Matrix effects in $^{206}Pb/^{238}U$ were corrected following established protocols detailed by Fletcher et al. (2010). 9 analyses of

Z2908 yielded a mean $^{207}Pb/^{206}Pb$ age of 1796.7 ± 5.4 Ma (mean square weighted deviation, MSWD = 1.7). An insignificant fractionation correction (0.02%) was applied to sample data, with no augmentation of sample precision required based on the reproducibility of $^{207}Pb/^{206}Pb$ in the reference materials. $^{207}Pb/^{206}Pb$ dates from individual analyses are presented with 1σ internal precision, whereas weighted mean $^{207}Pb/^{206}Pb$ dates are reported at 95% confidence limits.

1.2 LA-SS-ICPMS of Zircon – Trace elements and Hf isotopes

Zircon Lu–Hf isotopes and rare earth element (REE) abundances were measured over two analytical sessions using laser ablation split stream inductively coupled plasma mass spectrometry (LA-SS-ICPMS). The analyses were conducted in zircons from the same samples that were analysed by SHRIMP, but not necessarily on the same grain or over the same spot as the SHRIMP analysis. Isotopic and elemental data were collected simultaneously using a Resonetics S-155-LR 193 nm excimer laser coupled to a Nu Plasma II multicollector and Agilent 7700s quadrupole mass spectrometer in the GeoHistory Facility, JdLC at Curtin University.

Samples 15BUDD120 – 228.42 and 15BUDD120 – 226.04 m, from the Transitional andesite (unit III) were analysed with a laser spot diameter of 24 μm, with 2.7 J/cm^2 on-sample laser energy, repetition rate of 10 Hz, ablation time of 25 seconds and ~30 seconds of background capture before and after each analysis. Two cleaning pulse preceded analysis. The spot size and ablation time in this case were limited by the smaller size of the zircons.

The remaining samples were analysed with a laser spot diameter of 50 μm, with 2.7 J/cm^2 on-sample laser energy, repetition rate of 10 Hz, ablation time of 40 seconds and ~45 seconds of total baseline acquisition.

Zircon standard P1 (Li et al., 2010; chips of Penglai zircon characterised in-house for trace element composition) was used as the primary standard to calculate element concentrations

using ^{91}Zr as the internal reference isotope and assuming 43.14% Zr in zircon, and to correct for instrument drift.

Lu–Hf isotopic data were measured simultaneously for ^{172}Yb, ^{173}Yb, ^{175}Lu, $^{176}Hf+Yb+Lu$, ^{177}Hf, ^{178}Hf, ^{179}Hf and ^{180}Hf on the Faraday array. Time resolved data was baseline subtracted and reduced using Iolite3.5 (DRS after Woodhead et al., 2004), where ^{176}Yb and ^{176}Lu were removed from the 176 mass signal using $^{176}Yb/^{173}Yb = 0.7962$ (Chu et al., 2002) and $^{176}Lu/^{175}Lu = 0.02655$ (Chu et al., 2002) with an exponential law mass bias correction assuming $^{172}Yb/^{173}Yb = 1.35274$ (Chu et al., 2002). The interference corrected $^{176}Hf/^{177}Hf$ was normalized to $^{179}Hf/^{177}Hf = 0.7325$ (Patchett and Tatsumoto, 1980) for mass bias correction. Zircons from the Mud Tank carbonatite locality were analysed together with the samples in each session to determine corrected, standard referenced $^{176}Hf/^{177}Hf$ (Table 1). Zircon standards with a range of REE contents (FC1 91500, Plešovice and GJ-1; references and data in Table 1) were run to verify the method. All analysed standards fell within 2σ error of reported $^{176}Hf/^{177}Hf$ values, although uncertainties on the 24 micron beam run were, understandably, significantly higher. In addition, the corrected $^{178}Hf/^{177}Hf$ and $^{180}Hf/^{177}Hf$ ratios (for the 50 micron beam run) were calculated to monitor the accuracy of the mass bias correction and yielded an average value of 1.467193 ± 12 and 1.886808 ± 11 (n=184), which is within the range of values reported by Thirlwall and Anczkiewicz (2004). Calculation of εHf values employed the decay constant of Scherer et al. (2001) and the Chondritic Uniform Reservoir (CHUR) values of Blichert-Toft and Albarède (1997).

Table 1: Summary of the Hf isotope measurements of standard materials used interspersed with analyses of unknown zircons. Mean values were calculated using the built-in statistics from the Iolite software (Paton et al., 2011)

Standard Material	**50 µm**	**24 µm**	**Reference Value**
	Corrected $^{176}Hf/^{177}Hf$	**Corrected $^{176}Hf/^{177}Hf$**	
Mud Tank	**0.282505 ± 14** (MSWD = 0.70, n = 14)	**0.282507 ± 64** (MSWD = 2.9, n = 6)	0.282505 ± 44 (Woodhead and Hergt, 2005)
FC1	**0.282182 ± 9** (MSWD = 0.31, n = 9)	**0.282229 ± 150** (MSWD = 3.9, n = 6)	0.282172 ± 42 (Woodhead and Hergt, 2005)

91500	**0.282306 ± 11** (MSWD = 0.71, n = 14)	**0.282235 ± 130** (MSWD = 2.4, n = 6)	0.282306 ± 40 (Woodhead et al., 2004)
Plešovice	**0.282477 ± 8** (MSWD = 0.3, n = 10)	**0.282470 ± 51** (MSWD = 0.49, n = 6)	0.282482 ± 13 (Sláma et al., 2008)
GJ-1	**0.282016 ± 12** (MSWD = 0.69, n = 14)	**0.281201 ± 110** (MSWD = 1.1, n = 6)	0.282000 ± 5 (Morel et al., 2008)

1.3 References

Black, L.P., Kamo, S.L., Allen, C.M., Aleinikoff, J.N., Davis, D.W., Korsch, R.J., Foudoulis, C., 2003. TEMORA 1: a new zircon standard for Phanerozoic U–Pb geochronology. Chem. Geol. 200, 155–170. https://doi.org/10.1016/S0009-2541(03)00165-7

Blichert-Toft, J., Albarède, F., 1997. The Lu-Hf isotope geochemistry of chondrites and the evolution of the mantle-crust system. Earth Planet. Sci. Lett. 148, 243–258. https://doi.org/10.1016/S0012-821X(97)00040-X

Claoué-Long, J.C., Compston, W., Roberts, J., Fanning, C.M., 1995. Two Carboniferous Ages: A Comparison of Shrimp Zircon Dating with Conventional Zircon Ages and 40Ar/39Ar Analysis, in: Berggren, W.A., Kent, D.V., Aubry, M.-P., Hardenbol, J. (Eds.), Geochronology, Time Scales, and Global Stratigraphic Correlation, Society for Sedimentary Geology Special Publications. SEPM (Society for Sedimentary Geology), pp. 3–21. https://doi.org/10.2110/pec.95.54

Compston, W., Williams, I.S., Meyer, C., 1984. U-Pb geochronology of zircons from lunar breccia 73217 using a sensitive high mass-resolution ion microprobe. Proc. 14th Lunar Planet. Sci. Conf. J. Geophys. Res. Suppl 89, B525–B534. https://doi.org/10.1029/JB089iS02p0B525

Chu, N.-C., Taylor, R.N., Chavagnac, V., Nesbitt, R.W., Boella, R.M., Milton, J.A., German, C.R., Bayon, G., Burton, K., 2002. Hf isotope ratio analysis using multi-collector inductively coupled plasma mass spectrometry: an evaluation of isobaric interference corrections. J. Anal. At. Spectrom. 17, 1567–1574. https://doi.org/10.1039/b206707b

de Laeter, J.R., Kennedy, A.K., 1998. A double focusing mass spectrometer for geochronology. Int. J. Mass Spectrom. 178, 43–50. https://doi.org/10.1016/S1387-3806(98)14092-7

Fletcher, I.R., McNaughton, N.J., Davis, W.J., Rasmussen, B., 2010. Matrix effects and calibration limitations in ion probe U–Pb and Th–Pb dating of monazite. Chem. Geol. 270, 31–44. https://doi.org/10.1016/j.chemgeo.2009.11.003

Kennedy, A.K., De Laeter, J.R., 1994. The performance characteristics of the WA SHRIMP II ion microprobe., in: Abstracts Vol., U.S. Geological Survey Circular. Presented at the Eighth International Conference on Geochronology, Cosmochronology and Isotope Geology, Berkeley, USA, p. 166.

Li, X.-H., Long, W.-G., Li, Q.-L., Liu, Y., Zheng, Y.-F., Yang, Y.-H., Chamberlain, K.R., Wan, D.-F., Guo, C.-H., Wang, X.-C., Tao, H., 2010. Penglai Zircon Megacrysts: A Potential New Working Reference Material for Microbeam Determination of Hf-O Isotopes and U-Pb Age. Geostand. Geoanalytical Res. 34, 117–134. https://doi.org/10.1111/j.1751-908X.2010.00036.x

Ludwig, K.R., 2011. User's manual for Isoplot 4.15: a geochronological toolkit for Microsoft Excel, Berkeley Geochronology Center Special Publication.

Ludwig, K.R., 2009. Squid 2.50, A User's Manual, Berkeley Geochronology Centre Special Publication.

Morel, M.L.A., Nebel, O., Nebel-Jacobsen, Y.J., Miller, J.S., Vroon, P.Z., 2008. Hafnium isotope characterization of the GJ-1 zircon reference material by solution and laser-

ablation MC-ICPMS. Chem. Geol. 255, 231–235. https://doi.org/10.1016/j.chemgeo.2008.06.040

Nasdala, L., Hofmeister, W., Norberg, N., Martinson, J.M., Corfu, F., Dörr, W., Kamo, S.L., Kennedy, A.K., Kronz, A., Reiners, P.W., Frei, D., Kosler, J., Wan, Y., Götze, J., Häger, T., Kröner, A., Valley, J.W., 2008. Zircon M257 - a Homogeneous Natural Reference Material for the Ion Microprobe U-Pb Analysis of Zircon. Geostand. Geoanalytical Res. 32, 247–265. https://doi.org/10.1111/j.1751-908X.2008.00914.x

Patchett, P.J., Tatsumoto, M., 1980. Hafnium isotope variations in oceanic basalts. Geophys. Res. Lett. 7, 1077–1080. https://doi.org/10.1029/GL007i012p01077

Paton, C., Hellstrom, J., Paul, B., Woodhead, J., Hergt, J., 2011. Iolite: Freeware for the visualisation and processing of mass spectrometric data. J. Anal. At. Spectrom. 26, 2508. https://doi.org/10.1039/c1ja10172b

Scherer, E., 2001. Calibration of the Lutetium-Hafnium Clock. Science 293, 683–687. https://doi.org/10.1126/science.1061372

Sláma, J., Košler, J., Condon, D.J., Crowley, J.L., Gerdes, A., Hanchar, J.M., Horstwood, M.S.A., Morris, G.A., Nasdala, L., Norberg, N., Schaltegger, U., Schoene, B., Tubrett, M.N., Whitehouse, M.J., 2008. Plešovice zircon — A new natural reference material for U–Pb and Hf isotopic microanalysis. Chem. Geol. 249, 1–35. https://doi.org/10.1016/j.chemgeo.2007.11.005

Stern, R.A., Bodorkos, S., Kamo, S.L., Hickman, A.H., Corfu, F., 2009. Measurement of SIMS Instrumental Mass Fractionation of Pb Isotopes During Zircon Dating. Geostand. Geoanalytical Res. 33, 145–168. https://doi.org/10.1111/j.1751-908X.2009.00023.x

Thirlwall, M.F., Anczkiewicz, R., 2004. Multidynamic isotope ratio analysis using MC–ICP–MS and the causes of secular drift in Hf, Nd and Pb isotope ratios. Int. J. Mass Spectrom. 235, 59–81. https://doi.org/10.1016/j.ijms.2004.04.002

Williams, I.S., 1998. Geochronology by Ion Microprobe, in: McKibben, M.A., Shanks, W.C., Ridley, W.I. (Eds.), Applications of Microanalytical Techniques to Understanding Mineralizing Processes, Reviews in Economic Geology. pp. 1–35.

Woodhead, J., Hergt, J., Shelley, M., Eggins, S., Kemp, R., 2004. Zircon Hf-isotope analysis with an excimer laser, depth profiling, ablation of complex geometries, and concomitant age estimation. Chem. Geol. 209, 121–135. https://doi.org/10.1016/j.chemgeo.2004.04.026

Woodhead, J.D., Hergt, J.M., 2005. A Preliminary Appraisal of Seven Natural Zircon Reference Materials for In Situ Hf Isotope Determination. Geostand. Geoanalytical Res. 29, 183–195. https://doi.org/10.1111/j.1751-908X.2005.tb00891.x